

DESIGN, ANALYSIS, AND CHANNEL MODELING OF  
MOLECULAR MULTIPLE-RECEIVER COMMUNICATION SYSTEMS

by

Gökberk Yaylalı

B.S., Electrical and Electronics Engineering, Boğaziçi University, 2020

Submitted to the Institute for Graduate Studies in  
Science and Engineering in partial fulfillment of  
the requirements for the degree of  
Master of Science

Graduate Program in Electrical and Electronics Engineering  
Boğaziçi University

2022

## ACKNOWLEDGEMENTS

I would like to dedicate this thesis to my little brother, Doruk, to inspire him on his journey to come. I hope to set an example for him to explore his future.

I cannot express how grateful and lucky I am to be working with Prof. Ali Emre Pusane, my thesis supervisor. I am honored to be guided by his brilliance since the beginning of my journey, and very thankful for his continuous support, patience, and understanding. I would like to thank Prof. Tuna Tuğcu and Asst. Prof. Birkan Yılmaz, for their continuous assistance during my time in NRG Boğaziçi. I would also like to thank Assoc. Prof. Ertuğrul Başar for participating in my thesis jury.

This work would not be possible without the endless support and care I received from my dearest mother, Mine Yaylalı, and my dearest father, Cemil Yaylalı. I cannot find enough words to express my gratitude to them, and their values made me the person I am today. I am blessed to carry their love in my heart.

I would like to express my sincere gratitudes to İlayda, who supported me and believed in me at all times, for holding my hand at every turn.

I want to thank my friends Özgür Göldoğan and Burak Bora Kapan, for their constant support in the problems I have encountered. I also want to thank the rest of the Se7en, Berk Filcan, Alperen Gürer and Fatih Pervanlar, for their eternal companionship. I am also grateful to my dearest friends from the Mongols: Ahmet Yavuz Demir, Barış Ege Sevgili, Ege Şükrü Tahmaz, and Yiğit Korkmaz. Without their brotherhood and all those memories together, life would be a lot less colored and joyful.

This thesis has been supported by the Scientific and Technological Research Council of Turkey (TÜBİTAK) under project number 119E190.

## ABSTRACT

# DESIGN, ANALYSIS, AND CHANNEL MODELING OF MOLECULAR MULTIPLE-RECEIVER COMMUNICATION SYSTEMS

Molecular communication is a prominent technology that emerged from contemporary needs. Due to its low energy cost and simple system designs, it is an effective approach to communication on the nanoscale. Among the molecular system designs in the literature, although molecular single-input single-output (SISO) systems are one of the primary systems, they cannot match the required data transmission rate demands. Inspired by the direction of the field, this thesis focuses on molecular multiple-receiver networks. Interference is a crucial problem for molecular multiple-receiver systems which needs to be analyzed. To this point, a comprehensive investigation of molecular multiple-input multiple-output (MIMO) systems in terms of communication performance and channel state information is performed. Results exhibit the channel characteristics in detail. As the analysis becomes the backbone of further designs, two interference-mitigating methods for molecular SISO systems are applied to molecular MIMO systems. The expectations of the interference at each receiver can be estimated and subtracted from signals to detect the information more accurately. Additionally, a pre-equalization method is employed in molecular MIMO systems. Utilizing different molecule types to remove interference from signals has shown an increase in performance for higher data transmission rates. Furthermore, a novel channel modeling for molecular multiple-receiver systems is proposed, as it is the foundation of developing sophisticated systems and modulation schemes. Computer-based simulations showed that the proposed model offers well channel characterization of such systems, and the model is aimed to be the pioneer of future developments in nanonetworks.

## ÖZET

# ÇOK ALICILI MOLEKÜLER İLETİŞİM SİSTEMLERİNDE TASARIM, ANALİZ, VE KANAL MODELLEMESİ

Moleküler haberleşme günümüz ihtiyaçlarından doğan ve öne çıkan bir teknolojidir. Düşük enerji tüketimi ve basit sistem tasarımlarıyla, nano ölçekte etkili bir haberleşme yöntemi olmaktadır. Literatürdeki moleküler sistem tasarımları arasından moleküler tek-girdi tek-çıkı (SISO) sistemleri, en temel sistemlerden biri olmasına karşın, artan veri aktarım hızı ihtiyaçlarına cevap verememektedir. Alanın ilerleyiş yönünden temel alarak bu tez, moleküler çok alıcılı ağlar üzerine odaklanmaktadır. Girişim, moleküler çok alıcılı sistemler için analiz edilmesi gereken kritik bir problemdir. Bu noktada, moleküler çok-girdi çok-çıkı (MIMO) sistemlerde, haberleşme performansı ve kanal durum bilgisi açısından kapsamlı bir analiz yapılmıştır. Elde edilen sonuçlar, kanal karakteristiklerini detaylı şekilde ortaya koymaktadır. Yapılan analiz ilerleyen tasarımlarda temel alınarak, moleküler SISO sistemler için tasarlanan iki girişim azaltıcı metot, moleküler MIMO sistemlerine uygulanmıştır. Her alıcı için beklenen girişim değerleri tahminlenerek daha isabetli bilgi kestirimi için işaretlerden çıkarılmaktadır. Buna ek olarak, bir ön-eşitleme metodu moleküler MIMO sistemlerde uygulanmıştır. Farklı molekül tiplerinin girişim azaltmak için kullanımıyla yüksek veri aktarım hızlarında performans artışı gözlemlenmiştir. Bunlara ek olarak, moleküler çok alıcılı sistemler için sofistike sistem ve kipleme şemalarının gelişiminin temeli olan yeni bir kanal modellemesi önerilmektedir. Bilgisayar-temelli simülasyonlar önerilen modelin bahsedilen sistemler için isabetli kanal davranış kestirimi yaptığını göstermektedir, ve modelin gelecekte nanoağlarda yapılacak geliştirmelerin öncüsü olması hedeflenmektedir.

## TABLE OF CONTENTS

ACKNOWLEDGEMENTS . . . . .	iii
ABSTRACT . . . . .	iv
ÖZET . . . . .	v
LIST OF FIGURES . . . . .	ix
LIST OF TABLES . . . . .	xv
LIST OF SYMBOLS . . . . .	xvi
LIST OF ACRONYMS/ABBREVIATIONS . . . . .	xix
1. INTRODUCTION . . . . .	1
1.1. Fundamentals of Molecular Communication . . . . .	2
1.2. Fundamentals of Molecular SISO Systems . . . . .	3
1.2.1. Fundamentals of Molecular BCSK . . . . .	5
1.2.2. Arrival Modeling of Messenger Molecules . . . . .	6
1.2.3. Detection in Molecular BCSK . . . . .	7
1.2.3.1. Hypothesis-0 Case . . . . .	8
1.2.3.2. Hypothesis-1 Case . . . . .	10
1.3. Molecular Multiple-Receiver Systems . . . . .	11
1.3.1. Fundamentals of Molecular SIMO Systems . . . . .	12
1.3.2. Fundamentals of Molecular MIMO Systems . . . . .	13
1.3.3. Fundamentals of Molecular Index Modulation . . . . .	14
1.4. Contributions of the Thesis . . . . .	15
1.5. Organization of the Thesis . . . . .	17
2. TOPOLOGICAL ANALYSIS OF MOLECULAR MIMO SYSTEMS . . . . .	18
2.1. Parameter Optimization For Large Molecular MIMO Systems . . . . .	18
2.1.1. Tx-Rx Coverage . . . . .	18
2.1.2. Displacement of Neighboring Antennas . . . . .	21
2.2. Analysis of Molecular MIMO Systems with Varying Number of Antennas . . . . .	25
2.2.1. Communication Performance Analysis . . . . .	27
2.2.1.1. Performance of Molecular MIMO of 2 Antennas . . . . .	28

2.2.1.2.	Performance of Molecular MIMO of 4 Antennas . . . .	29
2.2.1.3.	Performance of Molecular MIMO of 8 Antennas . . . .	30
2.2.1.4.	Performance of Molecular MIMO of 16 Antennas . . . .	31
2.2.1.5.	Performance of Molecular MIMO of 32 Antennas . . . .	32
2.2.2.	Channel State Information Analysis . . . . .	33
2.2.2.1.	CSI for Molecular MIMO of 2 Antennas . . . . .	35
2.2.2.2.	CSI for Molecular MIMO of 4 Antennas . . . . .	35
2.2.2.3.	CSI for Molecular MIMO of 8 Antennas . . . . .	36
2.2.2.4.	CSI for Molecular MIMO of 16 Antennas . . . . .	36
2.2.2.5.	CSI for Molecular MIMO of 32 Antennas . . . . .	38
2.3.	Analysis of Molecular MIMO Systems with Varying Spatial Parameters	39
2.3.1.	Analysis of Varying Tx-Rx Distance . . . . .	39
2.3.2.	Analysis of Varying UCA Radius . . . . .	42
3.	MOLECULAR MIMO MODULATION ANALYSIS . . . . .	45
3.1.	Molecular Space Shift Keying . . . . .	46
3.2.	Generalized Molecular Space Shift Keying . . . . .	47
3.2.1.	Antenna Selection Strategy . . . . .	48
3.3.	Interference-Mitigating Methods . . . . .	51
3.3.1.	Constant-Weight Code-Based Iterative Sorting Decoding in Molecular MIMO Systems . . . . .	51
3.3.1.1.	MSSK with Iterative Sorting Decoder . . . . .	52
3.3.1.2.	MGSSK with Iterative Sorting Decoder . . . . .	54
3.3.2.	Beamforming in Molecular MIMO Systems . . . . .	55
3.3.2.1.	Beamforming via Signal-to-Interference Ratio . . . . .	55
3.3.2.2.	Beamforming via Signal-Interference Difference . . . . .	59
4.	CHANNEL MODELING FOR MOLECULAR SIMO SYSTEMS . . . . .	62
4.1.	Recursive Model . . . . .	63
4.1.1.	Absorption Rate Derivation for Molecular SIMO Systems . . . . .	64
4.1.2.	Closed-form Solution Derivation . . . . .	70
4.2.	Simplified Model . . . . .	74

4.2.1. Absorption Rate Approximation Based on the Recursive Model for Molecular SIMO Systems . . . . .	75
4.2.2. Closed-form Solution Derivation . . . . .	76
4.3. Channel Modeling for Molecular SIMO Systems With More Than Two Receivers . . . . .	78
4.4. Performance Evaluations . . . . .	82
4.4.1. Angular Analysis . . . . .	82
4.4.1.1. Scenario 1–Smaller Rx to be Closer to Tx . . . . .	83
4.4.1.2. Scenario 2–Larger Rx to be Closer to Tx . . . . .	85
4.4.1.3. Scenario 3–Same Radii Rxs . . . . .	88
4.4.2. Compatibility Between Models . . . . .	91
4.5. Applications of Channel Modeling in Molecular SIMO Systems . . . . .	93
4.5.1. Positioning & Localization of Tx . . . . .	93
4.5.1.1. Topology-Peak Time Relationship via The Recursive Model . . . . .	94
4.5.1.2. Topology-Peak Time Relationship via The Simplified Model . . . . .	95
4.5.2. Synchronization in Molecular SIMO Systems . . . . .	97
4.5.3. Applicability to Molecular MIMO Systems . . . . .	99
5. CONCLUSION . . . . .	100
REFERENCES . . . . .	103
APPENDIX A: REGION OF CONVERGENCE OF THE LAPLACE TRANSFORMATIONS OF THE ABSORPTION RATE FUNCTIONS IN THE RECURSIVE MODEL . . . . .	109

## LIST OF FIGURES

Figure 1.1.	An example of a molecular SISO model. . . . .	3
Figure 1.2.	The graph of absorption rate of MMs by Rx in a molecular SISO system. . . . .	4
Figure 1.3.	An example molecular SIMO model with two receivers. . . . .	12
Figure 1.4.	An example molecular MIMO model with four transmitters (small spheres) and four receivers (large spheres), placed in UCA formation. . . . .	14
Figure 2.1.	An example of the coverage angle of Tx towards an Rx. . . . .	19
Figure 2.2.	The graph of $d_x$ versus $n_{\text{TRx}}$ , from 2 to 32. . . . .	20
Figure 2.3.	An example of the displacement angle among receivers. . . . .	22
Figure 2.4.	The graph of $d_{yz}$ versus $n_{\text{TRx}}$ , from 2 to 32. . . . .	24
Figure 2.5.	An illustration of the receiver planes of the molecular MIMO systems with a varying number of antennas. . . . .	25
Figure 2.6.	The graphs of ER versus $t_b$ and $M_b$ of MSSK in molecular MIMO with $n_{\text{TRx}} = 2$ . . . . .	28
Figure 2.7.	The graphs of ER versus $t_b$ and $M_b$ of MSSK in molecular MIMO with $n_{\text{TRx}} = 4$ . . . . .	30

Figure 2.8.	The graphs of ER versus $t_b$ and $M_b$ of MSSK in molecular MIMO with $n_{\text{TRx}} = 8$ . . . . .	31
Figure 2.9.	The graphs of ER versus $t_b$ and $M_b$ of MSSK in molecular MIMO with $n_{\text{TRx}} = 16$ . . . . .	32
Figure 2.10.	The graphs of ER versus $t_b$ and $M_b$ of MSSK in molecular MIMO with $n_{\text{TRx}} = 32$ . . . . .	33
Figure 2.11.	The graph of the magnitude of several channel taps versus $t_b$ of molecular MIMO system with $n_{\text{TRx}} = 2$ , normalized with respect to the signal tap. . . . .	35
Figure 2.12.	The graph of the magnitude of several channel taps versus $t_b$ of molecular MIMO system with $n_{\text{TRx}} = 4$ , normalized with respect to the signal tap. . . . .	36
Figure 2.13.	The graph of the magnitude of several channel taps versus $t_b$ of molecular MIMO system with $n_{\text{TRx}} = 8$ , normalized with respect to the signal tap. . . . .	37
Figure 2.14.	The graph of the magnitude of several channel taps versus $t_b$ of molecular MIMO system with $n_{\text{TRx}} = 16$ , normalized with respect to the signal tap. . . . .	37
Figure 2.15.	The graph of the magnitude of several channel taps versus $t_b$ of molecular MIMO system with $n_{\text{TRx}} = 32$ , normalized with respect to the signal tap. . . . .	38
Figure 2.16.	A visualization of the coverage area of Tx on spherical Rx. . . . .	40

Figure 2.17.	The graph of ER versus $t_b$ of MSSK in molecular MIMO with $n_{\text{TRX}} = 8$ , for different $d_x$ 's. . . . .	41
Figure 2.18.	The graphs of the magnitude of several channel taps versus $t_b$ of molecular MIMO system with $n_{\text{TRX}} = 8$ , for different $d_x$ 's. . . . .	42
Figure 2.19.	The graphs of ER versus $d_{yz}$ of MSSK in molecular MIMO system with $n_{\text{TRX}} = 8$ , for different $t_b$ 's. . . . .	43
Figure 2.20.	The graphs of the magnitude of several channel taps versus $t_b$ of molecular MIMO system with $n_{\text{TRX}} = 8$ , for different $d_{yz}$ 's. . . . .	44
Figure 3.1.	A molecular MIMO system with $n_{\text{TRX}} = 4$ . . . . .	45
Figure 3.2.	The graph of ER versus $M_b$ of MSSK in molecular MIMO system with $n_{\text{TRX}} = 8$ , $d_x = 10 \mu\text{m}$ , $d_{yz} = 10 \mu\text{m}$ , $t_b = 0.30 \text{ s}$ . . . . .	47
Figure 3.3.	The undesirable antenna pairs for MGSSK with $k = 2$ on molecular MIMO with 8 antennas, due to increased ILI on unintended neighbor antennas. . . . .	49
Figure 3.4.	The preferable antenna pairs for MGSSK with $k = 2$ on molecular MIMO with 8 antennas, due to positive-feeding ILI between the selected antennas. . . . .	49
Figure 3.5.	The undesirable antenna pairs for MGSSK with $k = 2$ on molecular MIMO with 8 antennas, due to non-feeding ILI between the selected antennas. . . . .	50
Figure 3.6.	The graph of ER versus $M_b$ of MGSSK in molecular MIMO system with $n_{\text{TRX}} = 8$ , $k = 2$ , $d_x = 10 \mu\text{m}$ , $d_{yz} = 10 \mu\text{m}$ , $t_b = 0.30 \text{ s}$ . . . . .	50

Figure 3.7. Iterative Sorting Decoding Algorithm . . . . . 53

Figure 3.8. The graph of ER versus  $M_b$  of MSSK with ISD in molecular MIMO system with  $n_{\text{TRx}} = 8$ ,  $d_x = 10 \mu\text{m}$ ,  $d_{yz} = 10 \mu\text{m}$ ,  $t_b = 0.30 \text{ s}$ . . . . . 54

Figure 3.9. The graph of ER versus  $M_b$  of MGSSK with ISD in molecular MIMO system with  $n_{\text{TRx}} = 8$ ,  $k = 2$ ,  $d_x = 10 \mu\text{m}$ ,  $d_{yz} = 10 \mu\text{m}$ ,  $t_b = 0.30 \text{ s}$ . . . . . 55

Figure 3.10. The heatmap of SIR with respect to  $t_b$  and  $\alpha$  on the left, the CSI of molecular MIMO system with  $n_{\text{TRx}} = 8$ ,  $t_b = 0.30 \text{ s}$ , and  $\alpha = 0.593$ , before and after pre-equalization on the right. . . . . 58

Figure 3.11. The graphs of ER versus  $M_b$  of MSSK with Beamforming via SIR in molecular MIMO system with  $n_{\text{TRx}} = 8$ ,  $d_x = 10 \mu\text{m}$ ,  $d_{yz} = 10 \mu\text{m}$ ,  $t_b = 0.15 \text{ s}$ ,  $\alpha = 0.593$  on the left,  $t_b = 0.30 \text{ s}$ ,  $\alpha = 0.659$  on the right. 59

Figure 3.12. The heatmap of SID with respect to  $t_b$  and  $\alpha$  on the left, the CSI of molecular MIMO system with  $n_{\text{TRx}} = 8$ ,  $t_b = 0.30 \text{ s}$ , and  $\alpha = 0.659$ , before and after pre-equalization on the right. . . . . 60

Figure 3.13. The graphs of ER versus  $M_b$  of MSSK with Beamforming via SID in molecular MIMO system with  $n_{\text{TRx}} = 8$ ,  $d_x = 10 \mu\text{m}$ ,  $d_{yz} = 10 \mu\text{m}$ ,  $t_b = 0.15 \text{ s}$ ,  $\alpha = 0.659$  on the left,  $t_b = 0.30 \text{ s}$ ,  $\alpha = 0.799$  on the right. 61

Figure 4.1. An illustration of a molecular SIMO system with 2 receivers. . . . . 63

Figure 4.2. A heatmap of the distribution of MMs arriving at a receiver in a molecular SISO system, generated via computer-aided diffusion simulation. . . . . 66

Figure 4.3.	An illustration of the molecular SIMO topology examined in Scenario 1. . . . .	83
Figure 4.4.	The graph of RMS error between the computer-based absorption probability of MMs and the absorption probability of MMs acquired by the recursive model versus the separation angle $\phi$ for Scenario 1. . . . .	84
Figure 4.5.	The graphs of absorption rate of MMs and absorption probability of MMs over time for Scenario 1, when the separation angle $\phi$ is half-eclipse angle $\arcsin \frac{r_1}{r_{01}}$ . . . . .	85
Figure 4.6.	The graphs of absorption rate of MMs and absorption probability of MMs over time for Scenario 1, when the separation angle $\phi$ is $\frac{\pi}{2}$ . . . . .	85
Figure 4.7.	An illustration of the molecular SIMO topology examined in Scenario 2. . . . .	86
Figure 4.8.	The graph of RMS error between the computer-based absorption probability of MMs and the absorption probability of MMs acquired by the recursive model versus the separation angle $\phi$ for Scenario 2. . . . .	87
Figure 4.9.	The graphs of absorption rate of MMs and absorption probability of MMs over time for Scenario 2, when the separation angle $\phi$ is half-eclipse angle $\arcsin \frac{r_1}{r_{01}}$ . . . . .	87
Figure 4.10.	The graphs of absorption rate of MMs and absorption probability of MMs over time for Scenario 2, when the separation angle $\phi$ is $\frac{\pi}{2}$ . . . . .	88
Figure 4.11.	An illustration of the molecular SIMO topology examined in Scenario 3. . . . .	89

- Figure 4.12. The graph of RMS error between the computer-based absorption probability of MMs and the absorption probability of MMs acquired by the recursive model versus the separation angle  $\phi$  for Scenario 3. 89
- Figure 4.13. The graphs of absorption rate of MMs and absorption probability of MMs over time for Scenario 3, when the separation angle  $\phi$  is half-eclipse angle  $\arcsin \frac{r_1}{r_{0_1}}$ . . . . . 90
- Figure 4.14. The graphs of absorption rate of MMs and absorption probability of MMs over time for Scenario 3, when the separation angle  $\phi$  is  $\frac{\pi}{2}$ . 90
- Figure 4.15. The graphs of absorption probability of MMs over time for Scenario 1 by the recursive model and the simplified model, when the separation angle  $\phi$  is half-eclipse angle  $\arcsin \frac{r_1}{r_{0_1}}$  on the left,  $\frac{\pi}{2}$  on the right. . . . . 92
- Figure 4.16. The graphs of absorption probability of MMs over time for Scenario 3 by the recursive model and the simplified model, when the separation angle  $\phi$  is half-eclipse angle  $\arcsin \frac{r_1}{r_{0_1}}$  on the left,  $\frac{\pi}{2}$  on the right. . . . . 92

## LIST OF TABLES

Table 2.1.	Parameter table for molecular MIMO system with $n_{\text{TRx}} = 2$ . . . .	28
Table 2.2.	Parameter table for molecular MIMO system with $n_{\text{TRx}} = 4$ . . . .	29
Table 2.3.	Parameter table for molecular MIMO system with $n_{\text{TRx}} = 8$ . . . .	29
Table 2.4.	Parameter table for molecular MIMO system with $n_{\text{TRx}} = 16$ . . . .	31
Table 2.5.	Parameter table for molecular MIMO system with $n_{\text{TRx}} = 32$ . . . .	32
Table 4.1.	Spatial parameters for Scenario 1. . . . .	83
Table 4.2.	Spatial parameters for Scenario 2. . . . .	86
Table 4.3.	Spatial parameters for Scenario 3. . . . .	88

## LIST OF SYMBOLS

<b>A</b>	Conditional absorption rate of MMs matrix
$A_{\text{area}}$	Total circular area confining Rxs
$A_{\text{cap}}$	Cap area of the sphere confined by the tangents of Rx
$A_{\text{ring}}$	Ring area confining Rxs
$A_{\text{Rx}}$	Total area covered by Rxs
<b>b</b>	Molecular SISO absorption rate of MMs vector
$C_i$	Center point of $\text{Rx}_i$
$D$	Diffusion coefficient
$d$	Shortest distance between Tx and Rx in molecular SISO
$d_x$	Shortest distance between Tx and Rx in molecular MIMO
$d_{yz}$	Shortest distance between the center of Rx UCA and Txs
<b>I</b>	Interference
$L$	Channel memory
$M$	Number of MMs released
$M_b$	Number of MMs per bit
$m[k]$	Message bit at $k$ th symbol
$\hat{m}[k]$	Estimated message bit at $k$ th symbol
$\mathbf{M}_{k,l}^{\text{Tx}}$	MMs released vector of $l$ th past sequence at $k$ th symbol
$M_k^{\text{Rx}}$	Number of MMs received by Rx at $k$ th symbol
$M_k^{\text{Tx}}$	Number of MMs released by Tx at $k$ th symbol
$n_{\text{Rx}}$	Number of Rxs
$n_{\text{TRx}}$	Number of Tx and Rxs
$n_{\text{Tx}}$	Number of Txs
<b>P</b>	The channel taps vector
$\mathbf{P}_{\text{ISI}}$	The interference channel taps vector
$P_k$	Channel taps at $k$ th upcoming symbol
$P_k^A$	Channel taps of type-A MMs at $k$ th upcoming symbol
$P_k^B$	Channel taps of type-B MMs at $k$ th upcoming symbol

$P_k^{ij}$	Channel taps from Tx <sub><i>j</i></sub> to Rx <sub><i>i</i></sub> at <i>k</i> th upcoming symbol
$r_0$	Center-to-center distance between Tx and Rx
$r_{0_i}$	Center-to-center distance between Tx and Rx <sub><i>i</i></sub>
$r_{0_{i j}}$	Distance from Rx <sub><i>j</i></sub> towards Rx <sub><i>i</i></sub>
$r_{\text{coverage}}$	The ratio of $A_{\text{cap}}$ by the total area of the imaginary sphere
$r_{\text{efficiency}}$	The ratio of $A_{\text{Rx}}$ by $A_{\text{ring}}$
$r_i$	Radius of the Rx <sub><i>i</i></sub>
$r_{\text{occupancy}}$	The ratio of $A_{\text{Rx}}$ by $A_{\text{area}}$
$r_r$	Radius of the Rx
$r_{\text{UCA}}$	Radius of the Rx UCA
Rx <sub><i>i</i></sub>	<i>i</i> th receiver
$S$	Size of the symbol set
S	Signal
$t$	Time
$t_b$	Bit duration
$t_s$	Symbol duration
$t_{\text{peak}}$	Peak time of the absorption rate of MMs by Rx
$\hat{t}_{\text{peak}}$	Observed peak time of the absorption rate of MMs by Rx
$t_{\text{peak}_i}$	Peak time of the absorption rate of MMs by Rx <sub><i>i</i></sub>
$\hat{t}_{\text{peak}_i}$	Observed peak time of the absorption rate of MMs by Rx <sub><i>i</i></sub>
Tx <sub><i>j</i></sub>	<i>j</i> th transmitter
$\mathbf{v}$	Estimated bit batch–sequence
$\mathbf{x}$	Molecular SIMO absorption rate of MMs vector
$\mathbf{y}$	Number of received MMs batch–sequence
$\alpha$	Signal power portion
$\beta$	Angular displacement between Rxs
$\gamma$	Molecular BCSK demodulation threshold
$\Delta t$	Incremental time step
$\theta$	Polar angle on Rx, Coverage angle of Tx-Rx pair
$\mu_{k,l}$	Mean of number of MMs of <i>l</i> th past sequence at <i>k</i> th symbol

$\mu_{v_i}$	Mean of the $i$ th element of the estimated sequence $v_i$
$\sigma_{k,l}^2$	Variance of number of MMs of $l$ th past sequence at $k$ th symbol
$\sigma_{v_i}$	Variance of the $i$ th element of the estimated sequence $v_i$
$\tau$	Time delay
$\phi$	Separation angle between Rxs
$\phi_{\text{Half-eclipse}}$	Separation angle of half-eclipse occurrence
$\phi_{\text{No-eclipse}}$	Separation angle of no-eclipse occurrence

## LIST OF ACRONYMS/ABBREVIATIONS

3D	Three-Dimensional
BCSK	Binary Concentration Shift Keying
BER	Bit Error Rate
BER-N	Bit Error Rate–Natural Coded
BER-G	Bit Error Rate–Gray Coded
CIR	Channel Impulse Response
CSI	Channel State Information
CWC	Constant-Weight Code
ER	Error Rate
GSSK	Generalized Space Shift Keying
ILI	Inter-Link Interference
IM	Index Modulation
ISD	Iterative Sorting Decoder
ISI	Inter-Symbol Interference
MC	Molecular Communication
MCD	Maximum Count Decoder
MCvD	Molecular Communication via Diffusion
MGSSK	Molecular Generalized Space Shift Keying
MIMO	Multiple-Input Multiple-Output
MISO	Multiple-Input Single-Output
MM	Messenger Molecule
MSSK	Molecular Space Shift Keying
ROC	Region Of Convergence
RV	Random Variable
Rx	Receiver
SER	Symbol Error Rate
SID	Signal-Interference Difference
SIMO	Single-Input Multiple-Output

SIR	Signal-to-Interference Ratio
SISO	Single-Input Single-Output
SM	Spatial Modulation
SMUX	Spatial Multiplexer
SSK	Space Shift Keying
TRx	Transceiver
Tx	Transmitter
UCA	Uniform Circular Array

## 1. INTRODUCTION

Molecular communication (MC) is a novel communication technology inspired by nature itself [1]. The communication among nanoscale machines within small ranges is orchestrated with this technology, under the laws of diffusion. Based on the physical phenomenon of diffusion, MC exploits the random motion of micro and nanoscale particles to transmit information in very small-scale applications [1]. The field is founded on the laws of diffusion [2], and the statistical diffusion models [3–5]. In recent years, the progress in the MC realm has escalated, and the development in the field has been enhanced over the years. It is believed that MC technology will be the pioneer of biocompatible nanoscale device communication, and the theoretical background of the field is being illuminated with the extensive work of the people in the field.

There are multiple methods in MC, and one of the most prominent approaches in the field is molecular communication via diffusion (MCvD) [6]. The variety of MCvD systems includes several system designs from simple molecular single-input single-output (SISO) systems to molecular multiple-input multiple-output (MIMO) systems. MCvD systems use diffusive messenger molecules (MM) to convey information through a fluidic medium. There are many different modulation schemes for MCvD systems in the literature that utilize different features of the MMs. For example, information can be encoded in the type of the MM used [7], the quantity of MM [8], or temporal position [9, 10] in molecular SISO MCvD systems, and the transmitter (Tx) antenna to be used for MM transmission, namely the index of the Tx antenna [11], in molecular MIMO MCvD systems. There are studies in the literature with extensive work to exploit many other characteristics. The proposed modulations in the MC realm aim to increase communication performances and data transmission rates. The information is generally conveyed through impulsive MM releases through the channel. These MMs are subject to the laws of diffusion, and they propagate randomly through three-dimensional (3D) space.

### 1.1. Fundamentals of Molecular Communication

Multiple receiver (Rx) designs are proposed in MC, such as fully-permeable receivers [12, 13] and fully-absorbing receivers [11, 14]. Fully-permeable receivers, also named passive or transparent receivers, do not interact with MMs. They count MMs within their coverage volume for a predefined period of time, and the MMs continue their movement without interruption [13]. This permeability causes the accumulation of MMs in the channel over consecutive impulses, impacting the future transmissions [12]. There are modulations in the literature utilizing fully-permeable receivers to overcome the cumulative channel [12]. On the other hand, a more realizable receiver design, namely the fully-absorbing receiver, is a well-examined design in the literature. Fully-absorbing receivers have a perfect absorbent surface that captures any MMs coming to its surface [15]. The absorbed MMs are trapped within the receiver and stopped from their movement. This way, the channel is kept cleaner compared to a fully-permeable receiver case. The shape of the receivers can vary. However, in general, they are modeled as spherical receivers. In this study, receivers are assumed to be fully-absorbing spherical receivers throughout the thesis.

The motion of the MMs is random in all directions. The diffusion of the particles is described by Fick's law [14], and the motion of the MMs is the Brownian motion, which is modeled as a Wiener process [16]. The displacement of MMs is a 3D random walk with Gaussian distributed increments in each direction. The means of Gaussian increments are zero in a driftless medium, and the variances are  $2D\Delta t$ , where  $D$  is the diffusion coefficient which depends on the Stokes' radius of the MM, the viscosity of the medium, and the absolute temperature, and  $\Delta t$  is the incremental time step [17]. The displacements in each direction are

$$x(t + \Delta t) = x(t) + \mathcal{N}(0, 2D\Delta t), \quad (1.1)$$

$$y(t + \Delta t) = y(t) + \mathcal{N}(0, 2D\Delta t), \quad (1.2)$$

$$z(t + \Delta t) = z(t) + \mathcal{N}(0, 2D\Delta t). \quad (1.3)$$

The arrival of MMs at a receiver is spread over time, since they are free to propagate in all directions. This spread causes a significant portion of the released MMs to not arrive within the designated time interval for a communication scenario. Consecutive symbols leave a quite large number of MMs roaming in the channel and arriving later than their designated time interval, causing interference among symbols, namely inter-symbol interference (ISI). ISI is a common problem for all communication systems, and worsens the communication performance in MCvD systems [18].

## 1.2. Fundamentals of Molecular SISO Systems

Molecular SISO systems are simple-designed MC systems consisting of one transmitter and one receiver. The receiver is widely assumed and modeled as a spherical receiver. Studies in the literature [19] model the transmitter as a sphere with a smaller radius compared to the receiver. However, generally, it is modeled as a point transmitter. The radius of the receiver is  $r_r$ , and the center-to-center distance between Tx and Rx is  $r_0$ .

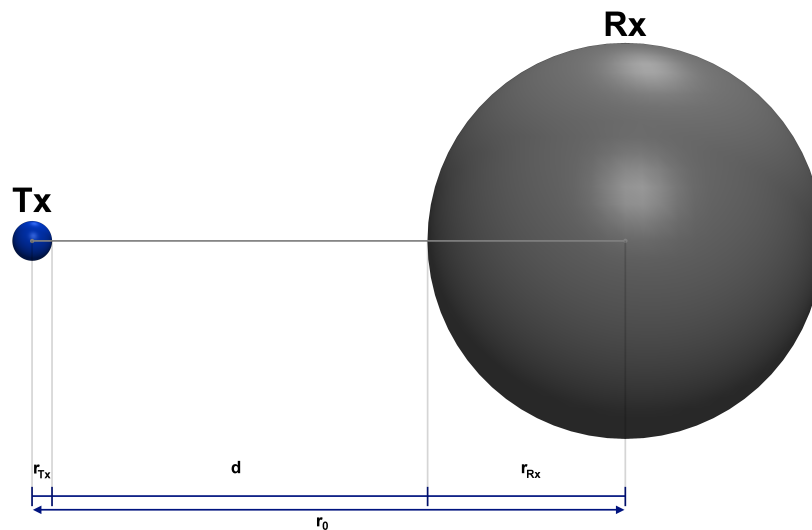


Figure 1.1. An example of a molecular SISO model.

The fluidic medium in which the MMs propagate is isotropic and boundless 3D space. The MMs released from the Tx arrive at Rx over time. The arrival of the MMs

depends on spatial parameters like  $r_r$  and  $r_0$ , the diffusion coefficient  $D$  of the MMs used for communication, and time  $t$ . In [14], the channel characteristics of a molecular SISO system with a fully-absorbing receiver are thoroughly examined and derived. The absorption rate of the MMs arriving at the receiver over time is given [14] as

$$p_{\text{Rx}}^{\text{SISO}}(t | r_0, r_r) = \frac{r_r}{r_0} \frac{1}{\sqrt{4\pi Dt}} \frac{r_0 - r_r}{t} \exp \left[ -\frac{(r_0 - r_r)^2}{4Dt} \right], \quad (1.4)$$

which is a characteristic feature of a molecular SISO system.

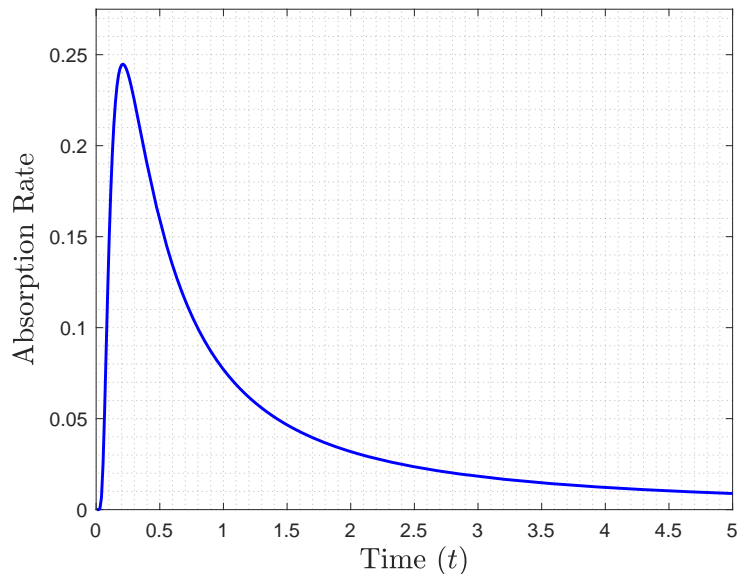


Figure 1.2. The graph of absorption rate of MMs by Rx in a molecular SISO system.

The center-to-center distance between Tx and Rx  $r_0$  is  $15 \mu\text{m}$ , the radius of Rx is  $5 \mu\text{m}$ , and the diffusion coefficient is  $D = 79.4 \mu\text{m}^2/\text{s}$ .

The expression in (1.4) also corresponds to the channel impulse response (CIR) of a molecular SISO system, and it is essential to develop sophisticated modulation schemes. By integrating (1.4) over time, one can derive the absorption probability of

MMs over time, as

$$P_{\text{Rx}}^{\text{SISO}}(t | r_0, r_r) = \int_0^t p_{\text{Rx}}^{\text{SISO}}(\tau | r_0, r_r) d\tau = \frac{r_r}{r_0} \operatorname{erfc} \left[ \frac{r_0 - r_r}{\sqrt{4Dt}} \right]. \quad (1.5)$$

Molecular SISO channel characteristics are extensively studied in the literature [7], specifically, the topology of point transmitter and spherical fully-absorbing receiver is well-examined [14] with solid analytically-derived foundations on CIR of molecular SISO systems.

### 1.2.1. Fundamentals of Molecular BCSK

Over all different modulation schemes designed for molecular SISO systems, molecular binary concentration shift keying (BCSK) is one of the most straightforward modulation schemes [7]. In molecular BCSK, the information is transmitted bit by bit, by releasing a predefined amount of MMs for bit-1, and releasing zero MMs for bit-0, as

$$M_k^{\text{Tx}} = \begin{cases} M_b, & m[k] = 1, \\ 0, & m[k] = 0, \end{cases} \quad (1.6)$$

where  $M_k^{\text{Tx}}$  is the number of MMs released from Tx at  $k$ th symbol duration of communication,  $M_b$  is the predefined amount of MMs to be released per bit, and  $m[k]$  is the message bit at  $k$ th symbol duration of the communication. Assuming bit-1 and bit-0 have equal probability, the average MMs released per one-bit information is  $\frac{M_b}{2}$ . For MC modulation schemes, power is measured by the number of MMs released. The comparison metric, the number of MMs released per bit, is generally used by normalizing the number of released MMs according to the corresponding bit package length.

The modulated information is conveyed through a diffusive channel. However, not all the MMs that are released arrive at the receiver. Also, the effect of ISI from

previous symbols in the channel interrupts the current symbol. Theoretically, the impact of the previous symbols lasts forever in the channel. However, after some time, the impact converges to zero, therefore the effect of ISI is generally assumed to exist for the last  $L$  symbols, which is the channel memory. The demodulation is conducted by simply comparing the number of MMs absorbed by the Rx  $M_k^{\text{Rx}}$  at the  $k$ th symbol duration of communication with a predefined threshold  $\gamma$  as

$$\hat{m}[k] = \begin{cases} 1, & M_k^{\text{Rx}} > \gamma, \\ 0, & M_k^{\text{Rx}} < \gamma, \end{cases} \quad (1.7)$$

where  $\hat{m}[k]$  is the estimate of the message bit at  $k$ th symbol duration of the communication. As shown above, the absorption probability of an MM until time  $t$  is calculated by (1.5). Then, the absorption probability of an MM during a symbol duration –current or previous– can be calculated as

$$P_k = P_{\text{Rx}}^{\text{SISO}}(kt_s | r_0, r_r) - P_{\text{Rx}}^{\text{SISO}}([k-1]t_s | r_0, r_r), \quad k \in \{1, \dots, L\}, \quad (1.8)$$

where  $t_s$  is the symbol duration of communication, and  $L$  is the channel memory of ISI. As seen,  $P_1$  is the absorption probability of an MM during its designated symbol duration, and  $P_k$  for  $k \in \{2, \dots, L\}$  is the absorption probability of an MM during the upcoming symbol durations, as ISI.  $P_k$  is the channel taps, and together they form the channel state information (CSI).

### 1.2.2. Arrival Modeling of Messenger Molecules

The absorption probability of an MM is calculated in (1.8). For a molecular BCSK modulation,  $M$  distinct MMs with the same absorption probability are released instantly for bit–1, which makes this probabilistic event a binomial of  $M$  trials with probability  $P_1$ . The number of MMs absorbed then becomes a binomial random vari-

able (RV) [20], as

$$M_1^{\text{Rx}} \sim \mathcal{B}(M_1^{\text{Tx}}, P_1). \quad (1.9)$$

Now, when ISI is taken into consideration, the number of MMs absorbed in the  $k$ th symbol duration of communication becomes a sum of independent binomial RVs. The sum of binomial RVs can be formulated as

$$M_k^{\text{Rx}} \sim \sum_{i=1}^L \mathcal{B}(M_{k-i+1}^{\text{Tx}}, P_i). \quad (1.10)$$

Since working with the sum of binomials is analytically intractable and the number of MMs released is generally large enough [21], the distribution of the sum of binomials can be approximated to Gaussian distribution [20], as

$$M_k^{\text{Rx}} \sim \mathcal{N}\left(\sum_{i=1}^L P_i M_{k-i+1}^{\text{Tx}}, \sum_{i=1}^L P_i(1 - P_i) M_{k-i+1}^{\text{Tx}}\right). \quad (1.11)$$

The distribution of the sum of binomials can also be approximated to Poisson distribution [20], as

$$M_k^{\text{Rx}} \sim \mathcal{P}\left(\sum_{i=1}^L P_i M_{k-i+1}^{\text{Tx}}\right). \quad (1.12)$$

The performance comparison of both approximations is also studied [20] in the literature. For convention purposes, the Gaussian approximation of the arrival of MMs will be used throughout the thesis.

### 1.2.3. Detection in Molecular BCSK

The threshold of the molecular BCSK modulation in (1.7) is an intricate parameter to determine. The optimum threshold is channel-dependent, therefore it needs to

be determined by an empirical approach since it is analytically intractable.

To propose a semi-analytical approach to determine the threshold  $\gamma$  of molecular BCSK, we start with the number of MMs arriving at the Rx at  $k$ th symbol duration as in (1.11), as

$$M_k^{\text{Rx}} \sim \mathcal{N} \left( \sum_{i=1}^L P_i M_{k-i+1}^{\text{Tx}}, \sum_{i=1}^L P_i (1 - P_i) M_{k-i+1}^{\text{Tx}} \right). \quad (1.13)$$

Assuming the CSI is known, the channel taps  $P_k$  for  $k \in \{1, \dots, L\}$  where  $L$  is the channel memory for ISI can be represented in vector notation as  $\mathbf{P} = [P_1 \ P_2 \ \dots \ P_L]^T$ . To determine the expected number of MMs at  $k$ th symbol duration, we need to consider the number of MMs released by Tx for the past  $L$  symbol durations, excluding the current symbol duration. The past  $L - 1$  releases can be represented in vector notation as  $\mathbf{M}_{k,l}^{\text{Tx}} = [M_{k-1}^{\text{Tx}} \ M_{k-2}^{\text{Tx}} \ \dots \ M_{k-L+1}^{\text{Tx}}]^T$ , where  $l$  represents the index of  $2^{L-1}$  different  $\mathbf{M}_{k,l}^{\text{Tx}}$  sequences.

We need to employ a Bayesian decision rule to determine which hypothesis is the most probable, assuming the vector  $\mathbf{M}_{k,l}^{\text{Tx}}$  is known.

1.2.3.1. Hypothesis-0 Case. Utilizing the (1.11), we can formulate the conditional probability distribution of the number of MMs received at the  $k$ th symbol duration, as

$$p(M_k^{\text{Rx}} | H_0, \mathbf{M}_{k,l}^{\text{Tx}}) = \mathcal{N} \left( \sum_{i=2}^L P_i M_{k-i+1}^{\text{Tx}}, \sum_{i=2}^L P_i (1 - P_i) M_{k-i+1}^{\text{Tx}} \right). \quad (1.14)$$

We simplify the notation by vector representation as

$$p(M_k^{\text{Rx}} | H_0, \mathbf{M}_{k,l}^{\text{Tx}}) = \mathcal{N}(\mu_{k,l}, \sigma_{k,l}^2), \quad (1.15)$$

where

$$\mu_{k,l} = \mathbf{P}_{\text{ISI}}^T \mathbf{M}_{k,l}^{\text{Tx}}, \quad (1.16)$$

$$\sigma_{k,l}^2 = (\mathbf{P}_{\text{ISI}} \odot (\mathbf{1} - \mathbf{P}_{\text{ISI}}))^T \mathbf{M}_{k,l}^{\text{Tx}}, \quad (1.17)$$

$$\mathbf{P}_{\text{ISI}} = \begin{bmatrix} P_2 & P_3 & \dots & P_L \end{bmatrix}^T, \quad (1.18)$$

and  $\odot$  is Hadamard product. There are  $2^{L-1}$  different  $\mathbf{M}_{k,l}^{\text{Tx}}$  sequences which are equiprobable as

$$P(\mathbf{M}_{k,l}^{\text{Tx}} | H_0) = \frac{1}{2^{L-1}}. \quad (1.19)$$

The joint probability distribution is formulated by

$$p(M_k^{\text{Rx}}, \mathbf{M}_{k,l}^{\text{Tx}} | H_0) = p(M_k^{\text{Rx}} | H_0, \mathbf{M}_{k,l}^{\text{Tx}}) P(\mathbf{M}_{k,l}^{\text{Tx}} | H_0). \quad (1.20)$$

To eliminate the conditionality on  $\mathbf{M}_{k,l}^{\text{Tx}}$ , we sum the joint probability distribution as

$$\sum_{l=1}^{2^{L-1}} p(M_k^{\text{Rx}}, \mathbf{M}_{k,l}^{\text{Tx}} | H_0) = \sum_{l=1}^{2^{L-1}} p(M_k^{\text{Rx}} | H_0, \mathbf{M}_{k,l}^{\text{Tx}}) P(\mathbf{M}_{k,l}^{\text{Tx}} | H_0), \quad (1.21)$$

$$= p(M_k^{\text{Rx}} | H_0). \quad (1.22)$$

Calculating  $p(M_k^{\text{Rx}} | H_0)$  as

$$p(M_k^{\text{Rx}} | H_0) = \frac{1}{2^{L-1}} \sum_{l=1}^{2^{L-1}} p(M_k^{\text{Rx}} | H_0, \mathbf{M}_{k,l}^{\text{Tx}}), \quad (1.23)$$

$$= \frac{1}{2^{L-1}} \sum_{l=1}^{2^{L-1}} \mathcal{N}(\mu_{k,l}, \sigma_{k,l}^2), \quad (1.24)$$

$$= \sum_{l=1}^{2^{L-1}} \frac{1}{\sqrt{2\pi\sigma_{k,l}^2}} \exp\left(-\frac{(M_k^{\text{Rx}} - \mu_{k,l})^2}{2\sigma_{k,l}^2}\right). \quad (1.25)$$

It should be noticed that (1.25) is a Gaussian mixture model.

1.2.3.2. Hypothesis-1 Case. In a similar approach, we utilize (1.11) to formulate the conditional probability distribution of the number of MMs at the  $k$ th symbol duration, as

$$p(M_k^{\text{Rx}} | H_1, \mathbf{M}_{k,l}^{\text{Tx}}) = \mathcal{N} \left( P_1 M_k^{\text{Tx}} + \sum_{i=2}^L P_i M_{k-i+1}^{\text{Tx}}, P_1(1-P_1)M_k^{\text{Tx}} + \sum_{i=2}^L P_i(1-P_i)M_{k-i+1}^{\text{Tx}} \right), \quad (1.26)$$

where  $M_k^{\text{Tx}}$  is equal to  $M_b$ , which is the amount molecular BCSK uses for bit-1 transmission. We simplify the notation by vector representation as

$$p(M_k^{\text{Rx}} | H_1, \mathbf{M}_{k,l}^{\text{Tx}}) = \mathcal{N}(\mu_{k,l}, \sigma_{k,l}^2), \quad (1.27)$$

where

$$\mu_{k,l} = P_1 M_b + \mathbf{P}_{\text{ISI}}^T \mathbf{M}_{k,l}^{\text{Tx}}, \quad (1.28)$$

$$\sigma_{k,l}^2 = P_1(1-P_1)M_b + (\mathbf{P}_{\text{ISI}} \odot (\mathbf{1} - \mathbf{P}_{\text{ISI}}))^T \mathbf{M}_{k,l}^{\text{Tx}}. \quad (1.29)$$

The joint probability distribution is again formulated by

$$p(M_k^{\text{Rx}}, \mathbf{M}_{k,l}^{\text{Tx}} | H_1) = p(M_k^{\text{Rx}} | H_1, \mathbf{M}_{k,l}^{\text{Tx}}) P(\mathbf{M}_{k,l}^{\text{Tx}} | H_1). \quad (1.30)$$

To eliminate the conditionality on  $\mathbf{M}_{k,l}^{\text{Tx}}$ , we sum the joint probability distribution as

$$\sum_{l=1}^{2^L-1} p(M_k^{\text{Rx}}, \mathbf{M}_{k,l}^{\text{Tx}} | H_1) = \sum_{l=1}^{2^L-1} p(M_k^{\text{Rx}} | H_1, \mathbf{M}_{k,l}^{\text{Tx}}) P(\mathbf{M}_{k,l}^{\text{Tx}} | H_1), \quad (1.31)$$

$$= p(M_k^{\text{Rx}} | H_1). \quad (1.32)$$

While considering the equiprobable  $\mathbf{M}_{k,l}^{\text{Tx}}$  sequences, we obtain

$$p(M_k^{\text{Rx}} | H_1) = \frac{1}{2^{L-1}} \sum_{l=1}^{2^{L-1}} \mathcal{N}(\mu_{k,l}, \sigma_{k,l}^2), \quad (1.33)$$

$$= \sum_{l=1}^{2^{L-1}} \frac{1}{\sqrt{2\pi\sigma_{k,l}^2}} \exp\left(-\frac{(M_k^{\text{Rx}} - \mu_{k,l})^2}{2\sigma_{k,l}^2}\right), \quad (1.34)$$

where the mean and the variance differ slightly. Provided the CSI is known, we can calculate the conditional probabilities  $p(M_k^{\text{Rx}} | H_0)$  and  $p(M_k^{\text{Rx}} | H_1)$  using all possible  $\mathbf{M}_{k,l}^{\text{Tx}}$  sequences of length  $L - 1$ , and formulate the Bayesian decision as

$$\frac{p(M_k^{\text{Rx}} | H_1)}{p(M_k^{\text{Rx}} | H_0)} \underset{H_0}{\overset{H_1}{\gtrless}} 1, \quad (1.35)$$

### 1.3. Molecular Multiple-Receiver Systems

Although the molecular SISO systems are well-examined systems with strong analytical foundations, they lack several requirements of today's technology [11]. One of them is that modulation schemes designed for molecular SISO systems cannot meet the high data transmission rate demands of today. There are multiple modulation schemes aiming to overcome the adverse effects of ISI and increase the communication performance and data transmission rate. However, the improvements are not quite enough compared to the modulations on other sophisticated molecular system designs. The other factor is that the MC realm is shifting towards multiple-entity networks, where multiple transmitters and receivers need to coexist [22]. Advanced modulations for multiple-entity networks are expected to be the future of the field, therefore the research focus of the field shifts toward the molecular multiple-entity networks.

Transmitters are generally modeled as point objects, so they do not interfere with MMs and they are statistically independent of other entities in a molecular network. However, receivers, specifically the fully-absorbing receivers, influence each other statis-

tically, therefore multiple-receiver networks are more difficult to work on. In this sense, two significant molecular topologies can be considered as bases of the multiple-receiver networks. They are molecular single-input multiple-output (SIMO) and molecular MIMO topologies.

### 1.3.1. Fundamentals of Molecular SIMO Systems

One of the most basic topologies in molecular multiple-entity networks is molecular SIMO systems. This topology consists of one transmitter, and multiple receivers distributed around it. Again, the Tx is generally modeled as a point object, and the Rxs are modeled as fully-absorbing spherical objects.

In case that the Rxs are modeled as fully-permeable, the statistical dependence would not exist, therefore the channel characteristics would be easily derived based on the analytical foundations of the molecular SISO channel model [14]. However, when the Rxs are fully-absorbing, they influence each other statistically, and the analytical examination needs to be revised. Several studies examine this problem [22–26], proposing analytical and semi-analytical methods for channel characteristics.

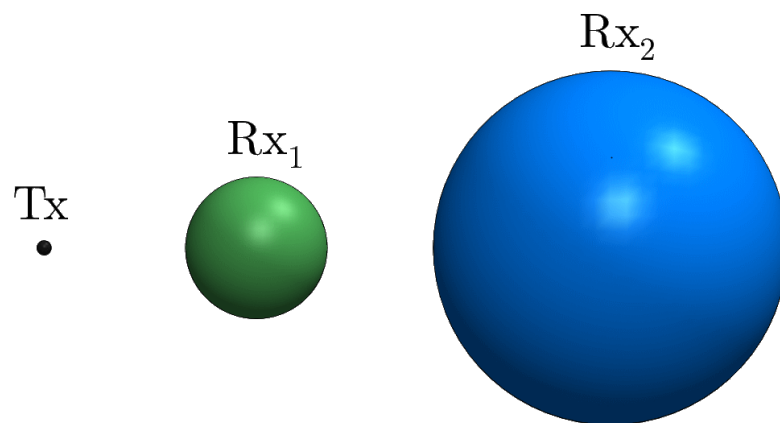


Figure 1.3. An example molecular SIMO model with two receivers.

Molecular SIMO systems are a step in the development of multiple-entity networks, and a significant milestone for the molecular MIMO networks. Throughout the thesis, the molecular SIMO systems are thoroughly examined.

### 1.3.2. Fundamentals of Molecular MIMO Systems

Molecular MIMO systems are fundamental examples of multiple-entity networks. As a generalized version of molecular SIMO systems, molecular MIMO systems show similar channel characteristics. Particularly for fully-absorbing receivers, the statistical dependence is a difficulty in channel characterization.

Molecular MIMO systems are suitable for more-sophisticated modulation schemes enabling more reliable communications and higher data transmission rates [11]. Therefore, it is expected for such systems to be a cornerstone in the development of MC technologies. Molecular MIMO systems bring their own challenges with them, such as positioning, localization, and alignment problems which impact the communication performance severely. However, several studies have shown progress in developing robust modulation schemes for combating these problems.

In general, there is no constraint for the spatial parameters of molecular MIMO systems such as the number of Rx and Tx antennas and the placement of antennas. However, for convention purposes, the numbers of Rx and Tx antennas are generally selected the same,  $n_{\text{TRx}}$ . There are different antenna placement examples in the literature. Uniform circular array (UCA) placement of the antennas is one of these topologies [11] proposed, and it shows feasibility in the analysis due to rotational symmetry around the center of UCA. With the help of symmetry, one can examine a single antenna and apply the impact by superpositioning the other antennas.

There are several advanced modulation schemes designed for molecular MIMO systems [11], and one of the most promising modulations presented is molecular index modulation [11].

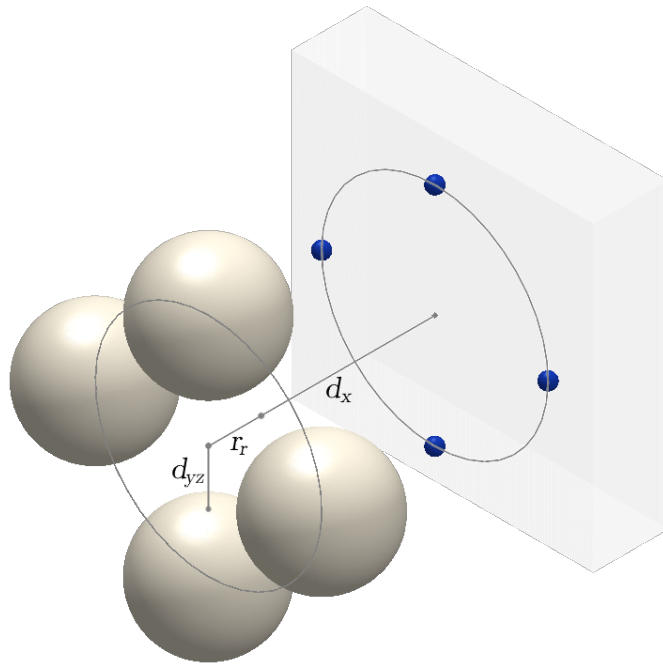


Figure 1.4. An example molecular MIMO model with four transmitters (small spheres) and four receivers (large spheres), placed in UCA formation.

### 1.3.3. Fundamentals of Molecular Index Modulation

Index modulation (IM) is a novel modulation method which is firstly proposed for wireless MIMO communication networks [27–29]. The basic principle of IM is to utilize the selection of antenna to convey information. The information is solely transmitted via the index of the selected antenna [30,31], or the index provides additional information [32,33].

A modulation scheme proposed for wireless communications, namely the space shift keying (SSK), utilizes the selection of antenna for each transmission to convey the information [30]. In this case, the sole information to be transmitted is carried by the index of the antenna. Another modulation scheme, namely the spatial modulation (SM), utilizes not only the selection of antenna, but also the signal to be transmitted

through the selected antenna [32]. In this way, the receiver side can merge these two pieces of information to de-map the information. The same principles are adapted to the MC realm [11]. Unlike wireless communications, there are no negative or complex signals in MC, other than the higher-complexity modulation schemes utilizing multiple MM types to conduct subtraction operations [34]. Therefore, there is no signal constellation formed by complex signals. In molecular SM, the signal constellation part of the information comes from the type of the MMs used [11], and the index part of the information comes from the selected antenna of the transmission. Merging two pieces, the receiver obtains the information package to be sent. Similarly, in molecular SSK (MSSK), the information is encoded to the selection of the antenna of the transmission [11]. Therefore, MC counterparts of the proposed IM-based schemes are examined in the literature.

#### 1.4. Contributions of the Thesis

The contributions of this thesis can be divided into three parts. The first part is the analysis of the existing molecular MIMO systems and modulation schemes. Upon the analysis and revisiting of the studies in the literature, we have proposed modified modulation schemes for the examined molecular MIMO systems.

The promising results of the existing studies in the literature show room for improvement. The modulation scheme proposed in [11] is a novel and high-performing modulation scheme, namely MSSK, for molecular MIMO systems. The inspiration of this study [30] handles the problem similarly in the wireless communication domain. The generalized version of this study [31] has a wider-perspective approach, namely the generalized SSK (GSSK), to the same problem. The adaptation of [31] into the MC realm is yet to be done, therefore we have proposed the adaptation of GSSK, the molecular GSSK (MGSSK), to increase the throughput of the modulation per symbol with solid foundations.

Following the proposition, we have observed that an ISI-mitigating receiver design proposed [35] for molecular SISO systems, namely the iterative sorting decoder (ISD), shows a significant performance increase with a specifically-designed codebook, constant-weight codes (CWC), while combating ISI in the time domain. We have proposed an adapted modulation scheme for molecular MIMO systems to achieve similar ISI and inter-link interference (ILI) mitigation, which is the interference among the Rx antennas for the same symbol duration. The adaptation aims to impact the interference in both the time and space domains.

The second part of the contributions is the comprehensive analysis of molecular MIMO systems, and a modulation scheme focusing on beamforming at the receiver side. Firstly, we have examined several molecular MIMO systems with a varying number of antennas, and analyzed the communication performance of large molecular MIMO topologies. Moreover, we have conducted the signal and interference power analysis on the mentioned topologies, with the impact of varying spatial parameters.

Another ISI-mitigating modulation scheme for molecular SISO systems is [34], which utilizes multiple MM types to pre-equalize the signal to mitigate ISI in the time domain. Similarly, ILI in molecular MIMO systems can be overcome by the pre-equalization with multiple MM types. We have proposed a beamforming modulation scheme to combat ILI before the receiver side. The aim is to mitigate the interference priorly to form a focused signal at the receiver side.

The third part, which can be considered the heart of this thesis, is a novel channel model for molecular SIMO systems. As mentioned above, the CIR of the molecular SISO systems can easily be obtained from solid analytical foundations [14]. However, the statistical dependence among multiple fully-absorbing receivers in a molecular SIMO system prevents an analogous derivation of the CIR of the receivers in molecular SIMO systems. To provide a proper solution to this problem, we have proposed a novel channel modeling [22] for a 2-Rx molecular SIMO system. The proposed model can be adjusted to a molecular MIMO system using the superposition principle. We,

then, have shown the potential applications of the channel model to combat common problems in communications systems such as synchronization, positioning, localization, and alignment problems.

### **1.5. Organization of the Thesis**

In Chapter 1, the thesis topics and the fundamentals of several topics are discussed. In Chapter 3, the analysis and design ideas of molecular MIMO systems based on existing modulation schemes are proposed. Interference-mitigating modifications for conventional molecular MIMO modulations are developed. In Chapter 2, the comprehensive analysis of larger molecular MIMO systems in terms of communication performance and signal power is performed. The effect of spatial parameters on communication performance is examined. A thorough channel model for molecular SIMO systems is proposed in Chapter 4.1, and in Chapter 4.2, a simplified version of that model is presented. Then, in Chapter 4.5, several applications of the proposed channel models on common communication problems such as synchronization, positioning, etc. are performed. Finally, Chapter 5 concludes the thesis and discusses the future work.

## 2. TOPOLOGICAL ANALYSIS OF MOLECULAR MIMO SYSTEMS

Molecular MIMO systems with antennas placed on UCA are previously studied in the literature [11, 36]. However, the spatial parameters of these molecular MIMO systems are generally eyeballed. These parameters correspond to both angular and spatial relationships between transmitters and receivers. For example, for a Tx-Rx pair, the distance  $d_x$  between the closest point on Rx and Tx affects the distance of MMs to travel, and the coverage angle of Tx towards Rx. Another example can be the distance between the center of Rx UCA to the closest point on Rx,  $d_{yz}$  affects the angular displacement among the Rxs, which influences interference. Based on the common molecular MIMO topologies that are used in the literature, the selection of the spatial parameters of molecular MIMO systems with a varying number of antennas  $n_{\text{TRx}}$ .

### 2.1. Parameter Optimization For Large Molecular MIMO Systems

#### 2.1.1. Tx-Rx Coverage

The absorption probability of MMs until time  $t$  for molecular SISO systems is given in (1.5). As seen, the absorption probability converges to  $\frac{r_r}{r_0} = \frac{r_r}{d+r_r}$  as time  $t$  goes to infinity. The behavior stays similar for the molecular MIMO systems. As the distance  $d_x$  increases, the number of MMs absorbed by receivers reduces significantly. Therefore, the distance  $d_x$  of molecular MIMO systems, especially larger systems with higher number of antennas  $n_{\text{TRx}}$ , needs to be in logarithmic relation with the number of antennas  $n_{\text{TRx}}$ .

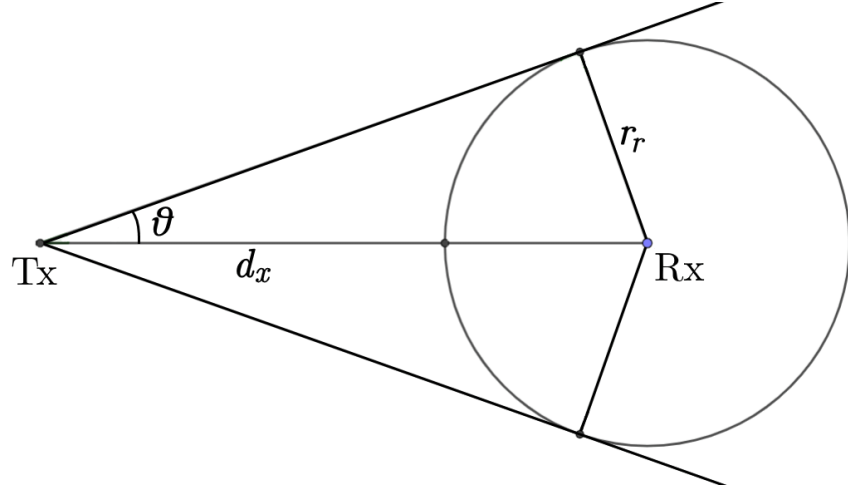


Figure 2.1. An example of the coverage angle of Tx towards an Rx.

In a Tx-Rx pair as shown in Figure 2.1, the coverage angle  $\theta$  is the angle between the tangent of the Rx and the center-to-center line of Tx and Rx. The relationship between  $\theta$  and  $d$  becomes

$$\sin \theta = \frac{r_r}{d + r_r}, \quad (2.1)$$

$$d = r_r \frac{1 - \sin \theta}{\sin \theta}. \quad (2.2)$$

For a molecular SISO system, the absorption probability of MMs by Rx converges to

$$\lim_{t \rightarrow \infty} P_{\text{Rx}}^{\text{SISO}}(t | r_0, r_r) = \frac{r_r}{d + r_r} = \sin \theta. \quad (2.3)$$

The trend of the absorption probability in molecular MIMO systems is similar. Then, the distance  $d_x$  is deduced by estimating  $\theta$  from a function of  $n_{\text{TRx}}$ , as

$$f(n_{\text{TRx}}) = m \log_2(n_{\text{TRx}}) + n = \sin \theta_{n_{\text{TRx}}}. \quad (2.4)$$

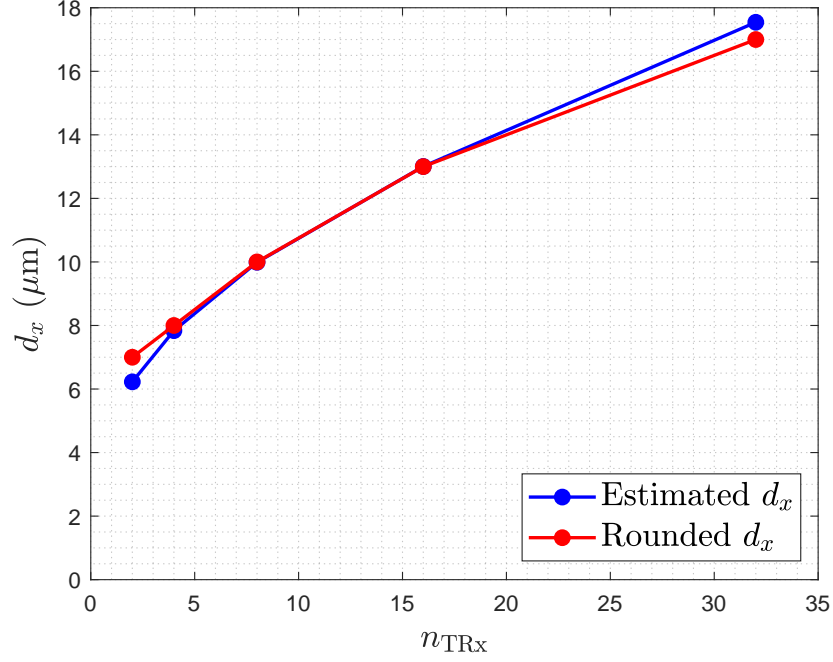


Figure 2.2. The graph of  $d_x$  versus  $n_{\text{TRx}}$ , from 2 to 32.

The molecular MIMO systems with  $n_{\text{TRx}} = 4$  [36] and  $n_{\text{TRx}} = 8$  [11, 37] are the systems commonly used in the literature. The parameters  $m$  and  $n$  of the estimation function can be found by selecting two angle values for systems with  $n_{\text{TRx}} = 4$  and  $n_{\text{TRx}} = 8$ , as

$$f(4) = 2m + n = \sin \theta_4, \quad \theta_4 = 0.40 \text{ rad}, \quad (2.5)$$

$$f(8) = 3m + n = \sin \theta_8, \quad \theta_8 = 0.34 \text{ rad}. \quad (2.6)$$

Solving the equation system gives

$$m = \sin \theta_8 - \sin \theta_4 = -0.0559, \quad (2.7)$$

$$n = 3 \sin \theta_4 - 2 \sin \theta_8 = 0.5013, \quad (2.8)$$

which results the function to be

$$f(n_{\text{TRx}}) = -0.0559 \log_2(n_{\text{TRx}}) + 0.5013, \quad (2.9)$$

$$= \sin \hat{\theta}_{n_{\text{TRx}}}. \quad (2.10)$$

The number of antennas is generally selected numbers which are powers of 2, since IM-based modulations such as MSSK carry the information by  $\log_2 n_{\text{TRx}}$  bit long packages by the index of the antenna used [11]. The numbers of interest lie from  $2^1 = 2$  to  $2^5 = 32$ , considering the realizability of the molecular MIMO systems. Rounding the estimated  $d_x$  distances, we get the first analytically-determined spatial parameter for defining larger molecular MIMO systems. The coefficients of the function in (2.9) depend on the initialization of two values, and the selected values for the molecular MIMO systems with  $n_{\text{TRx}} = 4$  and  $n_{\text{TRx}} = 8$  are educated guesses.

### 2.1.2. Displacement of Neighboring Antennas

Another significant spatial parameter of a molecular MIMO system with antennas placed on UCA is the radius of UCA. As shown in Figure 1.4, the radius of the Rx UCA is  $d_{yz} + r_r$ , so the variable part is  $d_{yz}$ . On the plane of UCA, the displacement among the Rxs depends on  $d_{yz}$ , which directly influences the interference among neighboring antennas.

For the regarding molecular MIMO topology, the number of Tx and Rx antennas is equal,  $n_{\text{Tx}} = n_{\text{Rx}}$ . Therefore the number of antennas is represented by  $n_{\text{TRx}}$  for notation conventions.  $n_{\text{TRx}}$  is generally selected a power of 2 for modulation purposes. All the Rx antennas are placed on UCA, with  $\frac{2\pi}{n_{\text{TRx}}}$  rad increments. As shown in Figure 2.3, a  $\frac{2\pi}{n_{\text{TRx}}}$  rad angular separation between two consecutive Rxs consists of two Rx-covering angles  $\alpha$ , and the displacement angle  $\beta$  between Rxs.

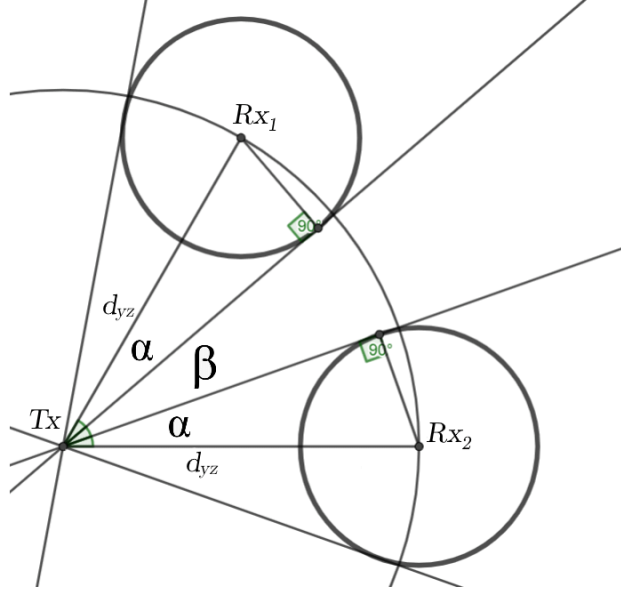


Figure 2.3. An example of the displacement angle among receivers.

The relation between  $\alpha$  and  $d_{yz}$  becomes

$$\sin \alpha = \frac{r_r}{d_{yz} + r_r}, \quad (2.11)$$

$$\alpha = \arcsin \frac{r_r}{d_{yz} + r_r}. \quad (2.12)$$

As mentioned, the angular separation between consecutive Rxs consists of

$$\frac{2\pi}{n_{\text{TRx}}} = 2\alpha + \beta, \quad (2.13)$$

$$\beta = \frac{2\pi}{n_{\text{TRx}}} - 2 \arcsin \frac{r_r}{d_{yz} + r_r}. \quad (2.14)$$

The relation between the displacement angle  $\beta$  and  $n_{\text{TRx}}$  can be modeled as an estimation function, with multiplicative inverse relation, as

$$f(n_{\text{TRx}}) = \hat{\beta}_{\text{TRx}}, \quad (2.15)$$

$$= \frac{m}{n_{\text{TRx}}} + n. \quad (2.16)$$

To find the coefficients, we again select two angle values for the common molecular MIMO topologies of  $n_{\text{TRx}} = 4$  and  $n_{\text{TRx}} = 8$ , as

$$f(4) = \frac{m}{4} + n = \beta_4, \quad \beta_4 = 0.22 \text{ rad}, \quad (2.17)$$

$$f(8) = \frac{m}{8} + n = \beta_8, \quad \beta_8 = 0.11 \text{ rad}. \quad (2.18)$$

Solving the equation system gives

$$m = 8(\beta_4 - \beta_8) = 0.88 \text{ rad}, \quad (2.19)$$

$$n = 2\beta_8 - \beta_4 = 0 \text{ rad}, \quad (2.20)$$

which results the function to be

$$f(n_{\text{TRx}}) = \frac{0.88}{n_{\text{TRx}}} \text{ rad}, \quad (2.21)$$

$$= \hat{\beta}_{\text{TRx}}. \quad (2.22)$$

The acquired  $\beta$  values are used to calculate  $d_{yz}$  from

$$\alpha = \frac{\pi}{n_{\text{TRx}}} - \frac{\beta}{2}, \quad (2.23)$$

$$d_{yz} = r_r \frac{1 - \sin \alpha}{\sin \alpha}. \quad (2.24)$$

The estimated  $d_{yz}$  distances are rounded, and the second spatial parameter for defining molecular MIMO systems is analytically calculated. The coefficients depend on the initialization of two values for molecular MIMO systems with  $n_{\text{TRx}} = 4$  and  $n_{\text{TRx}} = 8$ , which are selected by educated guesses.

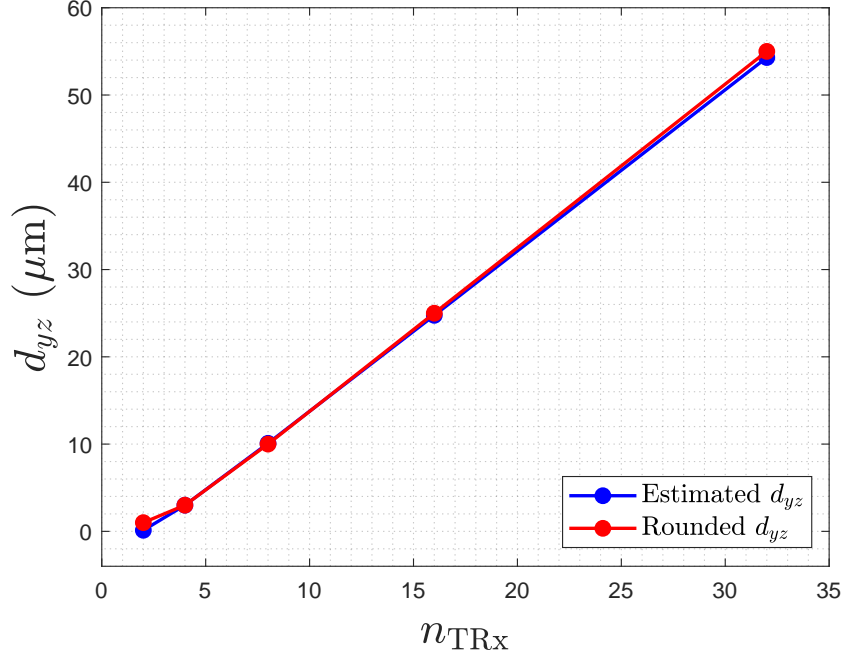


Figure 2.4. The graph of  $d_{yz}$  versus  $n_{\text{TRx}}$ , from 2 to 32.

On the Rx UCA plane, how efficient the area is being used can be discussed again numerically. On the Rx UCA plane,  $n_{\text{TRx}}$  antennas are placed on a circular array of radius  $d_{yz} + r_r$ , equidistantly. The total covered area becomes a circular area of radius  $d_{yz} + 2r_r$ , where the central circular area of radius  $d_{yz}$  remains empty, meaning that the Rx's occupy the ring area. The occupancy ratio of both areas can be geometrically calculated easily. The area covered by Rx's is

$$A_{\text{Rx}} = n_{\text{TRx}} \pi r_r^2, \quad (2.25)$$

whereas the total area occupied and the area of the ring is

$$A_{\text{area}} = \pi (d_{yz} + 2r_r)^2 \quad (2.26)$$

$$A_{\text{ring}} = \pi ((d_{yz} + 2r_r)^2 - d_{yz}^2) = 4\pi (d_{yz}r_r + r_r^2). \quad (2.27)$$

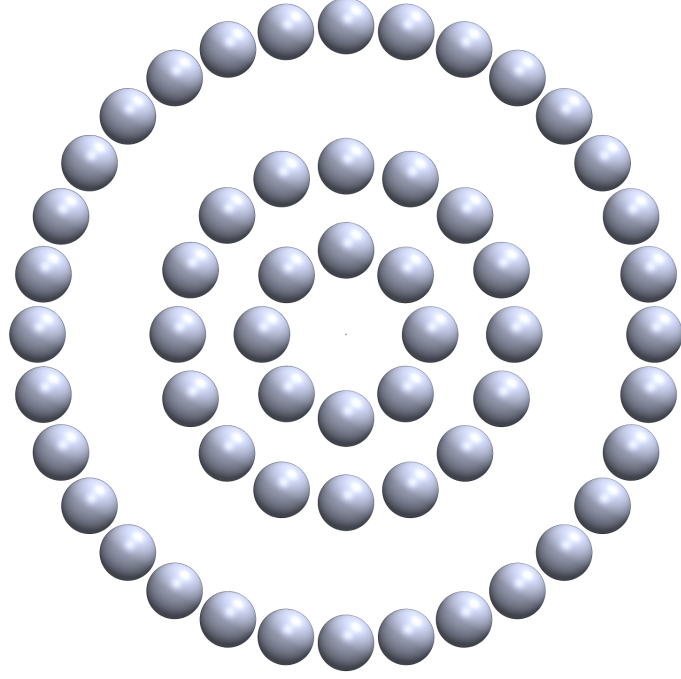


Figure 2.5. An illustration of the receiver planes of the molecular MIMO systems with a varying number of antennas from  $n_{\text{Rx}} = 8$  to  $n_{\text{Rx}} = 32$ .

The occupancy ratio and the efficiency ratio can be calculated as

$$r_{\text{occupancy}} = \frac{n_{\text{TRx}}\pi r_r^2}{\pi(d_{yz} + 2r_r)^2} = \frac{n_{\text{TRx}}r_r^2}{(d_{yz} + 2r_r)^2}, \quad (2.28)$$

$$r_{\text{efficiency}} = \frac{n_{\text{TRx}}\pi r_r^2}{4\pi(d_{yz}r_r + r_r^2)} = \frac{n_{\text{TRx}}r_r}{4(d_{yz} + r_r)}. \quad (2.29)$$

The determined spatial parameters of these molecular MIMO systems are used in the following analyses.

## 2.2. Analysis of Molecular MIMO Systems with Varying Number of Antennas

In this section, the performance and the CSI of the molecular MIMO systems with a varying number of antennas  $n_{\text{TRx}}$  are analyzed. As expected, each topology has

different characteristics, therefore the absorption probabilities of MMs by Rxs of each topology differ from each other. Increasing the symbol duration  $t_s$  evidently decreases ISI, since there is more time for Rxs to absorb MMs. However, This comes with a cost of increased ILI, since other Rxs also have more time to absorb [11]. Combining with the differing parameters, the sweet spot of the efficient bit duration  $t_b$  for each topology is then different. Additionally, The signal power in the MC realm is the amount of MMs released. Thus, as the number of MMs released increases, the error rate (ER) of the communication decreases.

For the analysis of molecular MIMO systems, MSSK modulation [11] is selected for its simplicity and interference-mitigating IM-based structure. MSSK, as will be explained in Chapter 3, is a modulation scheme designed for molecular MIMO systems, utilizing the indices of the antennas used for each transmission. The information is encoded by the index of the antenna [11], and the receivers count all the absorbed MMs. At the end of each symbol duration, the maximum count decoder (MCD) detects the antenna with the highest number of MMs absorbed.

For the data transmission rate comparison purposes, symbol durations are determined by the equivalent bit durations for compared molecular MIMO topologies, as

$$t_s = t_b \log_2 n_{\text{TRx}}. \quad (2.30)$$

Similarly, for power consumption comparison purposes, the number of MMs released is determined by the number of MMs released per bit for each topology, as

$$M = M_b \log_2 n_{\text{TRx}}. \quad (2.31)$$

The communication performances of different molecular MIMO systems are analyzed in terms of ER with varying signal power. The evaluations are conducted by

computer-based simulations. The communication simulations are exercised with different bit durations. Also, to emphasize the impact of ISI and ILI, communication performance simulations with varying bit durations are conducted for all topologies, with fixed signal power.

### 2.2.1. Communication Performance Analysis

The spatial parameters of large molecular MIMO systems are determined in Chapter 2.1. Systems with determined parameters are used for communication via MSSK modulation. The number of antennas  $n_{\text{TRx}}$  are selected powers of 2, from  $2^1$  to  $2^5$ . The CSI for each topology is calculated similarly to (1.8). The absorption probability of MMs by  $\text{Rx}_i$  when signal is released from  $\text{Tx}_j$  is represented as  $P_{\text{Rx}_i}^{\text{MIMO}}(t | \text{Tx}_j)$ , which is not analytically acquired for now. The channel taps become

$$P_k^{i|j} = P_{\text{Rx}_i}^{\text{MIMO}}(kt_s | \text{Tx}_j) - P_{\text{Rx}_i}^{\text{MIMO}}([k-1]t_s | \text{Tx}_j),$$

$$k \in \{1, \dots, L\}, \quad i, j \in \{1, \dots, n_{\text{TRx}}\}. \quad (2.32)$$

The absorption probabilities are obtained by computer-based diffusion simulations with parameters of  $D = 79.4 \mu\text{m}^2/\text{s}$ ,  $\Delta t = 10^{-4}$  s, the number of MMs released  $M = 10^6$ . The calculated CSI is used to simulate the number of arrivals of MMs at Rxs by (1.11). Then, MCD detects the antennas used for each symbol duration, and decodes the information according to the indices. For comparison purposes, the indexing of antennas is performed in two ways, natural-coded indexing and gray-coded indexing. Gray codes are commonly-known codes for their reduced bit error rate (BER) performances. Indexing of antennas by gray-mapping provides that there is only one bit difference between neighboring antennas, which is beneficial considering that ILI is a severe problem in communication performance.

Table 2.1. Parameter table for molecular MIMO system with  $n_{\text{TRx}} = 2$ .

$n_{\text{TRx}}$	2	$r_r$	$5 \mu\text{m}$
$d_x$	$7 \mu\text{m}$	$r_0$	$12 \mu\text{m}$
$d_{yz}$	$1 \mu\text{m}$	$r_{\text{UCA}}$	$6 \mu\text{m}$
$r_{\text{occupancy}}$	0.4132	$r_{\text{efficiency}}$	0.4167

2.2.1.1. Performance of Molecular MIMO of 2 Antennas. The molecular MIMO system with  $n_{\text{TRx}} = 2$  is a densely-packed MC topology consisting of 2 point TxS and 2 RxS. By utilizing MSSK modulation, the information is transmitted as  $\log_2 2 = 1$  bit long packages. Also, since there are 2 antennas, one works for bit-0, and the other works for bit-1. Since it is densely packed, ILI is quite strong. The error rates change as  $t_b$  increases, showing a flooring error rate. This is founded on the saturation of ILI as the bit duration increases.

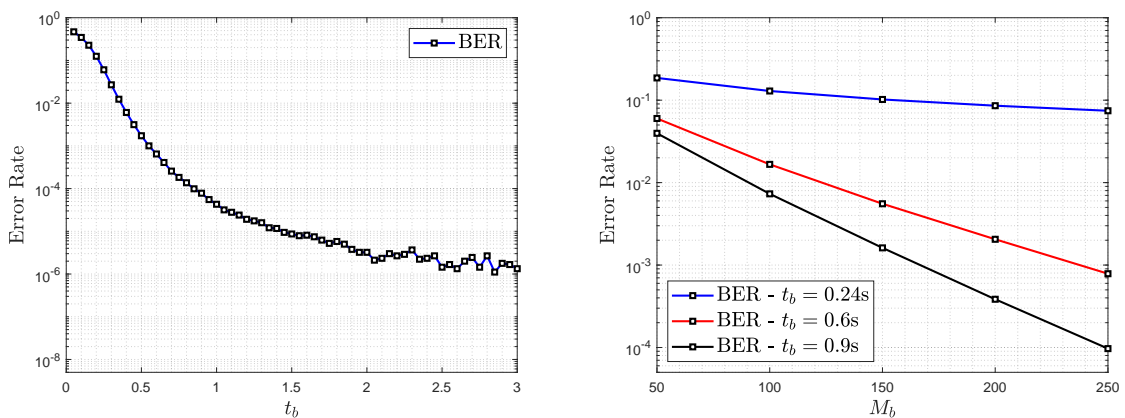


Figure 2.6. The graphs of ER versus  $t_b$  (on the left) and versus  $M_b$  (on the right) of MSSK in molecular MIMO with  $n_{\text{TRx}} = 2$ . The spatial parameters of the topology is given in Table 2.1.

Since bit duration and symbol duration is equal for a molecular MIMO system with  $n_{\text{TRx}} = 2$ , relatively short bit durations do not perform well, since the majority of MMs do not have enough time to be absorbed by RxS, hence the higher ISI. Therefore,

this topology works better in higher bit durations compared to the short ones.

Table 2.2. Parameter table for molecular MIMO system with  $n_{\text{TRx}} = 4$ .

$n_{\text{TRx}}$	4	$r_r$	5 $\mu\text{m}$
$d_x$	8 $\mu\text{m}$	$r_0$	13 $\mu\text{m}$
$d_{yz}$	3 $\mu\text{m}$	$r_{\text{UCA}}$	8 $\mu\text{m}$
$r_{\text{occupancy}}$	0.5917	$r_{\text{efficiency}}$	0.6250

2.2.1.2. Performance of Molecular MIMO of 4 Antennas. The molecular MIMO system with  $n_{\text{TRx}} = 4$  is the densest packing among the regarded molecular MIMO systems, with the highest occupancy ratio. By utilizing MSSK modulation, the information is transmitted as  $\log_2 4 = 2$  bit long packages. As shown in Chapter 2.1, the displacement among neighboring Rx antennas decreases as the number of antennas in the system increases. That is the main reason for increased ILI, along with the fact that the symbol duration is increased by the increased bit package length. The trade-off between ILI and ISI depends on the symbol duration, and as the symbol duration increases, ISI drops significantly whereas ILI gets stronger. As the symbol durations extend beyond the bit durations, the communication performance of this topology in terms of error rates gets better for shorter bit duration scenarios. Compared to the previous topology, the decrease in communication error rates has a steeper trend.

Table 2.3. Parameter table for molecular MIMO system with  $n_{\text{TRx}} = 8$ .

$n_{\text{TRx}}$	8	$r_r$	5 $\mu\text{m}$
$d_x$	10 $\mu\text{m}$	$r_0$	15 $\mu\text{m}$
$d_{yz}$	10 $\mu\text{m}$	$r_{\text{UCA}}$	15 $\mu\text{m}$
$r_{\text{occupancy}}$	0.5000	$r_{\text{efficiency}}$	0.6667

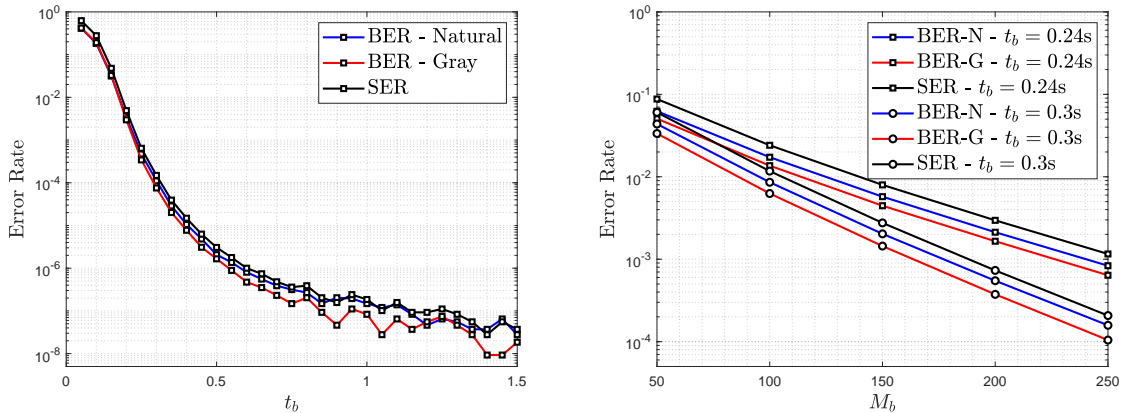


Figure 2.7. The graphs of ER versus  $t_b$  (on the left) and versus  $M_b$  (on the right) of MSSK in molecular MIMO with  $n_{\text{TRx}} = 4$ . The spatial parameters of the topology is given in Table 2.2.

2.2.1.3. Performance of Molecular MIMO of 8 Antennas. The molecular MIMO system with  $n_{\text{TRx}} = 8$  is one of the most efficiently packed among the regarding molecular MIMO systems, with the highest efficiency ratio. By utilizing MSSK modulation, the information is transmitted as  $\log_2 8 = 3$  bit long packages. This topology is often regarded as the sweet spot for the number of antennas, since the communication error rate slope is steeper than in other topologies despite the increase in ILI. Symbol duration for fixed bit duration is longer than the previous topologies, and shorter than the upcoming topologies, which enables ISI to be weaker compared to the previous topologies, and ILI not to stronger enough compared to the upcoming topologies.

Since the symbol duration is longer, the improvement in communication performance is higher, as the error rate curves have steeper slopes. However, since the Rx antennas are closer to each other as a result of smaller displacement angles, ILI becomes a severer problem in higher bit durations, therefore the error floor is higher than the one in the 4-antenna counterpart.

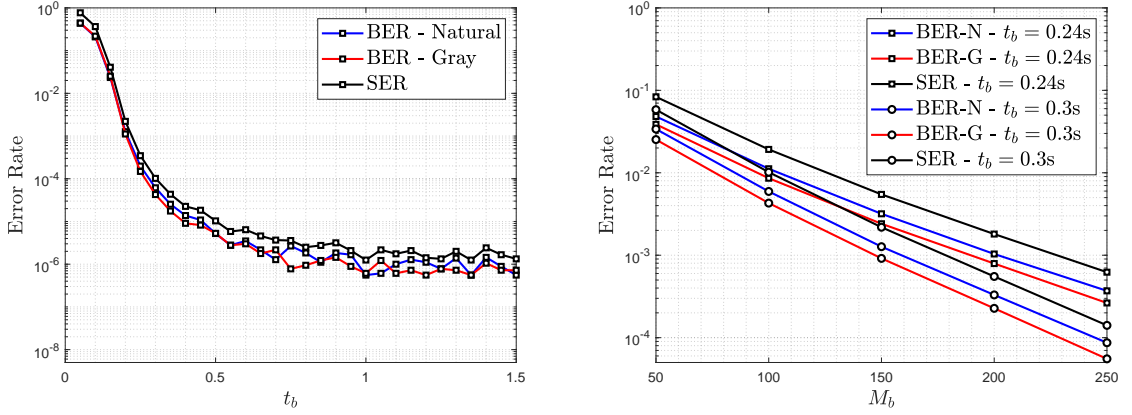


Figure 2.8. The graphs of ER versus  $t_b$  (on the left) and versus  $M_b$  (on the right) of MSSK in molecular MIMO with  $n_{\text{TRx}} = 8$ . The spatial parameters of the topology is given in Table 2.3.

Table 2.4. Parameter table for molecular MIMO system with  $n_{\text{TRx}} = 16$ .

$n_{\text{TRx}}$	16	$r_r$	$5 \mu\text{m}$
$d_x$	$13 \mu\text{m}$	$r_0$	$18 \mu\text{m}$
$d_{yz}$	$25 \mu\text{m}$	$r_{\text{UCA}}$	$30 \mu\text{m}$
$r_{\text{occupancy}}$	0.3265	$r_{\text{efficiency}}$	0.6667

2.2.1.4. Performance of Molecular MIMO of 16 Antennas. The molecular MIMO system with  $n_{\text{TRx}} = 16$  is a large example of molecular MIMO topologies with a radius twice the radius of its 8-antenna counterpart. It is effectively packed as its efficiency ratio is equal to the highest. By utilizing MSSK modulation, the information is transmitted as  $\log_2 16 = 4$  bit long packages. This densely-packed topology is prone to suffer from ILI as the impact of ILI is an increasing trend with the number of antennas. From this topology, ILI starts to hit the communication performance severely.

Again, since the symbol duration is longer than the previous topologies for a fixed bit duration, the saturation of the performance occurs rapidly. As expected, ILI is fed by the increasing bit durations  $t_b$ , therefore the error floor is considerably higher.

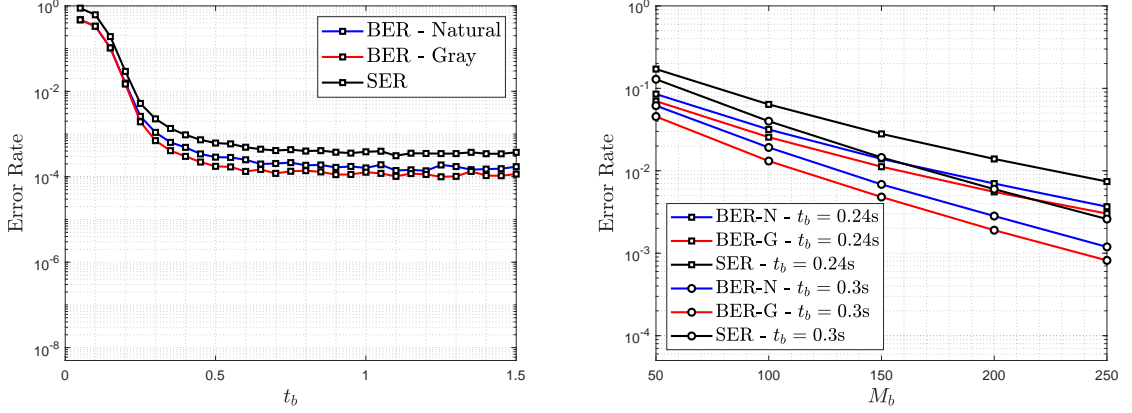


Figure 2.9. The graphs of ER versus  $t_b$  (on the left) and versus  $M_b$  (on the right) of MSSK in molecular MIMO with  $n_{\text{TRx}} = 16$ . The spatial parameters of the topology is given in Table 2.4.

Table 2.5. Parameter table for molecular MIMO system with  $n_{\text{TRx}} = 32$ .

$n_{\text{TRx}}$	32	$r_r$	5 $\mu\text{m}$
$d_x$	17 $\mu\text{m}$	$r_0$	22 $\mu\text{m}$
$d_{yz}$	55 $\mu\text{m}$	$r_{\text{UCA}}$	60 $\mu\text{m}$
$r_{\text{occupancy}}$	0.1893	$r_{\text{efficiency}}$	0.6667

2.2.1.5. Performance of Molecular MIMO of 32 Antennas. As the largest topology to be examined in this thesis, the molecular MIMO system with  $n_{\text{TRx}} = 32$  is a quite large molecular MIMO topology which consists of 64 entities –32 TxS and 32 RxS– in total. The radius is twice the radius of its 16–antenna counterpart, whereas the efficiency ratio is equal to the highest. This means RxS are densely-packed within their region. By utilizing MSSK modulation, the information is transmitted as  $\log_2 32 = 5$  bit long packages. This directly implies longer symbol durations for fixed bit durations, which mitigates ISI while strengthening the ILI.

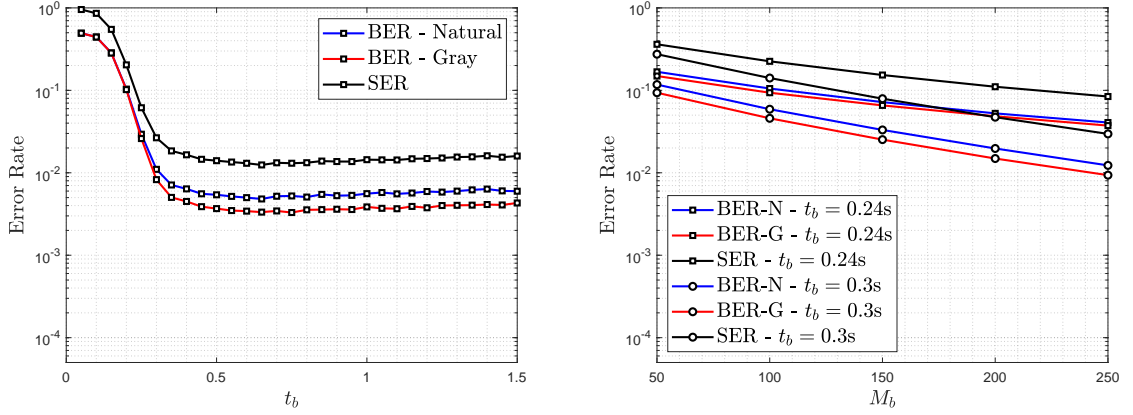


Figure 2.10. The graphs of ER versus  $t_b$  (on the left) and versus  $M_b$  (on the right) of MSSK in molecular MIMO with  $n_{\text{TRx}} = 32$ . The spatial parameters of the topology is given in Table 2.5.

With its densely-packed Rxs and higher symbol durations which enhance ILI, this topology is prone to suffer heavily from ILI as its communication performance hits the error floor quickly, and the error floor is quite high, compared to the other topologies. The room for improvement is quite small for the topology, as the error rate curve has an easier slope.

### 2.2.2. Channel State Information Analysis

As the spatial parameters of a variety of molecular MIMO topologies have been determined, the CSI of these topologies gain prominence. Based on the earlier results and deductions from analytical foundations of molecular SISO systems in (1.4) and (1.5), we can state these observations:

- (i) Depending on the spatial parameter  $d_x$ , MMs need enough time to arrive at and be absorbed by Rxs at the designated time interval.

As stated above, the CSI, as conventionally known as channel taps, are calculated via (2.32). These absorption probability functions are yet to be analytically formulated, which will be presented in Chapter 4, however, they are formed in a

similar trend to that of molecular SISO systems, as shown in (1.5). To give an example in molecular SISO, we want to have  $P_1$ , the absorption probability of an MM during its designated symbol duration as calculated by (1.8), to be greater than all ISI terms, the first ISI term  $P_2$  in particular. Then, we can formalize the inequality

$$P_1 \geq P_2, \quad (2.33)$$

$$\frac{r_r}{r_0} \operatorname{erfc} \left[ \frac{r_0 - r_r}{\sqrt{4Dt_s}} \right] \geq \frac{r_r}{r_0} \operatorname{erfc} \left[ \frac{r_0 - r_r}{\sqrt{4D(2t_s)}} \right] - \frac{r_r}{r_0} \operatorname{erfc} \left[ \frac{r_0 - r_r}{\sqrt{4Dt_s}} \right], \quad (2.34)$$

$$2 \operatorname{erfc} \left[ \frac{r_0 - r_r}{\sqrt{4Dt_s}} \right] \geq \operatorname{erfc} \left[ \frac{r_0 - r_r}{\sqrt{8Dt_s}} \right]. \quad (2.35)$$

Therefore,  $t_s$  should be longer than a certain value that satisfies (2.35), in order to avoid the ISI terms exceeding the signal term. A similar logic works for molecular MIMO systems, as well. For a numerically-calculated time, ISI terms may exceed the signal term, so the symbol duration  $t_s$  needs to be selected accordingly.

- (ii) For longer symbol durations  $t_s$ , the number of MMs absorbed by Rxs eventually converges to saturation as  $t_s$  goes to infinity.

Increased symbol durations help reduce ISI, while increasing ILI. As mentioned above, the absorption probability functions of Rxs in a molecular MIMO system show a similar form to those in molecular SISO systems. To show an example in molecular SISO, we can write

$$P_1 = \lim_{t_s \rightarrow \infty} \frac{r_r}{r_0} \operatorname{erfc} \left[ \frac{r_0 - r_r}{\sqrt{4Dt_s}} \right] = \frac{r_r}{r_0}, \quad (2.36)$$

while the remaining ISI terms converge to zero. Similarly, the channel taps of a molecular MIMO system  $P_k^{i|j}$  become saturated for  $k = 1$  symbol instance, as the remaining ISI terms for  $k \geq 2$  vanish. As ILI terms  $P_1^{i|j}$  for  $i \neq j$  saturate, the room for improvement in communication performance diminishes, hence the error floor in error rates with varying bit durations.

To emphasize the signal and interference power, we compare the magnitudes of significant channel taps of each topology, such as the first ISI term of the antenna to be used, and the ILI terms of the nearest neighboring antenna.

2.2.2.1. CSI for Molecular MIMO of 2 Antennas. Since the displacement angle is the greatest in this topology among the regarded molecular MIMO topologies, the only ILI term,  $P_1^{i|j}$  for  $i \neq j$  is relatively small. Since the symbol duration is equal to the bit duration, ISI terms have an advantage here due to the arrival of the MMs, which eventually fade out.

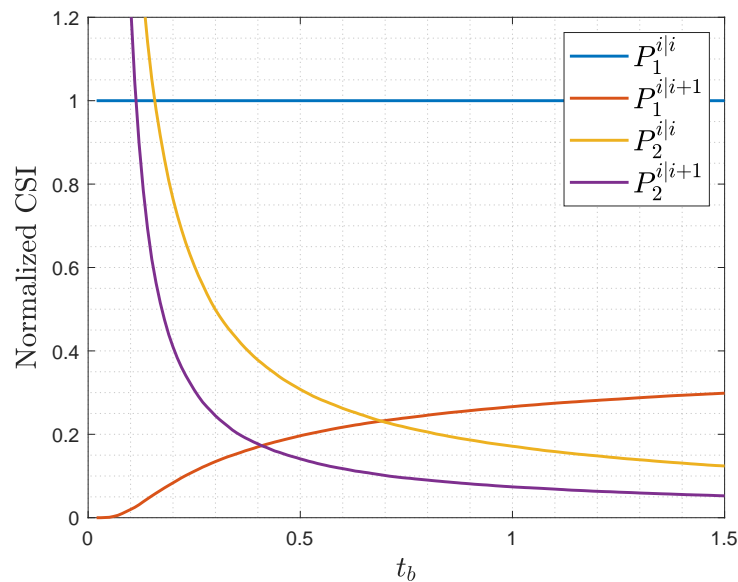


Figure 2.11. The graph of the magnitude of several channel taps versus  $t_b$  of molecular MIMO system with  $n_{\text{TRx}} = 2$ , normalized with respect to the signal tap.

2.2.2.2. CSI for Molecular MIMO of 4 Antennas. The symbol duration is enhanced as the bit package length increases, therefore the ISI terms lose strength earlier than the previous topology. As we can observe, ILI terms saturate to a greater value, due to the increased closeness among Rx antennas.

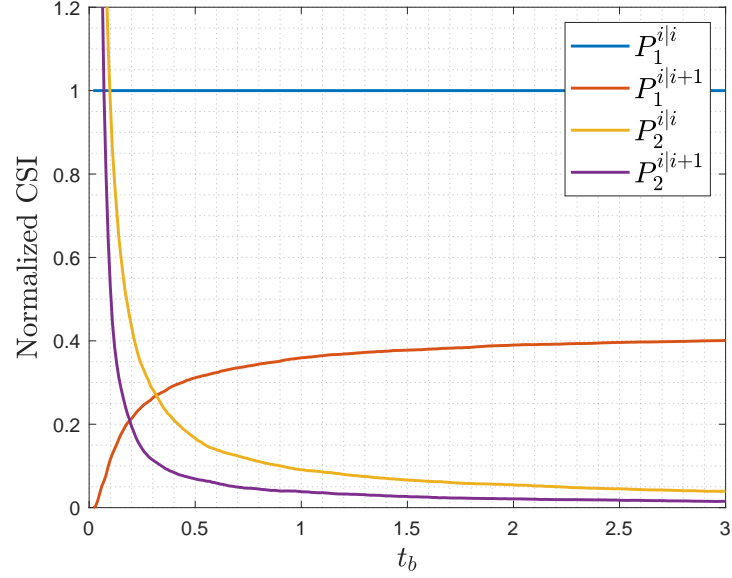


Figure 2.12. The graph of the magnitude of several channel taps versus  $t_b$  of molecular MIMO system with  $n_{\text{TRx}} = 4$ , normalized with respect to the signal tap.

2.2.2.3. CSI for Molecular MIMO of 8 Antennas. Two similar observations are made from the CSI of this topology. Firstly, the significance of the ISI terms again reduces rapidly as it verifies the trend between increasing the number of antennas and the evolution of ISI power for shorter bit durations. The second observation is that the ILI terms again have greater magnitudes compared to the previous topologies, as a result of reduced displacement angles among Rxs.

2.2.2.4. CSI for Molecular MIMO of 16 Antennas. In this topology, one significant observation can be stated, that is, ILI is a severe problem from now on, even for shorter bit durations which imply shorter symbol durations. The densely-packed Rxs and relatively longer symbol durations collectively result in a heavy interference among Rxs, which undermine the communication performance.

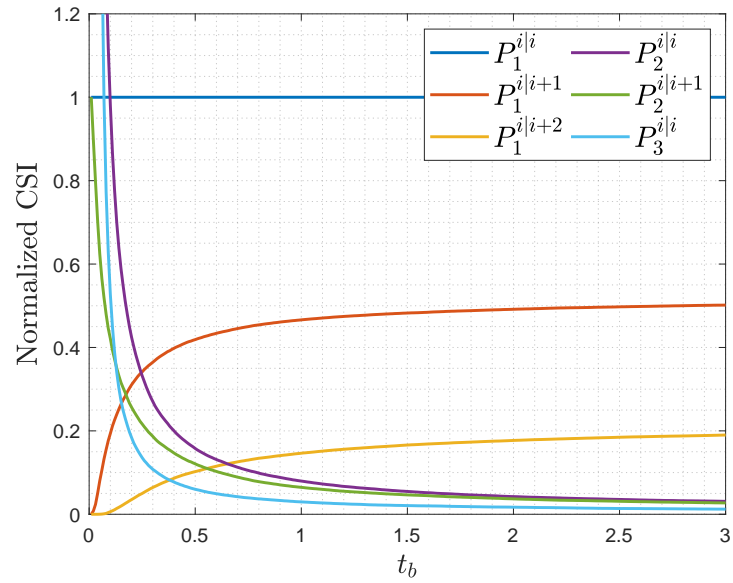


Figure 2.13. The graph of the magnitude of several channel taps versus  $t_b$  of molecular MIMO system with  $n_{\text{TRx}} = 8$ , normalized with respect to the signal tap.

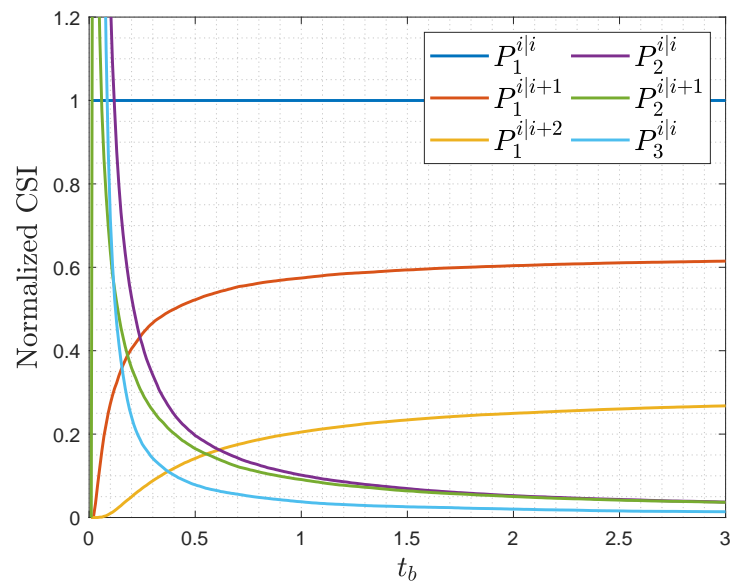


Figure 2.14. The graph of the magnitude of several channel taps versus  $t_b$  of molecular MIMO system with  $n_{\text{TRx}} = 16$ , normalized with respect to the signal tap.

2.2.2.5. CSI for Molecular MIMO of 32 Antennas. Combined with the increased  $d_x$ , the closely-placed Rxs are nearly at the same distance to an arbitrary Tx. This means the neighbor Rxs get nearly a similar amount of MMs as the intended Rx, which severely hurts the communication performance. These large topologies are extremely vulnerable to ILI with their reduced coverage angles between Tx-Rx pairs, and the closeness of their Rx antennas.

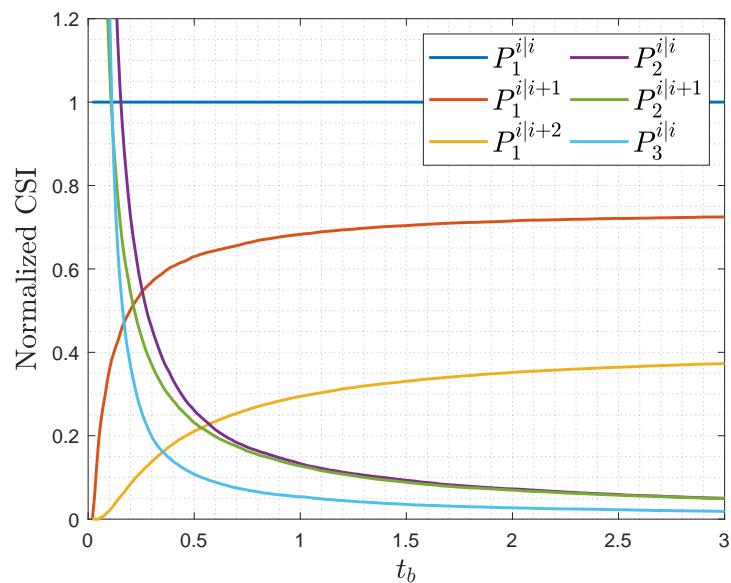


Figure 2.15. The graph of the magnitude of several channel taps versus  $t_b$  of molecular MIMO system with  $n_{\text{TRx}} = 32$ , normalized with respect to the signal tap.

To summarize, there are a few results to point out. Firstly, the molecular MIMO topologies where the Tx and Rx planes are distant  $-d_x$  is large- and Rxs are close to each other are ILI-prone topologies. These topologies require higher bit durations for MMs to arrive at Rxs, however, the ILI becomes still significant due to their low coverage angle and low displacement angle.

The second point is that, increasing bit duration to reduce error rate does not always pay off, since high bit durations also increase the ILI which causes the Rxs to achieve saturation in terms of MMs. Therefore the topology converges to its natural

limits in communication performance, hence the error floors. Depending on these observations, the communication performance generally decreases for molecular MIMO topologies which can be considered large, such as the topologies with 16 and 32 antennas.

### 2.3. Analysis of Molecular MIMO Systems with Varying Spatial Parameters

To define a molecular MIMO system with antennas placed on a UCA, there are 8 parameters to determine in general. These are  $n_{\text{Tx}}$  and  $n_{\text{Rx}}$ , which are system-related parameters, the radius of an Rx  $r_r$ , which is a topological parameter, the diffusion coefficient  $D$ , which depends on the MM type used,  $d_x$ ,  $d_{yz}$ ,  $r_0$  and  $r_{\text{UCA}}$ , which are spatial parameters. Among these, the parameters  $r_0$  and  $r_{\text{UCA}}$  are dependent parameters. The number of antennas  $n_{\text{TRx}}$  and  $n_{\text{Rx}}$  is set equal, and the effect of the number of antennas on communication performance is examined above. The radius  $r_r$  is generally constant for convention, which leaves us two variable parameters to examine,  $d_x$  and  $d_{yz}$ .

The molecular MIMO system with 8 antennas is widely regarded as the optimized molecular MIMO system due to its compact packing and its lower vulnerability to ILI. Therefore, the effects of variable spatial parameters are examined on this topology.

#### 2.3.1. Analysis of Varying Tx-Rx Distance

The distance between the Tx plane and the Rx plane is represented as  $r_0$ , which is constant for all Tx-Rx pairs since the planes are parallel to each other. The radii of Rxs are regarded constant, then the variable part is  $d_x$ , the shortest distance between Tx and the surface of its pair Rx. As mentioned, the angular coverage between Tx and Rx is governed by the variable  $d_x$ , as stated in (2.1). Another geometrical measurement, the coverage area, is visualized in Figure 2.16.

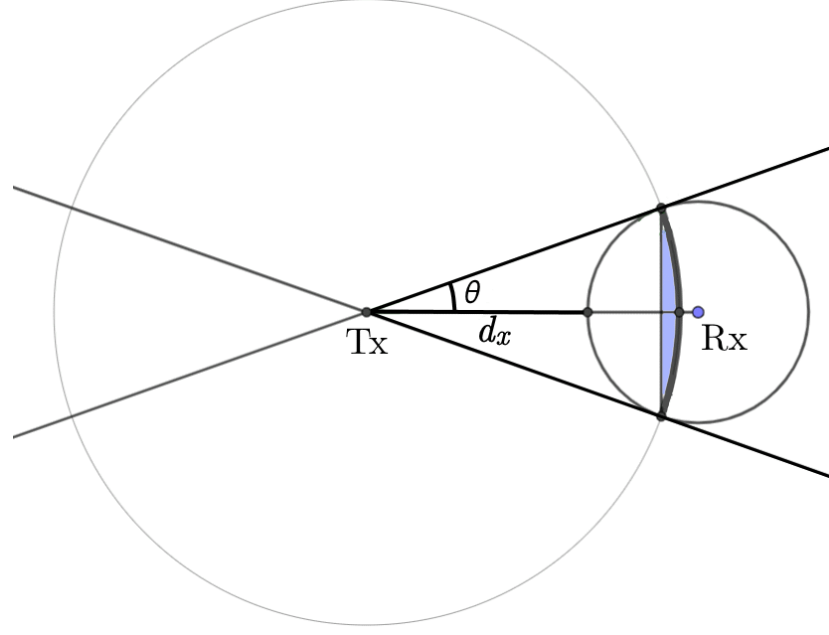


Figure 2.16. A visualization of the coverage area of Tx on spherical Rx.

The geometrical calculation of the covered cap is

$$A_{\text{cap}} = 2\pi r_r^2(1 - \cos \theta). \quad (2.37)$$

Then, the ratio of the covered area to the area of the imaginary 3D sphere becomes

$$r_{\text{coverage}} = \frac{2\pi r_r^2(1 - \cos \theta)}{4\pi r_r^2} = \frac{1 - \cos \theta}{2}. \quad (2.38)$$

As the coverage angle decreases due to an increase in  $d_x$ , the covered area ratio decreases. This metric and the coverage angle help us to infer the fact that we expect a decrease in the number of MMs arriving at Rxs and also a delay in the peak arrival time for increasing  $d_x$  values.

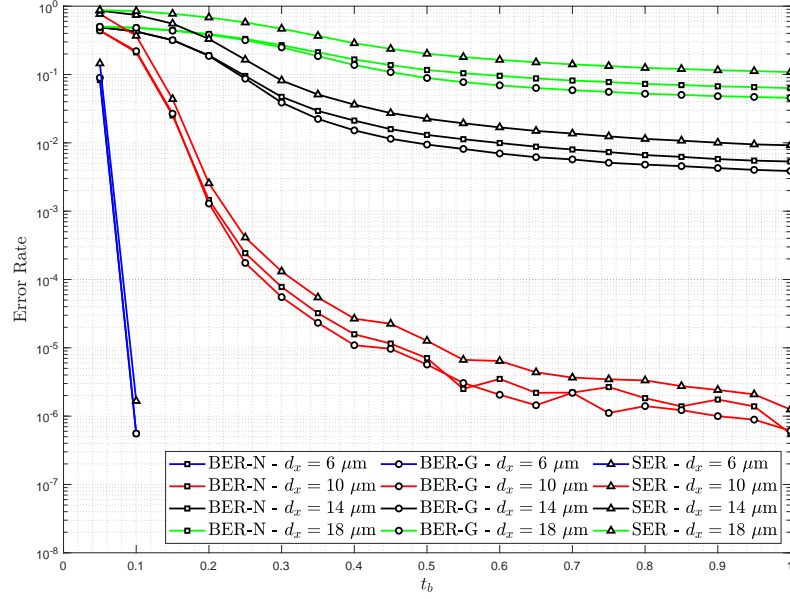


Figure 2.17. The graph of ER versus  $t_b$  of MSSK in molecular MIMO with  $n_{\text{TRx}} = 8$ , for different  $d_x$ 's.

From the results, we can state that:

- (i) Low  $d_x$  enables MMs to arrive at RxS more quickly, reducing ISI. On the other hand, as the  $d_x$  increases, MMs are prone to scatter around the diffusive medium randomly. Therefore, the absorption probability of MMs by the intended Rx antennas decreases, along with a delay in arrival, increasing ISI, and reducing signal power.
- (ii) Since low  $d_x$  leads to a higher coverage angle, MMs are prone to be absorbed by the intended Rx antenna, reducing ILI. Conversely, higher  $d_x$  causes the coverage angle to reduce, thus the MMs scatter around the medium more, increasing the number of MMs absorbed by unintended Rx antennas, hence the increase in ILI.

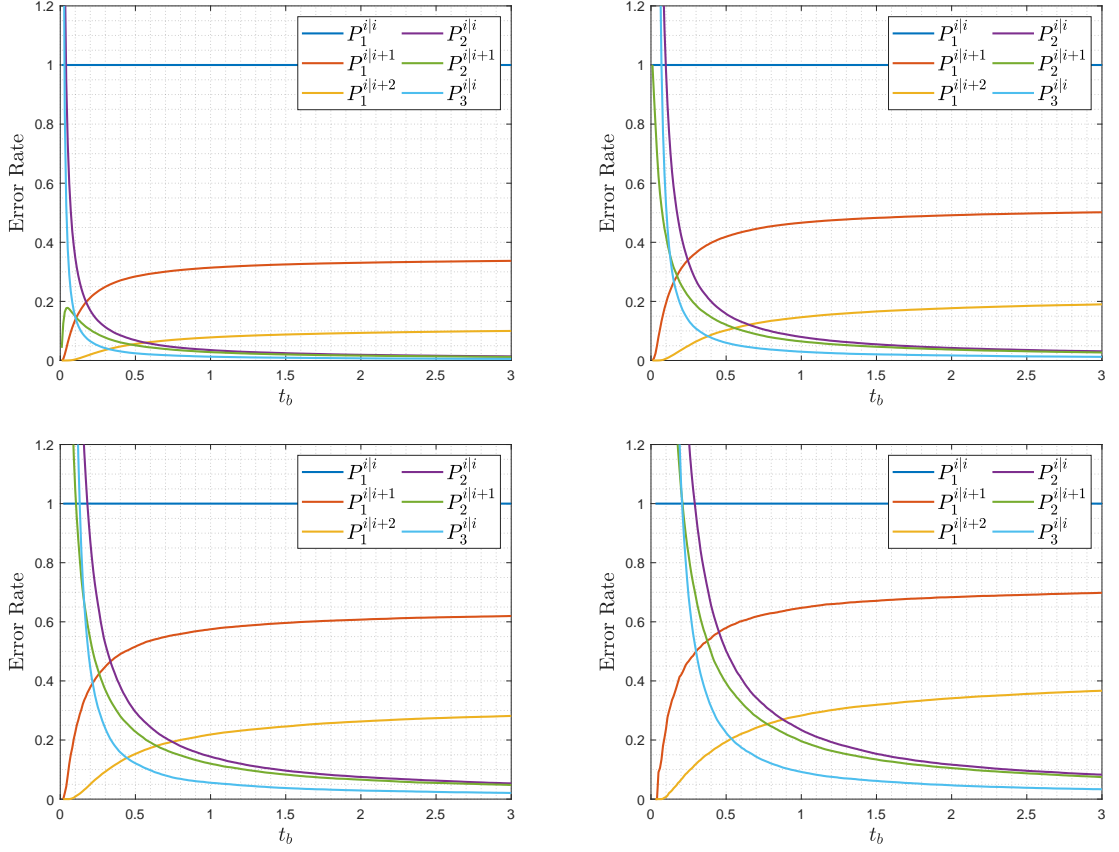


Figure 2.18. The graphs of the magnitude of several channel taps versus  $t_b$  of molecular MIMO system with  $n_{\text{TRx}} = 8$ , for  $d_x = 6 \mu\text{m}$  on the upper left,  $d_x = 10 \mu\text{m}$  on the upper right,  $d_x = 14 \mu\text{m}$  on the lower left,  $d_x = 18 \mu\text{m}$  on the lower right, normalized with respect to the signal tap.

In the light of these results and implications, it can be stated that lowering  $d_x$  has a significant positive impact on communication performance. However, it converges to resemble wired communication as  $d_x$  goes to 0, in contrast with the purpose of MC applications.

### 2.3.2. Analysis of Varying UCA Radius

On the Rx plane, the radius of the circular array on which the Rxes are placed is represented as  $r_{\text{UCA}}$ , where  $r_{\text{UCA}} = d_{yz} + r_r$ . The spatial parameter  $d_{yz}$  directly governs

the separation between spherical Rxs of radius  $r_r$ , where they are placed uniformly on the circular array. The center-to-center angular displacement between two neighboring antennas then becomes  $\frac{2\pi}{n_{\text{TRx}}}$ . As stated in Chapter 2.1, the angular displacement among Rxs is given as (2.14).

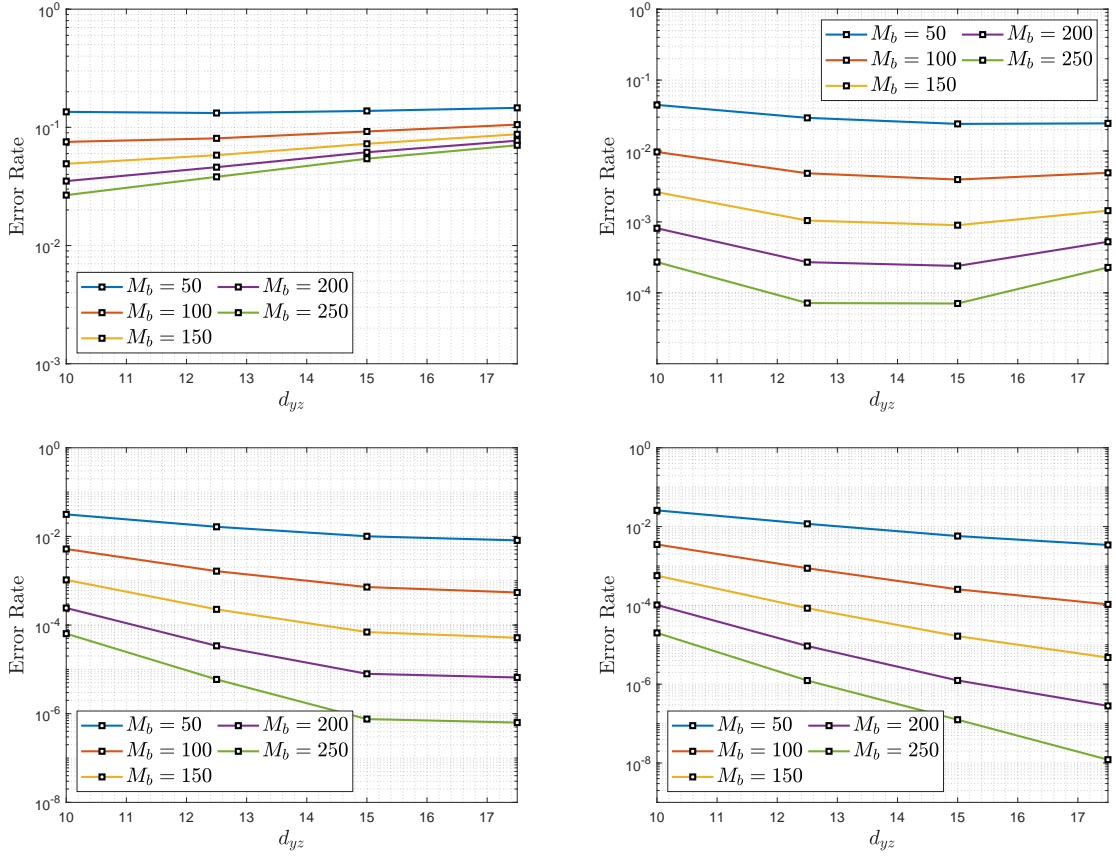


Figure 2.19. The graphs of ER versus  $d_{yz}$  of MSSK in molecular MIMO system with  $n_{\text{TRx}} = 8$ , for  $t_b = 0.15$  s on the upper left,  $t_b = 0.25$  s on the upper right,  $t_b = 0.32$  s on the lower left,  $t_b = 0.40$  s on the lower right.

Increasing  $d_{yz}$  helps Rxs to be placed more distant from each other, thus the ILI is expected to decrease. However, other Rx antennas absorb some portion of MMs released each symbol duration which helps the intended antenna to be protected from ISI due to those reduced free-roaming MMs [11]. Therefore, ILI from other antennas actually helps to reduce ISI for the upcoming symbol durations, by reducing the number

of MMs that roam freely in the medium [11]. This effect appears in shorter bit durations in particular, since shorter bit durations unintentionally increase the power of ISI. Then, as  $t_b$  increases, this phenomenon loses its significance, and increasing  $d_{yz}$  helps to improve the communication performance in terms of error rates. Although the CSI profiles look similar, one significant observation can be made: ISI terms reduce more power with increasing  $t_b$  for higher  $d_{yz}$  values, hence the improvement in the natural limit of communication performance for longer bit durations.

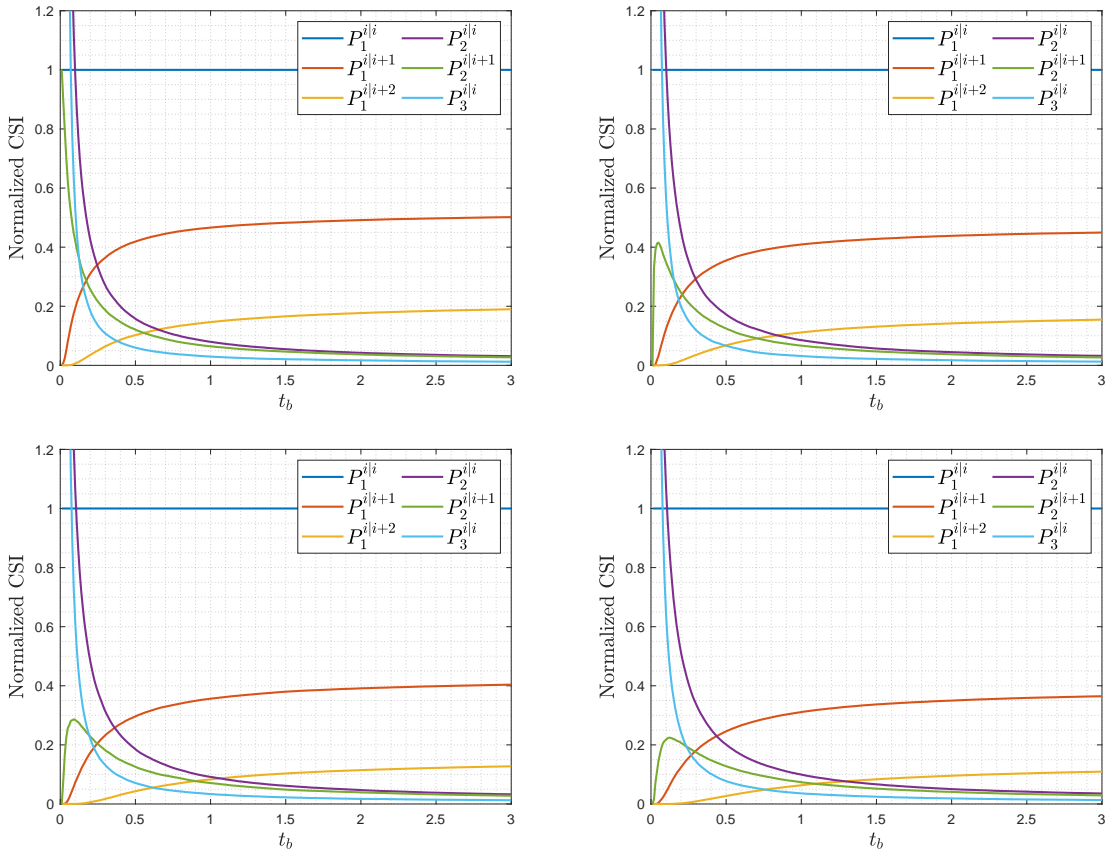


Figure 2.20. The graphs of the magnitude of several channel taps versus  $t_b$  of molecular MIMO system with  $n_{\text{TRX}} = 8$ , for  $d_{yz} = 10 \mu\text{m}$  on the upper left,  $d_{yz} = 12.5 \mu\text{m}$  on the upper right,  $d_{yz} = 15 \mu\text{m}$  on the lower left,  $d_{yz} = 17.5 \mu\text{m}$  on the lower right, normalized with respect to the signal tap.

### 3. MOLECULAR MIMO MODULATION ANALYSIS

In molecular SISO systems, ISI has a strong effect on the performance of communication, due to the MMs roaming freely in the diffusive channel. The interference is even stronger in molecular MIMO systems, due to the multiple antennas.

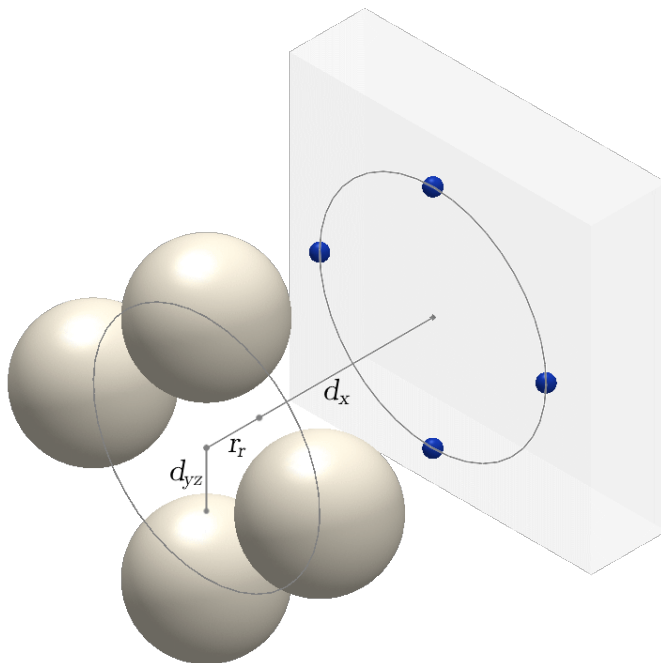


Figure 3.1. A molecular MIMO system with  $n_{\text{TRx}} = 4$ .

There are modulation schemes that utilize multiple antennas at once [11], such as spatial multiplexing (SMUX). In this scheme, the information is divided into the number of Tx-Rx pairs, and each pair communicates as molecular BCSK. The channel is used by each pair every symbol duration, therefore the number of MMs free-roaming increases dramatically, hence the increase in ISI. In order to mitigate the immense effects of ISI, IM-based modulation schemes have been proposed [11] for molecular MIMO systems.

### 3.1. Molecular Space Shift Keying

The inspiration of this scheme, the study [30] proposes to convey the information with the selection of the Tx antenna for the considered symbol duration of the communication. The information packages are carried by the index of the antenna. A similar approach in the MC realm, MSSK, is proposed in [11]. As mentioned, molecular MIMO systems with the same number of antennas are examined throughout the thesis. The Tx and Rx antennas are placed on a UCA. That way, each Tx and Rx pair are aligned with each other, and the Tx plane and the Rx plane are parallel, as shown in Figure 1.4.

For a molecular MIMO system whose number of Tx and Rx antennas  $n_{\text{Tx}}$  and  $n_{\text{Rx}}$  are the same, there are  $n_{\text{TRx}}$  potential single antenna selections. Each antenna is to a symbol, indicating that each antenna carries  $\log_2 n_{\text{TRx}}$ -bit long packages. The signal is an impulsive MM release into the channel, and the MMs propagate through the Rxs. Each Rx absorbs the MMs arriving at them during a symbol duration. The signal is demodulated via MCD, by detecting the Rx antenna with the highest number of MMs absorbed by the end of each symbol duration. The index of the detected Rx antenna is to be the detected bit package [11].

ISI and ILI are severe problems in communications in general, even more in the MC realm due to high-tailed CIR. Using the channel multiple times per symbol duration increases the interference which worsens the communication performance. Therefore, using the channel once per symbol duration, helps the channel remain relatively cleaner compared to other modulation schemes that use the channel more than once, such as SMUX [11]. Thus, the ISI and ILI are decreased along with the increase in communication performance.

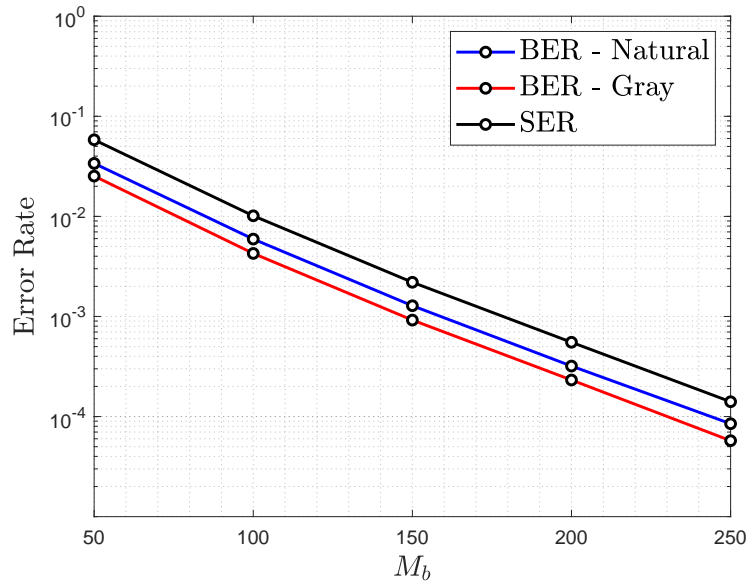


Figure 3.2. The graph of ER versus  $M_b$  of MSSK in molecular MIMO system with  $n_{\text{TRx}} = 8$ ,  $d_x = 10 \mu\text{m}$ ,  $d_{yz} = 10 \mu\text{m}$ ,  $t_b = 0.30 \text{ s}$ .

### 3.2. Generalized Molecular Space Shift Keying

The MSSK modulation scheme utilizes one single antenna per symbol, enabling transmission of  $\log_2 n_{\text{TRx}}$ -bit long packages. Although the channel remains relatively cleaner due to the single use of the channel, the throughput can be increased by utilizing more than one antenna per symbol. The generalized version of SSK modulation, GSSK, is proposed in [31]. The idea behind is to utilize the selection of more than one antenna to increase the throughput per symbol, at a cost of increased ILI. The trade-off between the increase in throughput and the increase in ILI is subject to communication preferences. For a similar molecular MIMO system with  $n_{\text{TRx}}$  antennas placed on a UCA, we can utilize  $k$  antennas per symbol,  $k$  ranging from 1 to  $n_{\text{TRx}}$  for MGSSK. The possible combinations of  $k$  antennas out of  $n_{\text{TRx}}$  is set  $S$ , and the size of  $S$  is

$$|S| = \binom{n_{\text{TRx}}}{k} = \frac{n_{\text{TRx}}!}{k!(n_{\text{TRx}} - k)!}. \quad (3.1)$$

The length of the bit packages needs to be integer, therefore the length is

$$\lfloor \log_2 |S| \rfloor = \left\lfloor \log_2 \left| \frac{n_{\text{TRx}}!}{k! (n_{\text{TRx}} - k)!} \right| \right\rfloor. \quad (3.2)$$

This directly indicates that if the size of set  $S$  is not a power of 2, there are symbols left out of communication. For instance, for a molecular MIMO system with  $n_{\text{TRx}} = 8$  antennas, the possible number of combinations of  $k = 2$  antennas is  $\frac{8!}{2! 6!} = 28$ . The length of the bit packages then becomes  $\lfloor \log_2 28 \rfloor = 4$ , which indicates that only  $2^4 = 16$  symbols are used, and 12 symbols are left out of communication.

### 3.2.1. Antenna Selection Strategy

In this case, the analysis and examination are conducted on molecular MIMO systems with 8 antennas placed on a UCA. The number of antennas to be activated per symbol is  $k = 2$ . Therefore, the number of potential antenna combinations is 28, as calculated above. As expected, there are 16 pairs that will be used in communication out of these 28 possibilities. The selection of the best 16 pairs is an optimization problem. Although the selection of the optimum 16 pairs by considering the effects of all the interference is a huge computational problem, there are several strategies to select a suboptimal set of pairs, based on controlling the ILI caused by the antennas:

**Remark.** *Interference of the selected antenna pairs is not preferable to strengthen the signals of the unintended antennas.*

For a molecular MIMO system with Rx's placed on a UCA, the neighboring Rx antennas receive the highest number of MMs of ILI caused by a Tx. The selection of an antenna causes the neighboring antennas to be influenced by ILI the most. For antenna pairs with a mutual neighbor antenna –the pairs with a single antenna gap–, the antennas both feed the common neighbor Rx antenna with ILI, inducing an unintended Rx antenna to be strengthened. There are 8 different antenna pairs, and such pairs are not preferable due to the increased ILI which worsens the communication performance, therefore they are to be eliminated from the selected pairs set.

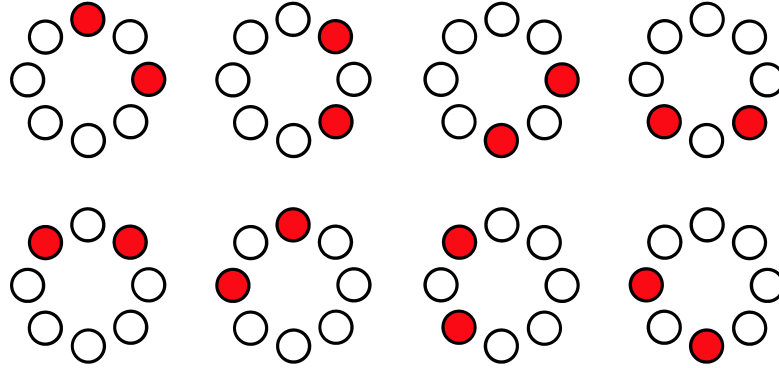


Figure 3.3. The undesirable antenna pairs for MGSSK with  $k = 2$  on molecular MIMO with 8 antennas, due to increased ILI on unintended neighbor antennas.

**Remark.** *Interference of the selected antenna pairs is preferable to strengthen the signals one another.*

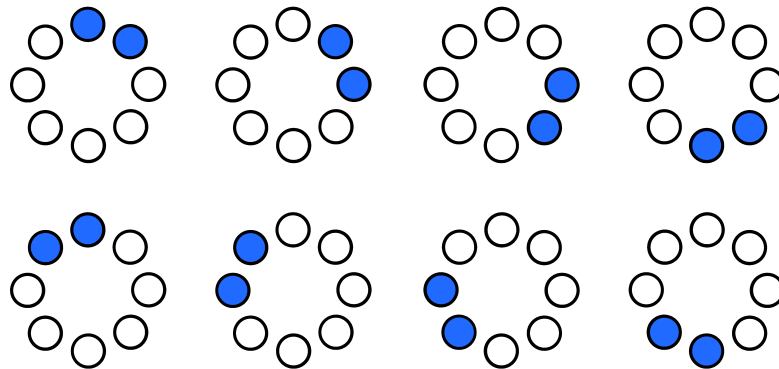


Figure 3.4. The preferable antenna pairs for MGSSK with  $k = 2$  on molecular MIMO with 8 antennas, due to positive-feeding ILI between the selected antennas.

The interference among neighbor antennas is the highest, since the neighbor Rx antennas have the shortest distance to the Tx antenna used among all unintended Rx antennas. This ILI can be controlled while selecting the antenna pairs. Neighboring antennas feed each other's signal strength with ILI, therefore ILI is used for good in

this selection principle. There are 8 different antenna pairs that strengthen each other's signal with controlled ILI. Due to the same principle, the antenna pairs that feed each other the least are also undesirable, since they do not benefit from the controlled ILI. The antennas with the highest distance on the plane of UCA affect each other lesser than any other antenna pair. There are 4 different antenna pairs to be eliminated that do not feed each other's signals.

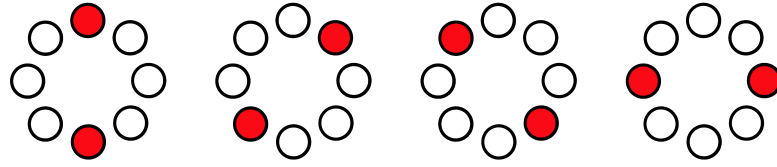


Figure 3.5. The undesirable antenna pairs for MGSSK with  $k = 2$  on molecular MIMO with 8 antennas, due to non-feeding ILI between the selected antennas.

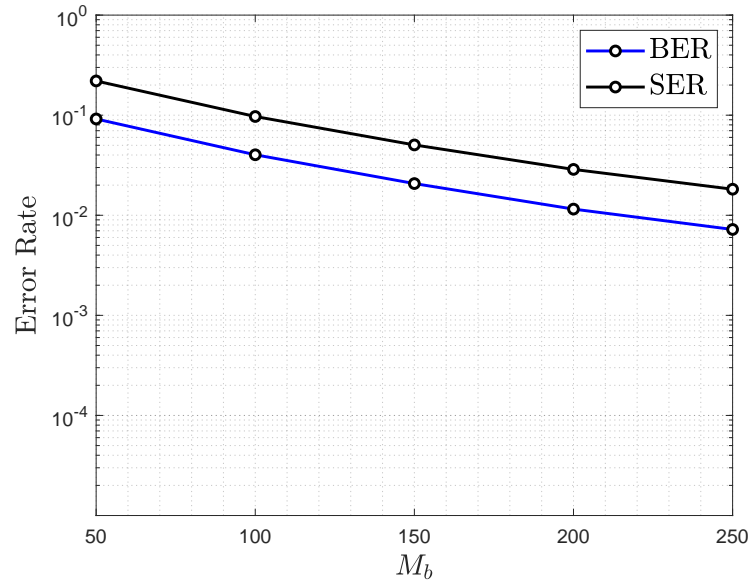


Figure 3.6. The graph of ER versus  $M_b$  of MGSSK in molecular MIMO system with  $n_{\text{TRx}} = 8$ ,  $k = 2$ ,  $d_x = 10 \mu\text{m}$ ,  $d_{yz} = 10 \mu\text{m}$ ,  $t_b = 0.30 \text{ s}$ .

The signal is demodulated via MCD, by detecting the Rx antennas with the two highest numbers of MMs absorbed by the end of each symbol duration. The detected Rx antennas are used to de-map the antenna pairs to the bit package to be transmitted. Even though the ILI caused by the antennas used is increased, the throughput per symbol is increased by the size of the symbol set.

### 3.3. Interference-Mitigating Methods

#### 3.3.1. Constant-Weight Code-Based Iterative Sorting Decoding in Molecular MIMO Systems

Constant-weight codes are codes with codewords of the same weight [38, 39]. There are several studies of various applications of CWC in the literature [35, 38–41]. In general, a CWC  $\mathcal{C}(n, k, m)$  is a code [35] such that

$$\mathbf{u} \in U = \{0, 1\}^k, \quad \mathbf{u} \xrightarrow{\text{CWC}(n, k, m)} \mathbf{v}, \quad \sum_{i=1}^n v_i = m, \quad (3.3)$$

where  $v_i$  is the  $i$ th bit of the codeword  $\mathbf{v}$  of length  $n$ . The importance of CWC is that, for IM-based modulation schemes for molecular MIMO systems, MSSK and MGSSK in particular, each symbol duration the antenna activation array whose elements are bit–1 for active antennas and bit–0 for inactive antennas can be regarded as a CWC of  $(n_{\text{TRx}}, \lfloor \log_2 |S| \rfloor, k)$ , where  $|S|$  is the size of the symbol set, and  $k$  is the number of active antennas per symbol. From (3.1), the size of the symbol set is obtained for MGSSK, and evidently for MSSK.

The decoding of the signals received by all the Rxs is done by MCD, in its simplest form. However, interference of the previous symbols influences the signal of the current symbol duration. In particular, ILI affects severely the other Rx antennas for a symbol duration, therefore smarter decoding designs are developed to increase the communication performance by considering the effects of interference. For molecular SISO systems, [35] suggests the iterative sorting decoder, which basically estimates and

subtracts the ISI iteratively.

In this study [35], the information is encoded in packages of length  $n$ . Each package is a codeword of weight  $m$ . That indicates that for each  $n$ -symbol package, only  $m$  symbol is bit-1. The codewords are formed by the symbols in the time domain. Each package is decoded by ISD, iteratively. At the start of the iterations, ISD detects the time indices of the highest  $m$  number of MMs with MCD to obtain an estimated bit package,  $\hat{\mathbf{v}}$ , tentatively. Then, it estimates the ISI on the MM absorption array of the package,  $\mathbf{y}$ , and subtracts it from  $\mathbf{y}$ , provided the CSI is known. Subsequently, the ISI-subtracted MM array  $\mathbf{y} - \text{ISI}$  is then used to detect the new estimated bit package,  $\hat{\mathbf{v}}'$ , again. Between two consecutive iterations, in case  $\hat{\mathbf{v}}$  and  $\hat{\mathbf{v}}'$  are not equal, and the estimation gets closer to  $\mathbf{y}$  in terms of distance, ISD continues to the next iteration, based on the estimated ISI from the last estimated bit package  $\hat{\mathbf{v}}'$  [35]. The distance is proposed in [35] as

$$\text{distance}(\mathbf{y}, \mathbf{v}) = \sum_{i=1}^n \frac{(y_i - \mu_{v_i})^2}{\sigma_{v_i}^2} + 2 \ln(\sigma_{v_i}). \quad (3.4)$$

In case  $\hat{\mathbf{v}}$  and  $\hat{\mathbf{v}}'$  are equal, the convergence is said to be occurred, and the package is decoded as  $\hat{\mathbf{v}}$ .

3.3.1.1. MSSK with Iterative Sorting Decoder. As explained above, the activated antennas of the symbols are modulated by IM-based modulations schemes such as MSSK and MGSSK in molecular MIMO systems. The analogous of the bit packages in the time domain of molecular SISO systems is the activated antenna arrays per symbol in molecular MIMO systems. The array is regarded as a CWC codeword of weight 1 to be decoded by ISD.

```

Input:  $\mathbf{y}$ ,  $m$ , CSI, maxIter
Output:  $\hat{\mathbf{v}}$ 
Initialize  $\hat{\mathbf{y}} \leftarrow \mathbf{y}$ 
Initialize  $\hat{\mathbf{v}} \leftarrow \text{MCD}(\hat{\mathbf{y}}, m)$ 
for  $i = 1$  to maxIter do
     $\hat{\mathbf{v}}' \leftarrow \text{MCD}(\hat{\mathbf{y}}, m)$ 
     $d' \leftarrow \text{distance}(\mathbf{y}, \hat{\mathbf{v}}')$ 
    if  $i == 1$  or  $(\hat{\mathbf{v}}' \neq \hat{\mathbf{v}} \text{ and } d' < d)$  then
        ISI  $\leftarrow \text{calculateISI}(\hat{\mathbf{v}}, \text{CSI})$ 
         $\hat{\mathbf{y}} \leftarrow \mathbf{y} - \text{ISI}$ 
         $d \leftarrow d'$ 
         $\hat{\mathbf{v}} \leftarrow \hat{\mathbf{v}}'$ 
    else
        break
    end if
end for
return  $\hat{\mathbf{v}}$ 

```

Figure 3.7. Iterative Sorting Decoding Algorithm.

The algorithm is similar for the MSSK case. An activated antenna array  $\hat{\mathbf{v}}$  is estimated to be compared with the estimation of the next iteration. Instead of ISI, ILI is estimated based on the estimated antenna array  $\hat{\mathbf{v}}$  of weight 1, and is subtracted from the MM absorption array of antennas,  $\mathbf{y}$ . The ILI-subtracted signal is then used to estimate the next iteration's activated antenna array,  $\hat{\mathbf{v}}'$ . In case the estimations of two consecutive iterations are not equal and the estimation gets closer to  $\mathbf{y}$  in terms of the distance shown in (3.4). In case the estimations of two consecutive iterations are equal, the convergence is said to have occurred, and the antenna used for transmission is detected from the activated antenna array. Following the detection of the antenna iteratively, the information bit package is decoded from the index of the antenna used.

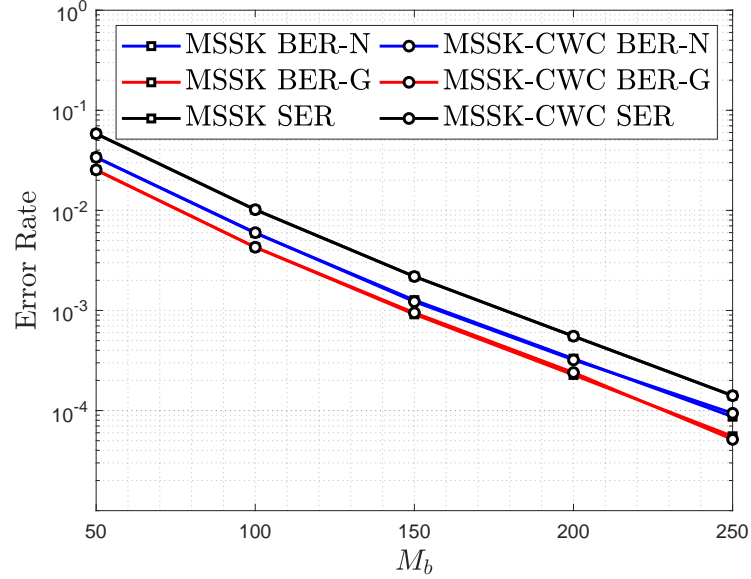


Figure 3.8. The graph of ER versus  $M_b$  of MSSK with ISD in molecular MIMO system with  $n_{\text{TRx}} = 8$ ,  $d_x = 10 \mu\text{m}$ ,  $d_{yz} = 10 \mu\text{m}$ ,  $t_b = 0.30 \text{ s}$ .

3.3.1.2. MGSSK with Iterative Sorting Decoder. Similar to the MSSK case, the activated antenna array is regarded as a CWC codeword of weight  $k$  to be decoded by ISD for the MGSSK case. ISD iteratively estimates the activated antenna array of weight  $k$ , by subtracting the estimated ILI based on the previous estimation of active antennas. Detected active antennas are used to de-map the information bit package to be transmitted.

Interference in MGSSK modulation, ILI in particular, is stronger than the one in MSSK, since the channel is used by not 1 but  $k$  antennas per symbol. For these IM-based modulation schemes for molecular MIMO systems, the ISD decodes the information bits in a smarter way by taking ILI into account. MSSK uses the channel once per symbol, and by its nature, it combats the ILI significantly even without a smart decoder design. The increase in communication performance of MGSSK is then evidently higher than the one of MSSK.

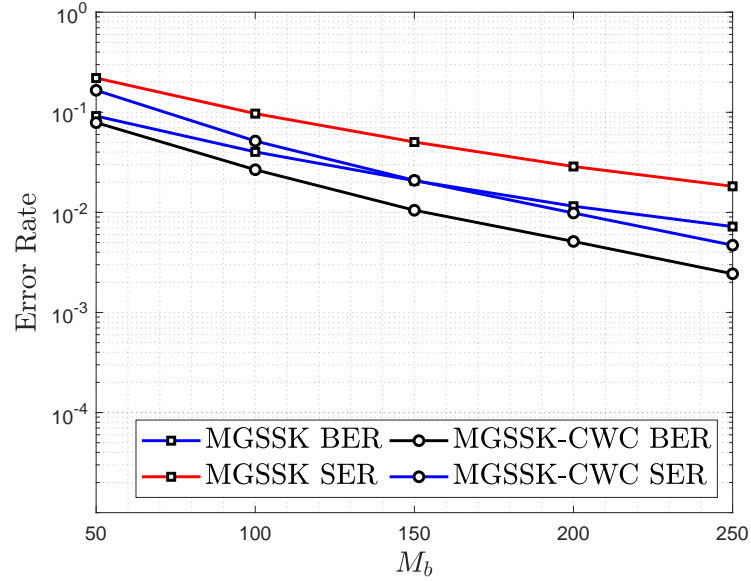


Figure 3.9. The graph of ER versus  $M_b$  of MGSSK with ISD in molecular MIMO system with  $n_{\text{TRx}} = 8$ ,  $k = 2$ ,  $d_x = 10 \mu\text{m}$ ,  $d_{yz} = 10 \mu\text{m}$ ,  $t_b = 0.30 \text{ s}$ .

### 3.3.2. Beamforming in Molecular MIMO Systems

Beamforming is a common signal processing technique that utilizes an antenna array to form a beam or directional signal in such a way that particular directions experience constructive interference while others experience destructive interference [42]. Like many of the MIMO communication systems, the molecular MIMO systems suffer from interference. For IM-based modulations for molecular MIMO systems, signals are impulsive MM releases at the Tx side, however, MMs propagate in the diffusive channel and can be absorbed by all RxS, which forms a non-impulsive signal at the Rx side. ILI in molecular MIMO systems is the result of the Brownian motion of the MMs in particular.

**3.3.2.1. Beamforming via Signal-to-Interference Ratio.** In the literature, several studies achieve beamforming [43], or equivalently, equalization [34, 37] in the MC realm. Especially [34] proposes a pre-equalization method in molecular SISO systems that

utilizes two different MM types that cancel each other at the Rx side in such a way that impulses of these MMs form an impulse as CIR. One type of the MMs carries the message signal, and the other type carries the poison signal which cancels the message signal at the Rx side. Tx releases a certain amount of poison signal with a certain amount of delay  $\tau$  in time to mitigate the ISI in the time domain for the upcoming symbols. The amount of the poison signal and the delay is an optimization problem, which is optimized with a signal-to-interference ratio (SIR) metric [34,44]. Let type-A is the MM type of the message signal, and type-B is the MM type of the poison signal. As shown in (1.8), the channel taps of the message signal and the poison signal are

$$P_k^A = P_{\text{Rx}}^{\text{SISO}}(kt_s | r_0, r_r) - P_{\text{Rx}}^{\text{SISO}}([k-1]t_s | r_0, r_r), \quad k \in \{1, \dots, L\}, \quad (3.5)$$

$$P_k^B = P_{\text{Rx}}^{\text{SISO}}(kt_s - \tau | r_0, r_r) - P_{\text{Rx}}^{\text{SISO}}([k-1]t_s - \tau | r_0, r_r), \quad k \in \{1, \dots, L\}. \quad (3.6)$$

Due to power consumption concerns, a total of  $M$  MMs are released per symbol. An  $\alpha$  portion of  $M$  is the type-A for the message, and  $1 - \alpha$  portion of  $M$  is the type-B for the poison [34]. The receiver counts both types of MMs each symbol duration, and subtracts the number of type-B MMs from the number of type-A MMs. The average signal power and the interference from both message and poison signals then become

$$S = \alpha MP_1^A - (1 - \alpha)MP_1^B, \quad (3.7)$$

$$I = \sum_{i=2}^L |\alpha MP_i^A - (1 - \alpha)MP_i^B|. \quad (3.8)$$

Therefore, the SIR [34] becomes

$$\text{SIR} = \frac{\alpha MP_1^A - (1 - \alpha)MP_1^B}{\sum_{i=2}^L |\alpha MP_i^A - (1 - \alpha)MP_i^B|}, \quad (3.9)$$

$$= \frac{\alpha(P_1^A + P_1^B) - P_1^B}{\sum_{i=2}^L |\alpha(P_i^A + P_i^B) - P_i^B|}. \quad (3.10)$$

The selection of  $\alpha$  and  $\tau$  is an optimization problem that needs to be optimized numerically [34] for the large number of  $L$  values.

This pre-equalization method can be adapted into molecular MIMO systems, in which the IM-based modulation schemes utilize the indices of antennas. The solution proposed for ISI in the time domain [34] is adjusted to solve ILI in the space domain with a similar approach. However, unlike the proposed method in molecular SISO where the poison is released with a delay in time, we need to release the poison with a *shift in space*, which means another Tx antenna. For the molecular MIMO topology we are interested in, the antennas are placed on a UCA. Then, due to rotational symmetry around the center of UCA, a rotationally-symmetric ILI around the antenna used is observed. Thus, the poison signal needs to be co-released symmetrically to the message antenna, from antennas with the same amount of shift in both rotational directions to cancel out the rotational components.

The notation of the CSI of molecular MIMO systems is mentioned above. The absorption probability of MMs by Rxs depends on the Tx antenna used. The channel taps are calculated by (2.32). The channel tap at the intended antenna,  $P_k^{i|i}$  is generally the strongest, depending on the symbol duration. The channel taps at the nearest neighbor antennas,  $P_k^{i|i-1}$  and  $P_k^{i|i+1}$ , are the strongest ILI taps among others. Therefore, it is reasonable to release the poison signals from the nearest neighbor antennas to mitigate the ILI at those antennas, since it reduces the power allocation for the poison signal which helps to keep the message signal power as high as possible. Due to the symmetry, the amount of poison MMs to be released from both neighbors needs to be equal. In an adaption of the pre-equalization method into molecular MIMO systems, the message signal power and the interference, ILI in particular, can be written as

$$S = \alpha M P_1^{i|i} - \frac{1-\alpha}{2} M \left( P_1^{i|i-1} + P_1^{i|i+1} \right), \quad (3.11)$$

$$I = \sum_{\substack{j=1 \\ j \neq i}}^{n_{\text{TRx}}} \left| \alpha M P_1^{j|i} - \frac{1-\alpha}{2} M \left( P_1^{j|i-1} + P_1^{j|i+1} \right) \right|. \quad (3.12)$$

Therefore, the SIR becomes

$$\text{SIR} = \frac{\alpha M P_1^{i|i} - \frac{1-\alpha}{2} M (P_1^{i|i-1} + P_1^{i|i+1})}{\sum_{\substack{j=1 \\ j \neq i}}^{n_{\text{TRx}}} \left| \alpha M P_1^{j|i} - \frac{1-\alpha}{2} M (P_1^{j|i-1} + P_1^{j|i+1}) \right|}, \quad (3.13)$$

$$= \frac{\alpha (2P_1^{i|i} + (P_1^{i|i-1} + P_1^{i|i+1})) - (P_1^{i|i-1} + P_1^{i|i+1})}{\sum_{\substack{j=1 \\ j \neq i}}^{n_{\text{TRx}}} \left| \alpha (2P_1^{j|i} + (P_1^{j|i-1} + P_1^{j|i+1})) - (P_1^{j|i-1} + P_1^{j|i+1}) \right|}. \quad (3.14)$$

The optimization needs to be done numerically, therefore an optimum  $\alpha$  value to maximize SIR is calculated by computer-based calculations.

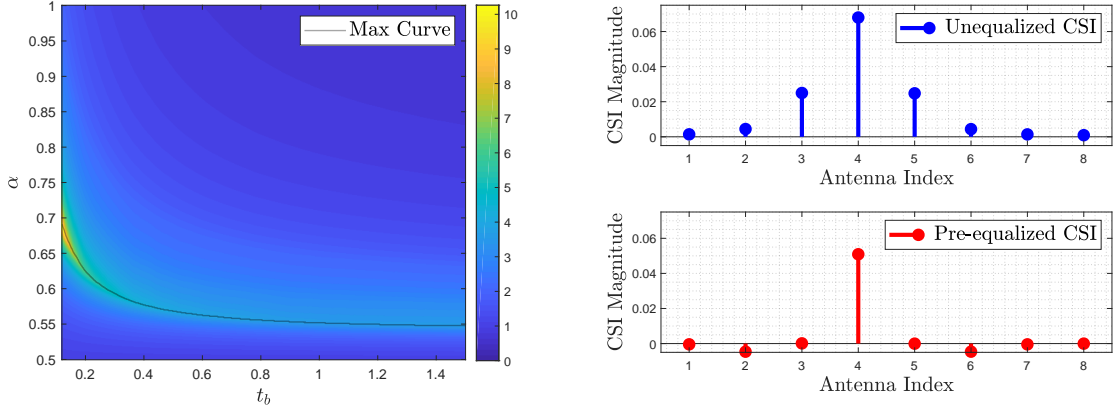


Figure 3.10. The heatmap of SIR with respect to  $t_b$  and  $\alpha$  on the left, the CSI of molecular MIMO system with  $n_{\text{TRx}} = 8$ ,  $t_b = 0.30$  s, and  $\alpha = 0.593$ , before and after pre-equalization on the right.

As we can see, the SIR metric does not work well enough in molecular MIMO systems, since it aims to maximize the ratio, whereas the magnitudes of message signal power would drop due to the poison signal. As shown in Figure 3.10, the SIR-maximizing  $\alpha$  values are shown. While these values maximize SIR, they do not have enough message signal power, which directly impacts the communication performance, as shown in Figure 3.11. Therefore, another metric used in molecular SISO applica-

tions, namely the signal-interference difference (SID), is presented in [45].

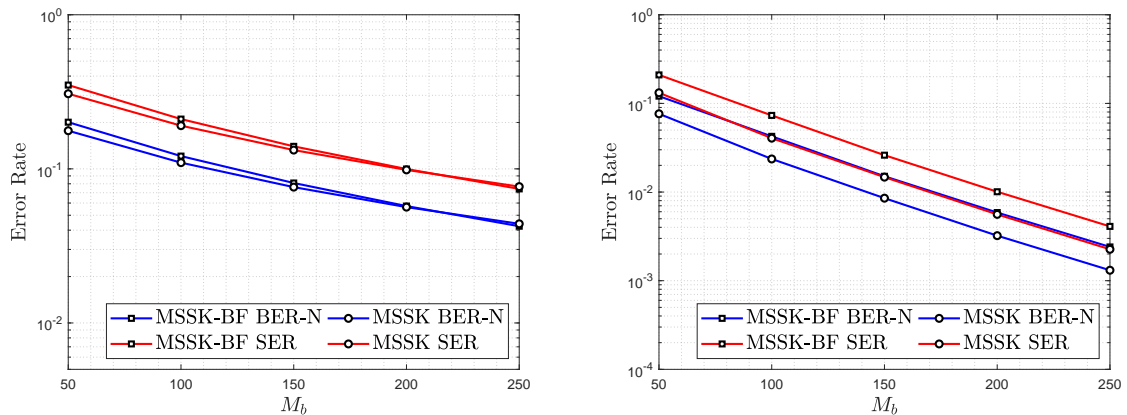


Figure 3.11. The graphs of ER versus  $M_b$  of MSSK with Beamforming via SIR in molecular MIMO system with  $n_{\text{TRx}} = 8$ ,  $d_x = 10 \mu\text{m}$ ,  $d_{yz} = 10 \mu\text{m}$ ,  $t_b = 0.15 \text{ s}$ ,  $\alpha = 0.593$  on the left,  $t_b = 0.30 \text{ s}$ ,  $\alpha = 0.659$  on the right.

3.3.2.2. Beamforming via Signal-Interference Difference. For many practical applications, the beamforming via SIR has several problems. First of all, the poison signal allocation reduces the message signal power, by being subtracted from the number of MMs belonging to the message signal at the Rx side. Furthermore, the arrival of MMs belonging to the poison signal again generates a random variable, which can be modeled as a Gaussian random variable [20]. Then, the addition –or subtraction– of two random variables generates a new random variable with higher variance, the sum of the variances of both message and poison signal in the Gaussian case. Therefore, although the expected value of the resultant signal at the Rx side converges to an interference-free beam, the variance is higher, and the communication performance suffers from the higher variance. In the light of these observations, the SID defined in [45] is utilized in a similar fashion to the beamforming via SIR. SID aims to maximize the power difference, rather than the ratio between the message signal and the interference. That way it helps to maintain the signal power considerably, compared to the beamforming via the SIR case.

The CSI of a molecular MIMO system is again represented as  $P_k^{i|j}$ , as defined in (2.32). Since the topology again requires the symmetrical release of the poison signal, the nearest neighboring antennas are used to deploy the poison signal MMs. Again, the message signal power and the interference are stated as

$$S = \alpha M P_1^{i|i} - \frac{1-\alpha}{2} M \left( P_1^{i|i-1} + P_1^{i|i+1} \right), \quad (3.15)$$

$$I = \sum_{\substack{j=1 \\ j \neq i}}^{n_{\text{TRx}}} \left| \alpha M P_1^{j|i} - \frac{1-\alpha}{2} M \left( P_1^{j|i-1} + P_1^{j|i+1} \right) \right|. \quad (3.16)$$

$M$  is a constant and to be canceled out from both terms. Therefore, the SID becomes

$$\text{SID} = \alpha P_1^{i|i} - \frac{1-\alpha}{2} M \left( P_1^{i|i-1} + P_1^{i|i+1} \right) - \sum_{\substack{j=1 \\ j \neq i}}^{n_{\text{TRx}}} \left| \alpha P_1^{j|i} - \frac{1-\alpha}{2} \left( P_1^{j|i-1} + P_1^{j|i+1} \right) \right|. \quad (3.17)$$

The optimum  $\alpha$  value that maximizes the SID needs to be numerically calculated via computer-based calculations.

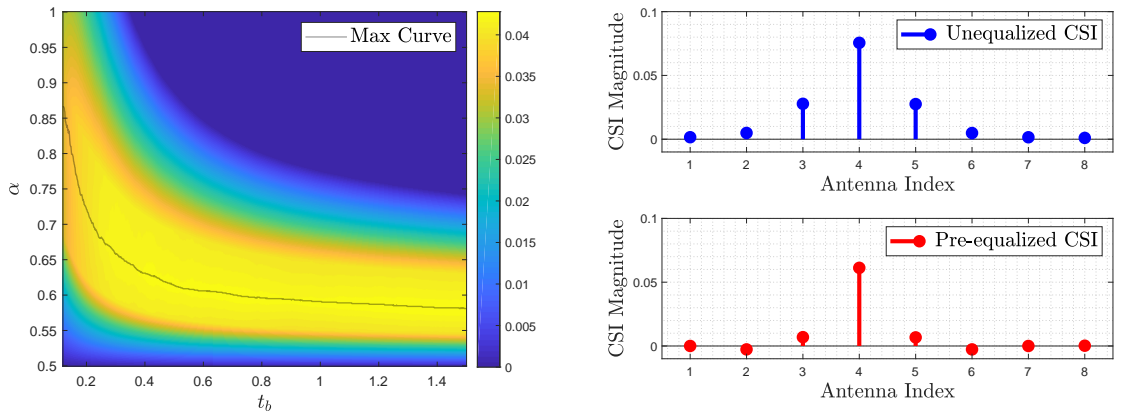


Figure 3.12. The heatmap of SID with respect to  $t_b$  and  $\alpha$  on the left, the CSI of molecular MIMO system with  $n_{\text{TRx}} = 8$ ,  $t_b = 0.30$  s, and  $\alpha = 0.659$ , before and after pre-equalization on the right.

As seen in Figure 3.12, the CSI of the molecular MIMO system is clarified from ILLI with the help of the poison signal. However, the magnitude of the channel tap of the signal after pre-equalization reduces, which impacts the communication performance. For the shorter bit durations  $t_b$ , interference dominates the signal, therefore the beamforming results in a slight performance increase for higher signal power in short bit durations. However, as the bit durations increase, the signal power overcomes the interference, which decreases the impact of the beamforming. In this case, the reduction in the signal power, as shown in 3.13, hinders the communication performance slightly.

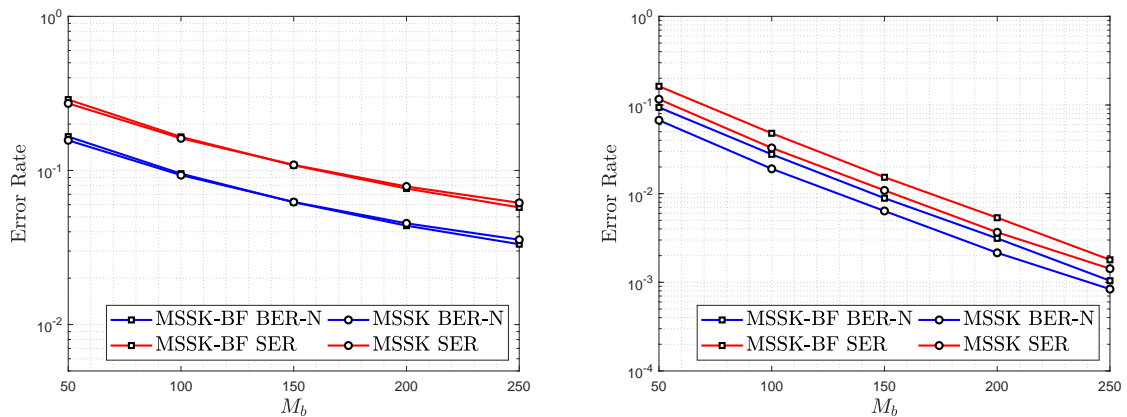


Figure 3.13. The graphs of ER versus  $M_b$  of MSSK with Beamforming via SID in molecular MIMO system with  $n_{\text{TRX}} = 8$ ,  $d_x = 10 \mu\text{m}$ ,  $d_{yz} = 10 \mu\text{m}$ ,  $t_b = 0.15$  s,  $\alpha = 0.659$  on the left,  $t_b = 0.30$  s,  $\alpha = 0.799$  on the right.

## 4. CHANNEL MODELING FOR MOLECULAR SIMO SYSTEMS

In recent years, the MC realm extended its reach beyond the molecular SISO systems to enable the development of higher-complexity systems. Many molecular multiple-entity systems, such as molecular MIMO systems [11, 36, 37] and molecular multiple-input single-output (MISO) systems [19] are being developed. However, there is a significant setback in the development of such sophisticated systems and modulations, which is the lack of proper analytical foundations in the molecular multiple-receiver domain. In fact, the molecular systems consisting of fully-permeable receivers are not affected by this adversity, since they are modeled not to interact with MMs which indicates that they do not interfere with each other. Therefore basic molecular SISO analytics apply to such systems. However, the need to design realistic molecular systems demands molecular systems with fully-absorbing receivers, which interact with MMs, and interfere with each other. Due to this statistical dependence, the molecular SISO analytics such as (1.4) and (1.5) cannot be applied in this domain. Therefore, a new channel modeling is required.

The molecular SIMO system in consideration is the simplest version of molecular SIMO systems with  $n_{\text{Rx}} = 2$ . The Rxs are spherical fully-absorbing Rxs of arbitrary radii placed in arbitrary center points in 3D space. The Tx is modeled as a point Tx, similar to the previous systems. As shown in Figure 4.1, the radius of  $\text{Rx}_i$  is  $r_i$ . The spatial parameter definitions are the same, as the center-to-center distance between the Tx and  $\text{Rx}_i$  is  $r_{0_i}$ . MMs are absorbed more by the front side of an Rx facing Tx [45]. Since the distribution of MMs on the surface of an Rx is not uniform, so the center of mass of the MMs absorbed is not the center of the spherical Rx. The point of the center of mass is a significant spatial point to be used in upcoming analyses, therefore we define a new spatial parameter,  $r_{0_{i|j}}$ , which is the distance between the center of mass of the MMs absorbed by  $\text{Rx}_j$  and the center of  $\text{Rx}_i$ .

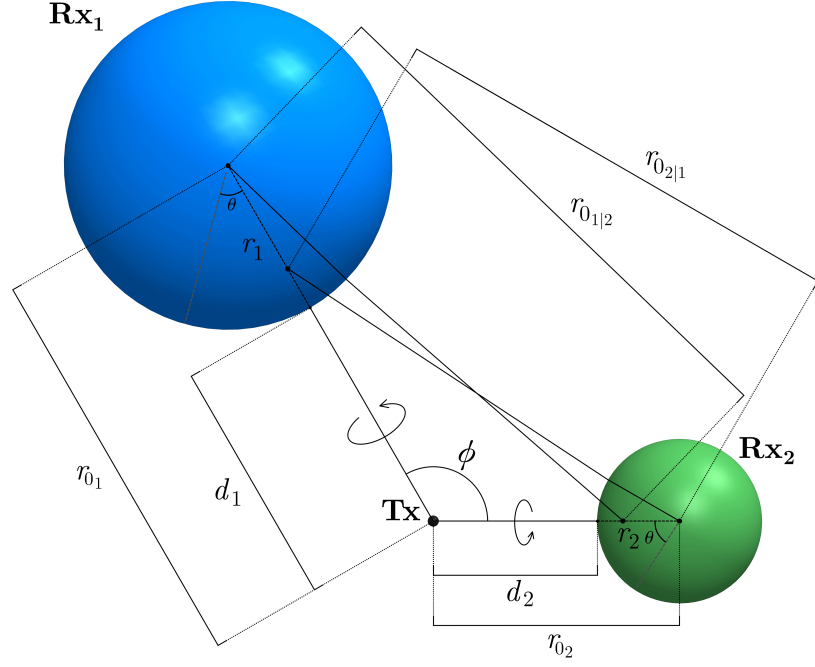


Figure 4.1. An illustration of a molecular SIMO system with 2 receivers.

#### 4.1. Recursive Model

The molecular SISO channel model analytically estimates the CIR of a molecular SISO system with an absorbing receiver [22]. However, when there are other absorbing receivers, the statistical dependence among the absorbing receivers violates the applicability of the molecular SISO channel model. The existence of another Rx reduces the number of MMs absorbed by a regarded Rx, which can be interrupted as Rxs compete for MMs with each other, and steal MMs from each other. This phenomenon is reciprocal, as the  $Rx_i$  steals from the  $Rx_j$  and vice versa [22]. Therefore, estimating the CIR of Rxs only by the molecular SISO channel model results in overcounting.

The motion of MMs in a diffusive medium is Brownian motion, which is characterized as a continuous Wiener process [16]. The motion is modeled as step increments independent of each other [16]. Based on the independence of step increments, it can be said that the motion of an MM can be split into parts that are independent of each

other. To emphasize this, let us assume an MM that is released from an arbitrary point  $A_1$ , and arrives at another arbitrary point  $A_2$  in space. With the help of the independence of step increments, the succeeding movement of that MM can be modeled as if it was released from  $A_2$ , provided that the MM is released from  $A_1$  and arrived at  $A_2$  priorly.

#### 4.1.1. Absorption Rate Derivation for Molecular SIMO Systems

The regarded molecular SIMO topology can be represented as that in Figure 4.1, where  $Rx_i$  is the Rx antenna in consideration for deriving the channel model analytics in presence of  $Rx_j$ ,  $i$  and  $j$  being the indices of Rxs, which are interchangeable. The absorption rate of MMs by  $Rx_i$  in presence of  $Rx_j$  in a molecular SIMO system is represented as  $p_{Rx_i}^{\text{SIMO}}(t | Rx_j, r_{0_i}, r_i)$ , and the absorption probability of MMs by  $Rx_i$  in presence of  $Rx_j$  until time  $t$  in a molecular SIMO system is represented as  $P_{Rx_i}^{\text{SIMO}}(t | Rx_j, r_{0_i}, r_i)$  throughout the thesis.

**Proposition 4.1.** *The presence of  $Rx_j$  does not help  $Rx_i$  in terms of MM absorption.*

One simple result can be inferred from Proposition 4.1, regarding the absorption rate of MMs by  $Rx_i$ .

**Corollary 4.2.** *For the absorption rate of MMs by  $Rx_i$  in presence of  $Rx_j$  in a molecular SIMO system, the upper bound is the absorption rate of MMs by  $Rx_i$  as if it was in a molecular SISO system, without the presence of  $Rx_j$ .*

The formulation of Corollary 4.2 then becomes

$$p_{Rx_i}^{\text{SIMO}}(t | Rx_j, r_{0_i}, r_i) \leq p_{Rx_i}^{\text{SISO}}(t | r_{0_i}, r_i). \quad (4.1)$$

As referred above, the Rxs compete for MMs. Hypothetically, the Rxs can be placed in such a way that they steal as many MMs as possible. For example,  $Rx_j$  can steal the amount of all the MMs it absorbs in presence of  $Rx_i$ , from  $Rx_i$  at most, and vice

versa. The sum of the absorption rates of MMs by both Rxs can be bounded as

$$\begin{aligned} \max \left[ p_{\text{Rx}_i}^{\text{SISO}}(t | r_{0_i}, r_i), p_{\text{Rx}_j}^{\text{SISO}}(t | r_{0_j}, r_j) \right] \\ \leq p_{\text{Rx}_i}^{\text{SIMO}}(t | \text{Rx}_j, r_{0_i}, r_i) + p_{\text{Rx}_j}^{\text{SIMO}}(t | \text{Rx}_i, r_{0_j}, r_j) \\ \leq p_{\text{Rx}_i}^{\text{SISO}}(t | r_{0_i}, r_i) + p_{\text{Rx}_j}^{\text{SISO}}(t | r_{0_j}, r_j). \quad (4.2) \end{aligned}$$

It is observed that some portion of MMs released is absorbed by  $\text{Rx}_j$  when trying to derive the absorption rate of MMs by  $\text{Rx}_i$  [22]. Let us assume  $\text{Rx}_j$  be a fully-permeable transceiver that does not interact with MMs, in contrast to  $\text{Rx}_j$  being a fully-absorbing Rx in the system model. In this assumption, let us expand the assumption by assuming that  $\text{Rx}_j$  releases every MMs to arrive at its surface instantly from the contact point on the surface. In this case, MMs that are released from Tx and arrived at  $\text{Rx}_j$  are released again. The absorption rate of those MMs by  $\text{Rx}_i$  can be modeled such that those MMs are released from the surface of  $\text{Rx}_j$  and absorbed by  $\text{Rx}_i$ , as if  $\text{Rx}_j$  did not exist at all. For instance, the absorption rate of MMs that are arriving at the surface of  $\text{Rx}_j$  at time  $\tau$  by  $\text{Rx}_i$  can be calculated by the molecular SISO channel analytics stated in (1.4). It should be noticed that the MMs arriving at  $\text{Rx}_j$  at time  $\tau$  which is smaller than  $t$  are in consideration to calculate the absorption rate of MMs referred above.

In order to get a better understanding of the assumption above, it should be noticed that the absorption rate –arrival rate in this assumed case– of MMs arriving at the surface of  $\text{Rx}_j$  at time  $\tau$  is also influenced by the MMs arriving at  $\text{Rx}_i$  at times smaller than  $\tau$ , and so on. Therefore, to take this nested influence into account, the absorption –arrival in this assumed case– rates of MMs arriving at both Rxs needs to be calculated in a recursive fashion.

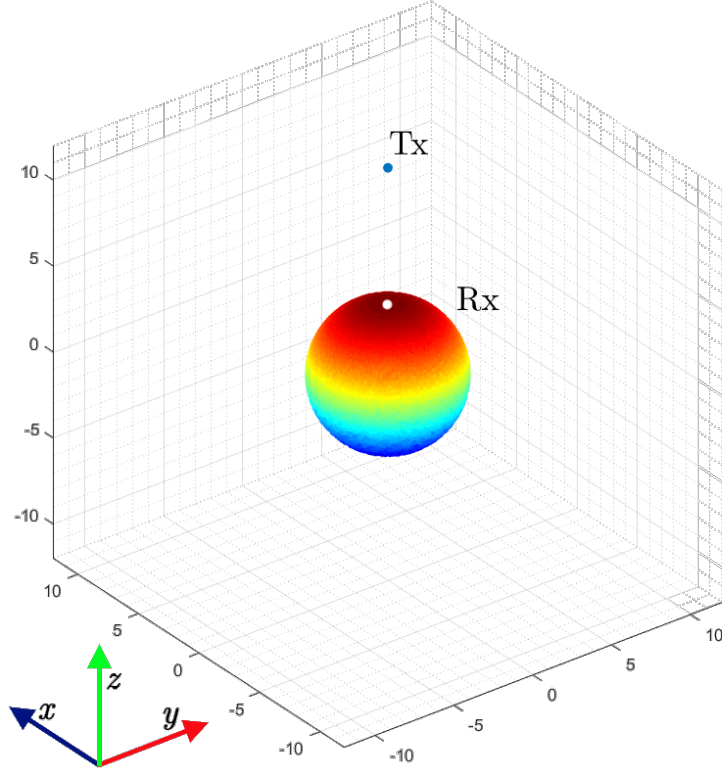


Figure 4.2. A heatmap of the distribution of MMs arriving at a receiver in a molecular SISO system, generated via computer-aided diffusion simulation. Tx is placed at  $(0, 0, 12 \mu\text{m})$  and center of Rx is placed in  $(0, 0, 0)$ .  $r_r = 4 \mu\text{m}$ ,  $M = 5 \times 10^4$ ,  $D = 79.4 \mu\text{m}^2/\text{s}$ , and  $\Delta t = 10^{-4}$  s. The closest point on Rx to Tx is shown.

In this assumed case, the MMs are said to be released again from the contact point on the surface of  $\text{Rx}_j$ . Then, the aggregate positions of all MMs arriving at  $\text{Rx}_j$  until time  $t$  gain prominence. In the molecular SISO case, MMs released from Tx are distributed on the surface of Rx nonuniformly [45]. Since the Tx-Rx pair is rotationally symmetrical around the center-to-center axis, the distribution of MMs arriving at the surface of Rx does only depend on polar angle  $\theta$ , as shown in Figure 4.1. The angular distribution of MMs on the surface of Rx is stated in [45] as

$$p_{\text{Rx}}^{\text{SISO}}(t, \theta | r_0, r_r) = \frac{\sin \theta \operatorname{erfc} \left( \frac{r_0^*}{\sqrt{4Dt}} \right) P_{\text{Rx}}^{\text{SISO}}(t | r_0, r_r)}{\left( 1 - \frac{2r_r}{r_0} \cos \theta + \frac{r_r^2}{r_0^2} \right)^{\frac{3}{2}} \int_0^\pi \frac{\sin \theta' \operatorname{erfc} \left( \frac{r_0^*}{\sqrt{4Dt}} \right)}{\left( 1 - 2\frac{2r_r}{r_0} \cos \theta' + \frac{r_r^2}{r_0^2} \right)^{\frac{3}{2}}} d\theta'}, \quad (4.3)$$

where

$$r_0^* = \sqrt{r_0^2 + r_r^2 - 2r_0r_r \cos \theta}. \quad (4.4)$$

As time goes to infinity, the angular distribution of MMs arriving at the surface of Rx in a molecular SISO system converges to saturation, and then becomes

$$p_{\text{Rx}}^{\text{SISO}}(\theta | r_0, r_r) = 2\pi r_r^2 \sin \theta \frac{\left(1 - \frac{r_r^2}{r_0^2}\right)}{4\pi r_r r_0 \left(1 - \frac{2r_r}{r_0} \cos \theta + \frac{r_r^2}{r_0^2}\right)^{3/2}}, \quad (4.5)$$

$$= \frac{r_r \sin \theta \left(1 - \frac{r_r^2}{r_0^2}\right)}{2r_0 \left(1 - \frac{2r_r}{r_0} \cos \theta + \frac{r_r^2}{r_0^2}\right)^{3/2}}. \quad (4.6)$$

To calculate the center of mass of MMs arriving at the surface of Rx, we need to calculate the expected value of  $r_r \cos \theta$ , where  $\theta$  is the polar angle. This gives us the distance from the center of Rx to the center of mass, as

$$E[r_r \cos \theta] = \int_0^\pi r_r \cos \theta' \frac{p_{\text{Rx}}^{\text{SISO}}(\theta | r_0, r_r)}{P_{\text{Rx}}^{\text{SISO}}(\infty | r_0, r_r)} d\theta', \quad (4.7)$$

$$= \frac{r_r \left(1 - \frac{r_r^2}{r_0^2}\right)}{2} \int_0^\pi \frac{\cos \theta' \sin \theta'}{\left(1 - \frac{2r_r}{r_0} \cos \theta' + \frac{r_r^2}{r_0^2}\right)^{3/2}} d\theta', \quad (4.8)$$

$$= r_r \frac{r_r}{r_0}. \quad (4.9)$$

The angle  $\theta$  is defined starting in the region of Rx closer to Tx. Then, the positive center of mass indicates that the center of mass is at the region of Rx closer to Tx.

Returning to the assumption case above, it is said that  $\text{Rx}_j$ , as a fully-permeable transceiver, releases the MMs arriving at its surface from the same contact point. This concept may be tractable for a single MM, however, it is intractable for an aggregate MM. Therefore the contact points need to be approximated for all MMs arriving at  $\text{Rx}_j$ , for analytical tractability.

The motion of all the MMs arriving at  $Rx_j$  can be split into two parts: the first being the arrival at the surface of  $Rx_j$ , the second being the motion towards  $Rx_i$  by being released from the surface of  $Rx_j$ . To utilize the molecular SISO analytics in this assumed scenario, all of the MMs arriving at the different points on the surface of  $Rx_j$  are assumed to arrive at the center of mass of  $Rx_j$ . The center of mass point, named virtual release point of  $Rx_j$  now, becomes the beginning point of the second part of the movement of MMs, which can be modeled by the molecular SISO analytics since there is no other fully-absorbing receiver to consider in this assumed case. The virtual release point of  $Rx_j$  is regarded as the release point for all the MMs arriving at  $Rx_j$ , as if there were no other Rxs. Following the assumption, we define the conditional absorption rate of MMs arriving at  $Rx_j$  at time  $\tau$  by  $Rx_i$  at time  $t$ , as

$$p_{R_{x_i}}^{\text{Conditional}}(t | R_{x_j}, \tau; r_{0_i}, r_i) = \begin{cases} p_{R_{x_i}}^{\text{SISO}}(t - \tau | r_{0_{i|j}}, r_i), & t > \tau, \\ 0, & t \leq \tau, \end{cases} \quad (4.10)$$

where  $r_{0_{i|j}}$  is the point-to-center distance between the virtual release point of  $Rx_j$  and the center of  $Rx_i$ .

To define the molecular SIMO topology with 2 Rx antennas, it should be noticed that the centers of two Rxs and one Tx are three points that define a plane in 3D space. Defined by the Tx corner, the angular separation between two Rxs is represented as  $\phi$ , as shown in Figure 4.1, and it is used to calculate  $r_{0_{j|i}}$  and  $r_{0_{i|j}}$  distances. Formulating the distances by the cosine rule gives

$$r_{0_{j|i}} = \sqrt{\left(r_{0_i} - r_i \frac{r_i}{r_{0_i}}\right)^2 + r_{0_j}^2 - 2 \left(r_{0_i} - r_i \frac{r_i}{r_{0_i}}\right) r_{0_j} \cos \phi}, \quad (4.11)$$

$$r_{0_{i|j}} = \sqrt{\left(r_{0_j} - r_j \frac{r_j}{r_{0_j}}\right)^2 + r_{0_i}^2 - 2 \left(r_{0_j} - r_j \frac{r_j}{r_{0_j}}\right) r_{0_i} \cos \phi}. \quad (4.12)$$

As referred before, the competition for MMs between the Rxs is reciprocal, as they both tend to reduce the other's capability of absorbing as many MMs as possible which is upper bounded by the molecular SISO absorption rate. Moreover, the amount of MMs

arriving at  $Rx_j$  at time  $\tau$  is affected by the prior effects of  $Rx_i$ , and so on. Therefore, the absorption rate –arrival rate in this assumed case– of MMs arriving at  $Rx_j$  at time  $\tau$  cannot be calculated by the molecular SISO absorption rate, rather it should be represented by the molecular SIMO representation  $p_{Rx_j}^{\text{SIMO}}(\tau | Rx_i, r_{0_j}, r_j)$  which is yet to be determined analytically. Combining this with the conditional absorption rate in (4.10) we obtain the joint absorption rate of MMs which arrive at  $Rx_j$  at time  $\tau$ , rereleased at time  $\tau$  and then absorbed by  $Rx_i$  at time  $t$ , as

$$p_{Rx_i}^{\text{Joint}}(t; Rx_j, \tau | r_{0_i}, r_i) = p_{Rx_j}^{\text{SIMO}}(\tau | Rx_i, r_{0_j}, r_j) p_{Rx_i}^{\text{Conditional}}(t | Rx_j, \tau; r_{0_i}, r_i), \quad (4.13)$$

$$= p_{Rx_j}^{\text{SIMO}}(\tau | Rx_i, r_{0_j}, r_j) p_{Rx_i}^{\text{SISO}}(t - \tau | r_{0_{i|j}}, r_i). \quad (4.14)$$

The joint absorption rate expression is defined for a single  $\tau$  time instance. Calculating the total absorption rate requires the integration of (4.14) over all  $\tau < t$ , as

$$p_{Rx_i}^{\text{Total}}(t; Rx_j | r_{0_i}, r_i) = \int_0^t p_{Rx_j}^{\text{SIMO}}(\tau | Rx_i, r_{0_j}, r_j) p_{Rx_i}^{\text{SISO}}(t - \tau | r_{0_{i|j}}, r_i) d\tau. \quad (4.15)$$

Finally, we have derived the total absorption rate of MMs arriving at  $Rx_j$  prior to being absorbed by  $Rx_i$ . Now, it is time to adapt this assumption into real features. When  $Rx_j$  is a fully-absorbing Rx, these MMs are absorbed by  $Rx_j$  and trapped, which prevents them from further propagating in the diffusive medium. Therefore, the total absorption rate of MMs arriving at  $Rx_j$  prior to being absorbed by  $Rx_i$  represents the absorption rate of MMs stolen from  $Rx_i$ , by  $Rx_j$  in reality, and it needs to be subtracted from the full potential of absorption of  $Rx_i$ , which is the molecular SISO absorption rate as if there were no other Rxs, as

$$\begin{aligned} p_{Rx_i}^{\text{SIMO}}(t | Rx_j, r_{0_i}, r_i) &= p_{Rx_i}^{\text{SISO}}(t | r_{0_i}, r_i) - p_{Rx_i}^{\text{Total}}(t; Rx_j | r_{0_i}, r_i), \\ &= p_{Rx_i}^{\text{SISO}}(t | r_{0_i}, r_i) - \int_0^t p_{Rx_j}^{\text{SIMO}}(\tau | Rx_i, r_{0_j}, r_j) p_{Rx_i}^{\text{SISO}}(t - \tau | r_{0_{i|j}}, r_i) d\tau. \end{aligned} \quad (4.16)$$

It should be noticed that the molecular SIMO absorption rate of MMs by  $Rx_i$  also has the molecular SIMO absorption rate of  $Rx_j$  as integrand. Consequently, the molecular SIMO absorption rate expressions have a recursive and mutually-feeding nature [22].

#### 4.1.2. Closed-form Solution Derivation

The integral proposed in (4.15) is a convolution integral, and can be rewritten in the form of

$$p_{Rx_i}^{\text{Total}}(t; Rx_j | r_{0_i}, r_i) = p_{Rx_j}^{\text{SIMO}}(t | Rx_i, r_{0_j}, r_j) * p_{Rx_i}^{\text{SISO}}(t | r_{0_{i|j}}, r_i), \quad (4.17)$$

which makes (4.16) become a simpler form as

$$p_{Rx_i}^{\text{SIMO}}(t | Rx_j, r_{0_i}, r_i) = p_{Rx_i}^{\text{SISO}}(t | r_{0_i}, r_i) - p_{Rx_j}^{\text{SIMO}}(t | Rx_i, r_{0_j}, r_j) * p_{Rx_i}^{\text{SISO}}(t | r_{0_{i|j}}, r_i). \quad (4.18)$$

To find a closed-form solution of (4.18), we transform the expression in (4.18) for both Rxs into the Laplace domain, as

$$P_{Rx_i}^{\text{SIMO}}(s) = P_{Rx_i}^{\text{SISO}}(s) - P_{Rx_j}^{\text{SIMO}}(s)P_{Rx_{i|j}}^{\text{SISO}}(s), \quad (4.19)$$

$$P_{Rx_j}^{\text{SIMO}}(s) = P_{Rx_j}^{\text{SISO}}(s) - P_{Rx_i}^{\text{SIMO}}(s)P_{Rx_{j|i}}^{\text{SISO}}(s), \quad (4.20)$$

where

$$\begin{aligned} P_{Rx_i}^{\text{SIMO}}(s) &= \mathcal{L} \{ p_{Rx_i}^{\text{SIMO}}(t | Rx_j, r_{0_i}, r_i) \}, & P_{Rx_j}^{\text{SIMO}}(s) &= \mathcal{L} \{ p_{Rx_j}^{\text{SIMO}}(t | Rx_i, r_{0_j}, r_j) \}, \\ P_{Rx_i}^{\text{SISO}}(s) &= \mathcal{L} \{ p_{Rx_i}^{\text{SISO}}(t | r_{0_i}, r_i) \}, & P_{Rx_j}^{\text{SISO}}(s) &= \mathcal{L} \{ p_{Rx_j}^{\text{SISO}}(t | r_{0_j}, r_j) \}, \\ P_{Rx_{i|j}}^{\text{SISO}}(s) &= \mathcal{L} \{ p_{Rx_i}^{\text{SISO}}(t | r_{0_{i|j}}, r_i) \}, & P_{Rx_{j|i}}^{\text{SISO}}(s) &= \mathcal{L} \{ p_{Rx_j}^{\text{SISO}}(t | r_{0_{j|i}}, r_j) \}. \end{aligned}$$

We substitute the molecular SIMO terms with each other to obtain the expression without the molecular SIMO terms, as

$$P_{\text{Rx}_i}^{\text{SIMO}}(s) = \frac{P_{\text{Rx}_i}^{\text{SISO}}(s) - P_{\text{Rx}_j}^{\text{SISO}}(s)P_{\text{Rx}_{i|j}}^{\text{SISO}}(s)}{1 - P_{\text{Rx}_{i|j}}^{\text{SISO}}(s)P_{\text{Rx}_{j|i}}^{\text{SISO}}(s)}. \quad (4.21)$$

Since all the remaining terms are in form of Laplace transformation of molecular SISO absorption rates, we can place the exact Laplace transformations of each term into (4.21). The Laplace transformation of a molecular SISO absorption rate is

$$\mathcal{L}\{p_{\text{Rx}_i}^{\text{SISO}}(t | r_{0_i}, r_i)\} = \frac{r_i}{r_{0_i}} \exp\left(-\frac{r_{0_i} - r_i}{\sqrt{D}}\sqrt{s}\right). \quad (4.22)$$

The Laplace transformations of each term can be implemented by replacing the relevant terms into (4.22). Substituting the Laplace transformations of each term into (4.21) gives

$$P_{\text{Rx}_i}^{\text{SIMO}}(s) = \frac{\frac{r_i}{r_{0_i}} \exp\left(-\frac{r_{0_i} - r_i}{\sqrt{D}}\sqrt{s}\right) - \frac{r_j r_i}{r_{0_j} r_{0_{i|j}}} \exp\left(-\frac{(r_{0_j} + r_{0_{i|j}}) - (r_j + r_i)}{\sqrt{D}}\sqrt{s}\right)}{1 - \frac{r_i r_j}{r_{0_{i|j}} r_{0_{j|i}}} \exp\left(-\frac{(r_{0_{i|j}} + r_{0_{j|i}}) - (r_i + r_j)}{\sqrt{D}}\sqrt{s}\right)}. \quad (4.23)$$

We need to derive the inverse Laplace transformation of (4.23), we split the fraction, and take the inverse Laplace transform of each part separately. Firstly, the left-hand side part is expanded as

$$\begin{aligned} & \frac{\frac{r_i}{r_{0_i}} \exp\left(-\frac{r_{0_i} - r_i}{\sqrt{D}}\sqrt{s}\right)}{1 - \frac{r_i r_j}{r_{0_{i|j}} r_{0_{j|i}}} \exp\left(-\frac{(r_{0_{i|j}} + r_{0_{j|i}}) - (r_i + r_j)}{\sqrt{D}}\sqrt{s}\right)} = \\ & \frac{r_i}{r_{0_i}} \exp\left(-\frac{r_{0_i} - r_i}{\sqrt{D}}\sqrt{s}\right) \sum_{k=0}^{\infty} \left[ \frac{r_i r_j}{r_{0_{i|j}} r_{0_{j|i}}} \exp\left(-\frac{(r_{0_{i|j}} + r_{0_{j|i}}) - (r_i + r_j)}{\sqrt{D}}\sqrt{s}\right) \right]^k \\ & = \sum_{k=0}^{\infty} \frac{r_i}{r_{0_i}} \left( \frac{r_i r_j}{r_{0_{i|j}} r_{0_{j|i}}} \right)^k \exp\left(-\frac{(r_{0_i} - r_i) + k \left( (r_{0_{i|j}} + r_{0_{j|i}}) - (r_i + r_j) \right)}{\sqrt{D}}\sqrt{s}\right), \quad (4.24) \end{aligned}$$

provided the region of convergence (ROC) is satisfied (ROC for expansion is derived in Appendix A). In a similar fashion, the right-hand side part is expanded as

$$\frac{\frac{r_j r_i}{r_{0_j} r_{0_{i|j}}} \exp\left(-\frac{(r_{0_j} + r_{0_{i|j}}) - (r_j + r_i)}{\sqrt{D}} \sqrt{s}\right)}{1 - \frac{r_i r_j}{r_{0_{i|j}} r_{0_j}} \exp\left(-\frac{(r_{0_{i|j}} + r_{0_j}) - (r_i + r_j)}{\sqrt{D}} \sqrt{s}\right)} = \sum_{k=0}^{\infty} \frac{r_j r_i}{r_{0_j} r_{0_{i|j}}} \left(\frac{r_i r_j}{r_{0_{i|j}} r_{0_j}}\right)^k \times \exp\left(-\frac{\left((r_{0_j} + r_{0_{i|j}}) - (r_i + r_j)\right) + k \left((r_{0_{i|j}} + r_{0_j}) - (r_i + r_j)\right)}{\sqrt{D}} \sqrt{s}\right). \quad (4.25)$$

We place substitutions to increase the readability of the equations and simplification, and the equation in (4.23) is converted into

$$P_{\text{Rxi}}^{\text{SIMO}}(s) = \sum_{k=0}^{\infty} A_{ik} \exp(-B_{ik} \sqrt{s}) - \sum_{k=0}^{\infty} A_{jk} \exp(-B_{jk} \sqrt{s}), \quad (4.26)$$

where

$$A_{ik} = \frac{r_i}{r_{0_i}} \left(\frac{r_i r_j}{r_{0_{i|j}} r_{0_{j|i}}}\right)^k, \quad A_{jk} = \frac{r_j r_i}{r_{0_j} r_{0_{i|j}}} \left(\frac{r_i r_j}{r_{0_{i|j}} r_{0_{j|i}}}\right)^k, \\ B_{ik} = \frac{(r_{0_i} - r_i) + k \left((r_{0_{i|j}} + r_{0_{j|i}}) - (r_i + r_j)\right)}{\sqrt{D}}, \quad (4.27) \\ B_{jk} = \frac{\left((r_{0_j} + r_{0_{i|j}}) - (r_i + r_j)\right) + k \left((r_{0_{i|j}} + r_{0_{j|i}}) - (r_i + r_j)\right)}{\sqrt{D}}.$$

Exploiting the linearity property of the Laplace transform, the time-domain solution of (4.26) is the sum of individual Laplace transformations of each term, as

$$p_{\text{Rxi}}^{\text{SIMO}}(t | \text{Rx}_j, r_{0_i}, r_i) = \mathcal{L}^{-1} \{P_{\text{Rxi}}^{\text{SIMO}}(s)\}, \quad (4.28)$$

$$= \sum_{k=0}^{\infty} \mathcal{L}^{-1} \{A_{ik} \exp(-B_{ik} \sqrt{s})\} - \sum_{k=0}^{\infty} \mathcal{L}^{-1} \{A_{jk} \exp(-B_{jk} \sqrt{s})\}. \quad (4.29)$$

Since all the terms in the Laplace domain are in form of the Laplace transform of a molecular SISO absorption rate, the inverse Laplace transform of each can be found

by utilizing (4.22) with the appropriate parameters, such as

$$\mathcal{L}^{-1} \{A_{ik} \exp(-B_{ik}\sqrt{s})\} = \frac{A_{ik} B_{ik}}{\sqrt{4\pi t} t} \exp\left(-\frac{B_{ik}^2}{4t}\right). \quad (4.30)$$

Therefore, the closed-form solution of the molecular SIMO absorption rate of MMs by  $Rx_i$  in presence of  $Rx_j$  becomes

$$p_{Rx_i}^{\text{SIMO}}(t | Rx_j, r_{0_i}, r_i) = \sum_{k=0}^{\infty} \frac{A_{ik} B_{ik}}{\sqrt{4\pi t} t} \exp\left(-\frac{B_{ik}^2}{4t}\right) - \sum_{k=0}^{\infty} \frac{A_{jk} B_{jk}}{\sqrt{4\pi t} t} \exp\left(-\frac{B_{jk}^2}{4t}\right). \quad (4.31)$$

The analytical closed-form solution presented in (4.31) consists of the sum of infinite terms. However, as the coefficients are defined above, it should be noticed that  $A_{ik}$  and  $A_{jk}$  are less than 1, and the exponents in (4.31)  $B_{ik}^2$  and  $B_{jk}^2$  grow rapidly as  $k$  increases which converge the exponential terms to 0 rapidly, the terms in sums converge to 0 after just several terms, and the expression (4.31) settles to convergence.

Now it is time to derive the molecular SIMO absorption probability of MMs by  $Rx_i$  in presence of  $Rx_j$  until time  $t$ . Integrating (4.31) gives

$$P_{Rx_i}^{\text{SIMO}}(t | Rx_j, r_{0_i}, r_i) = \int_0^t p_{Rx_i}^{\text{SIMO}}(\tau | Rx_j, r_{0_i}, r_i) d\tau. \quad (4.32)$$

Placing the explicit expression into the equation, we obtain

$$\begin{aligned} P_{Rx_i}^{\text{SIMO}}(t | Rx_j, r_{0_i}, r_i) &= \\ & \int_0^t \left[ \sum_{k=0}^{\infty} \frac{A_{ik} B_{ik}}{\sqrt{4\pi\tau} \tau} \exp\left(-\frac{B_{ik}^2}{4\tau}\right) - \sum_{k=0}^{\infty} \frac{A_{jk} B_{jk}}{\sqrt{4\pi\tau} \tau} \exp\left(-\frac{B_{jk}^2}{4\tau}\right) \right] d\tau, \\ P_{Rx_i}^{\text{SIMO}}(t | Rx_j, r_{0_i}, r_i) &= \\ & \sum_{k=0}^{\infty} \int_0^t \frac{A_{ik} B_{ik}}{\sqrt{4\pi\tau} \tau} \exp\left(-\frac{B_{ik}^2}{4\tau}\right) d\tau - \sum_{k=0}^{\infty} \int_0^t \frac{A_{jk} B_{jk}}{\sqrt{4\pi\tau} \tau} \exp\left(-\frac{B_{jk}^2}{4\tau}\right) d\tau. \end{aligned}$$

Calculating individual integrals gives us

$$P_{\text{Rx}_i}^{\text{SIMO}}(t | \text{Rx}_j, r_{0_i}, r_i) = \sum_{k=0}^{\infty} A_{ik} \operatorname{erfc} \left( \frac{B_{ik}}{\sqrt{4t}} \right) - \sum_{k=0}^{\infty} A_{jk} \operatorname{erfc} \left( \frac{B_{jk}}{\sqrt{4t}} \right), \quad (4.33)$$

and finally, substituting the coefficients we get

$$\begin{aligned} P_{\text{Rx}_i}^{\text{SIMO}}(t | \text{Rx}_j, r_{0_i}, r_i) = & \\ & \sum_{k=0}^{\infty} \frac{r_i}{r_{0_i}} \left( \frac{r_i r_j}{r_{0_{i|j}} r_{0_{j|i}}} \right)^k \operatorname{erfc} \left( \frac{(r_{0_i} - r_i) + k \left( (r_{0_{i|j}} + r_{0_{j|i}}) - (r_i + r_j) \right)}{\sqrt{4Dt}} \right) - \\ & \frac{r_j r_i}{r_{0_j} r_{0_{i|j}}} \left( \frac{r_i r_j}{r_{0_{i|j}} r_{0_{j|i}}} \right)^k \operatorname{erfc} \left( \frac{\left( (r_{0_j} + r_{0_{i|j}}) - (r_i + r_j) \right) + k \left( (r_{0_{i|j}} + r_{0_{j|i}}) - (r_i + r_j) \right)}{\sqrt{4Dt}} \right). \end{aligned} \quad (4.34)$$

The expression (4.34) is the absorption probability of MMs by  $\text{Rx}_i$  in presence of  $\text{Rx}_j$  until time  $t$ , which is a characteristic feature for each Rx in every MC system.

## 4.2. Simplified Model

The recursive model provides detailed analytics for molecular SIMO absorption probability of MMs by Rxs. However, the recursive nature of the exploited phenomenon led to a more sophisticated closed-form solution, which theoretically consists of infinite terms. This enormous computational requirement would be a burden for practical applications, and the requirement increases linearly depending on the precision constraint of the application. We propose a simplification of the proposed recursive model by exploiting the recursive nature itself.

#### 4.2.1. Absorption Rate Approximation Based on the Recursive Model for Molecular SIMO Systems

We start with the total absorption rate of MMs arriving at  $Rx_j$  prior to being absorbed by  $Rx_i$  in (4.15),

$$p_{Rx_i}^{\text{Total}}(t; Rx_j | r_{0_i}, r_i) = \int_0^t p_{Rx_j}^{\text{SIMO}}(\tau | Rx_i, r_{0_j}, r_j) p_{Rx_i}^{\text{SISO}}(t - \tau | r_{0_{i|j}}, r_i) d\tau, \quad (4.35)$$

and we replace the molecular SIMO term in the integrand by (4.16), as

$$p_{Rx_i}^{\text{Total}}(t; Rx_j | r_{0_i}, r_i) = \int_0^t \left[ p_{Rx_j}^{\text{SISO}}(\tau | r_{0_j}, r_j) - \int_0^\tau p_{Rx_i}^{\text{SIMO}}(\eta | Rx_j, r_{0_i}, r_i) p_{Rx_j}^{\text{SISO}}(\tau - \eta | r_{0_{j|i}}, r_j) d\eta \right] p_{Rx_i}^{\text{SISO}}(t - \tau | r_{0_{i|j}}, r_i) d\tau. \quad (4.36)$$

Arranging the terms gives

$$p_{Rx_i}^{\text{Total}}(t; Rx_j | r_{0_i}, r_i) = \int_0^t p_{Rx_j}^{\text{SISO}}(\tau | r_{0_j}, r_j) p_{Rx_i}^{\text{SISO}}(t - \tau | r_{0_{i|j}}, r_i) d\tau - \int_0^t \int_0^\tau p_{Rx_i}^{\text{SIMO}}(\eta | Rx_j, r_{0_i}, r_i) p_{Rx_j}^{\text{SISO}}(\tau - \eta | r_{0_{j|i}}, r_j) p_{Rx_i}^{\text{SISO}}(t - \tau | r_{0_{i|j}}, r_i) d\eta d\tau. \quad (4.37)$$

This expansion can be called *one-degree expansion*, since we placed the recursive term in the integrand with its explicit and again recursive expansion. The integral becomes the difference between one single integral and one double integral. It should be noticed that the double integral still consists of a molecular SIMO term, and two molecular SISO terms alongside it. We can further expand this integral and obtain higher integrals with more molecular SISO terms accumulating within these new integrals. However, the molecular SISO terms collected and multiplied together converge to zero, since they are less than 1. Therefore, the accumulated terms within the double integral, or any higher integrals converge to 0, and can be neglected.

Based on the assumption of the magnitudes of the probabilistic terms, the approximation of the total absorption rate examined in (4.35) becomes

$$\hat{p}_{\text{Rx}_i}^{\text{Total}}(t; \text{Rx}_j | r_{0_i}, r_i) = \int_0^t p_{\text{Rx}_j}^{\text{SISO}}(\tau | r_{0_j}, r_j) p_{\text{Rx}_i}^{\text{SISO}}(t - \tau | r_{0_{i|j}}, r_i) d\tau, \quad (4.38)$$

which is substituted in (4.16) to arrive at

$$\hat{p}_{\text{Rx}_i}^{\text{SIMO}}(t | \text{Rx}_j, r_{0_i}, r_i) = p_{\text{Rx}_i}^{\text{SISO}}(t | r_{0_i}, r_i) - \int_0^t p_{\text{Rx}_j}^{\text{SISO}}(\tau | r_{0_j}, r_j) p_{\text{Rx}_i}^{\text{SISO}}(t - \tau | r_{0_{i|j}}, r_i) d\tau, \quad (4.39)$$

which is the approximation of the absorption rate of MMs by  $\text{Rx}_i$  in presence of  $\text{Rx}_j$ . Provided that the molecular SISO terms are small enough, the simplified model is an accurate approximation of the recursive model, therefore it is a computationally feasible option of the recursive model.

#### 4.2.2. Closed-form Solution Derivation

The closed-form solution of the simplified model expression in (4.39) is rather straightforward compared to its recursive counterpart. In a similar fashion, we notice that the equation in (4.39) can be represented with a convolution integral, as

$$\hat{p}_{\text{Rx}_i}^{\text{SIMO}}(t | \text{Rx}_j, r_{0_i}, r_i) = p_{\text{Rx}_i}^{\text{SISO}}(t | r_{0_i}, r_i) - p_{\text{Rx}_j}^{\text{SISO}}(t | r_{0_j}, r_j) * p_{\text{Rx}_i}^{\text{SISO}}(t | r_{0_{i|j}}, r_i), \quad (4.40)$$

which is transformed into Laplace domain, as

$$\hat{P}_{\text{Rx}_i}^{\text{SIMO}}(s) = P_{\text{Rx}_i}^{\text{SISO}}(s) - P_{\text{Rx}_j}^{\text{SISO}}(s) P_{\text{Rx}_{i|j}}^{\text{SISO}}(s). \quad (4.41)$$

We have previously derived the Laplace transformations of these terms, thus we place the appropriate transformations in (4.41) to obtain the Laplace transform of the

simplified absorption rate of MMs in molecular SIMO system as

$$\hat{P}_{\text{Rx}_i}^{\text{SIMO}}(s) = \frac{r_i}{r_{0_i}} \exp\left(-\frac{r_{0_i} - r_i}{\sqrt{D}} \sqrt{s}\right) - \frac{r_j r_i}{r_{0_j} r_{0_{i|j}}} \exp\left(-\frac{(r_{0_j} + r_{0_{i|j}}) - (r_j + r_i)}{\sqrt{D}} \sqrt{s}\right). \quad (4.42)$$

As the final touch, the inverse Laplace transforms of each term separately for

$$\begin{aligned} \hat{p}_{\text{Rx}_i}^{\text{SIMO}}(t | \text{Rx}_j, r_{0_i}, r_i) &= \frac{r_i}{r_{0_i}} \frac{1}{\sqrt{4\pi Dt}} \frac{r_{0_i} - r_i}{t} \exp\left(-\frac{(r_{0_i} - r_i)^2}{4Dt}\right) - \\ &\frac{r_j r_i}{r_{0_j} r_{0_{i|j}}} \frac{1}{\sqrt{4\pi Dt}} \frac{(r_{0_j} + r_{0_{i|j}}) - (r_j + r_i)}{t} \exp\left(-\frac{(r_{0_j} + r_{0_{i|j}}) - (r_j + r_i)^2}{4Dt}\right). \end{aligned} \quad (4.43)$$

Purified from the infinite higher-complexity terms, the simplified model gives a computationally feasible approximation of the recursive model absorption rate expressions, by neglecting the effects of the recursively affected MMs, which converge to 0. To derive the approximation of the molecular SIMO absorption probability of MMs by  $\text{Rx}_i$  in presence of  $\text{Rx}_j$  until time  $t$ , we again integrate (4.43), as

$$\hat{P}_{\text{Rx}_i}^{\text{SIMO}}(t | \text{Rx}_j, r_{0_i}, r_i) = \int_0^t \hat{p}_{\text{Rx}_i}^{\text{SIMO}}(\tau | \text{Rx}_j, r_{0_i}, r_i) d\tau. \quad (4.44)$$

Substituting the integrand with 4.43 gives

$$\begin{aligned} \hat{P}_{\text{Rx}_i}^{\text{SIMO}}(t | \text{Rx}_j, r_{0_i}, r_i) &= \int_0^t \left[ \frac{r_i}{r_{0_i}} \frac{1}{\sqrt{4\pi D\tau}} \frac{r_{0_i} - r_i}{\tau} \exp\left(-\frac{(r_{0_i} - r_i)^2}{4D\tau}\right) - \right. \\ &\left. \frac{r_j r_i}{r_{0_j} r_{0_{i|j}}} \frac{1}{\sqrt{4\pi D\tau}} \frac{(r_{0_j} + r_{0_{i|j}}) - (r_j + r_i)}{\tau} \exp\left(-\frac{(r_{0_j} + r_{0_{i|j}}) - (r_j + r_i)^2}{4D\tau}\right) \right] d\tau. \end{aligned} \quad (4.45)$$

Individually integrating each term gives

$$\hat{P}_{\text{Rx}_i}^{\text{SIMO}}(t | \text{Rx}_j, r_{0_i}, r_i) = \frac{r_i}{r_{0_i}} \operatorname{erfc}\left(\frac{r_{0_i} - r_i}{\sqrt{4Dt}}\right) - \frac{r_j r_i}{r_{0_j} r_{0_{i|j}}} \operatorname{erfc}\left(-\frac{(r_{0_i} + r_{0_{i|j}}) - (r_i + r_j)}{\sqrt{4Dt}}\right), \quad (4.46)$$

which is the approximation of the molecular SIMO absorption probability of MMs by  $\text{Rx}_i$  in presence of  $\text{Rx}_j$ .

### 4.3. Channel Modeling for Molecular SIMO Systems With More Than Two Receivers

The proposed model is adaptable for channel modeling of molecular SIMO systems with the number of Rx antennas greater than 2. The single difference is that we now consider the effect of all other Rxs, rather than one single present Rx. By definition, the recursive model considers the recursive effects of Rxs on one another. For molecular SIMO systems with more than 2 Rxs, the bystander antennas are also affecting each other. However, due to simplicity concerns in derivation, we assume the effect between only the intended Rx and the other bystander Rxs.

The updated joint absorption rate of MMs by  $Rx_i$  in presence of  $Rx_j$  which is one of the  $n_{Rx} - 1$  antennas other than  $Rx_i$  is notationally similar with a slight change, as

$$p_{Rx_i}^{\text{Joint}}(t; Rx_j, \tau | r_{0_i}, r_i) = p_{Rx_j}^{\text{SIMO}}(\tau | Rx_1, \dots, Rx_{n_{Rx}}, r_{0_j}, r_j) p_{Rx_i}^{\text{SISO}}(t - \tau | r_{0_{i|j}}, r_i), \quad (4.47)$$

where the change is that the molecular SIMO term of  $Rx_j$  is now affected not only by  $Rx_i$  but all Rxs. The total effect of the presence of  $Rx_j$  is calculated by integrating (4.47) over time  $t$  as

$$p_{Rx_i}^{\text{Total}}(t; Rx_j | r_{0_i}, r_i) = \int_0^t p_{Rx_j}^{\text{SIMO}}(\tau | Rx_1, \dots, Rx_{n_{Rx}}, r_{0_j}, r_j) p_{Rx_i}^{\text{SISO}}(t - \tau | r_{0_{i|j}}, r_i) d\tau. \quad (4.48)$$

Now, the difference is here. Since there are now  $n_{Rx}$  Rxs in total, the accumulated effect of all Rxs, the aggregate absorption rate of MMs arriving at all other Rxs prior to being absorbed by  $Rx_i$  is

$$p_{Rx_i}^{\text{Aggregate}}(t; Rx_1, \dots, Rx_{n_{Rx}} | r_{0_i}, r_i) = \sum_{\substack{j=1 \\ j \neq i}}^{n_{Rx}} p_{Rx_i}^{\text{Total}}(t; Rx_j | r_{0_i}, r_i), \quad (4.49)$$

$$p_{\text{Rx}_i}^{\text{Aggregate}}(t; \text{Rx}_1, \dots, \text{Rx}_{n_{\text{Rx}}} | r_{0_i}, r_i) = \sum_{\substack{j=1 \\ j \neq i}}^{n_{\text{Rx}}} \int_0^t p_{\text{Rx}_j}^{\text{SIMO}}(\tau | \text{Rx}_1, \dots, \text{Rx}_{n_{\text{Rx}}}, r_{0_j}, r_j) p_{\text{Rx}_i}^{\text{SISO}}(t - \tau | r_{0_{i|j}}, r_i) d\tau. \quad (4.50)$$

Finally, by subtracting (4.50) from the molecular SISO absorption rate of  $\text{Rx}_i$ , we get

$$p_{\text{Rx}_i}^{\text{SIMO}}(t | \text{Rx}_1, \dots, \text{Rx}_{n_{\text{Rx}}}, r_{0_i}, r_i) = p_{\text{Rx}_i}^{\text{SISO}}(t | r_{0_i}, r_i) - \sum_{\substack{j=1 \\ j \neq i}}^{n_{\text{Rx}}} \int_0^t p_{\text{Rx}_j}^{\text{SIMO}}(\tau | \text{Rx}_1, \dots, \text{Rx}_{n_{\text{Rx}}}, r_{0_j}, r_j) p_{\text{Rx}_i}^{\text{SISO}}(t - \tau | r_{0_{i|j}}, r_i) d\tau, \quad (4.51)$$

which is the absorption rate of MMs by  $\text{Rx}_i$  in presence of  $n_{\text{Rx}} - 1$  other Rxs. The dependence among the terms makes the calculation quite complex, however, we may propose an approach on the way of deriving the closed-form solution of (4.51). Starting with transforming the terms in (4.51) into Laplace domain gives

$$P_{\text{Rx}_i}^{\text{SIMO}}(s) = P_{\text{Rx}_i}^{\text{SISO}}(s) - \sum_{\substack{j=1 \\ j \neq i}}^{n_{\text{Rx}}} P_{\text{Rx}_j}^{\text{SIMO}}(s) P_{\text{Rx}_{i|j}}^{\text{SISO}}(s). \quad (4.52)$$

Shifting the right-hand side sum of terms to the left-hand side of the equation gives

$$P_{\text{Rx}_i}^{\text{SIMO}}(s) + \sum_{\substack{j=1 \\ j \neq i}}^{n_{\text{Rx}}} P_{\text{Rx}_j}^{\text{SIMO}}(s) P_{\text{Rx}_{i|j}}^{\text{SISO}}(s) = P_{\text{Rx}_i}^{\text{SISO}}(s), \quad (4.53)$$

which can be shaped into matrix notation, as

$$\mathbf{Ax} = \mathbf{b}, \quad (4.54)$$

$$\begin{bmatrix}
1 & P_{\text{Rx}_1|2}^{\text{SISO}}(s) & \dots & P_{\text{Rx}_1|n_{\text{Rx}}}^{\text{SISO}}(s) \\
P_{\text{Rx}_2|1}^{\text{SISO}}(s) & 1 & \dots & P_{\text{Rx}_2|n_{\text{Rx}}}^{\text{SISO}}(s) \\
P_{\text{Rx}_3|1}^{\text{SISO}}(s) & P_{\text{Rx}_3|2}^{\text{SISO}}(s) & \dots & P_{\text{Rx}_3|n_{\text{Rx}}}^{\text{SISO}}(s) \\
\vdots & \vdots & \ddots & \vdots \\
P_{\text{Rx}_{n_{\text{Rx}}}|1}^{\text{SISO}}(s) & P_{\text{Rx}_{n_{\text{Rx}}}|2}^{\text{SISO}}(s) & \dots & 1
\end{bmatrix}
\begin{bmatrix}
P_{\text{Rx}_1}^{\text{SIMO}}(s) \\
P_{\text{Rx}_2}^{\text{SIMO}}(s) \\
P_{\text{Rx}_3}^{\text{SIMO}}(s) \\
\vdots \\
P_{\text{Rx}_{n_{\text{Rx}}}}^{\text{SIMO}}(s)
\end{bmatrix}
=
\begin{bmatrix}
P_{\text{Rx}_1}^{\text{SISO}}(s) \\
P_{\text{Rx}_2}^{\text{SISO}}(s) \\
P_{\text{Rx}_3}^{\text{SISO}}(s) \\
\vdots \\
P_{\text{Rx}_{n_{\text{Rx}}}}^{\text{SISO}}(s)
\end{bmatrix}. \quad (4.55)$$

Assuming the spatial parameters of the topology are known, the matrix  $\mathbf{A}$  and the vector  $\mathbf{b}$  are computable. Provided that the matrix  $\mathbf{A}$  is nonsingular, the vector that carries the Laplace transformations of the molecular SIMO absorption rate of MMs by individually all Rxs can be calculated by simple linear algebra. Following that, the inverse Laplace transform of the vector  $\mathbf{x}$  gives the time-domain solution of the molecular SIMO absorption rates of MMs by all Rxs, as

$$\mathbf{x} = \mathbf{A}^{-1}\mathbf{b}, \quad (4.56)$$

$$\begin{bmatrix}
p_{\text{Rx}_1}^{\text{SIMO}}(t | \text{Rx}_1, \dots, \text{Rx}_{n_{\text{Rx}}}, r_{0_1}, r_1) \\
p_{\text{Rx}_2}^{\text{SIMO}}(t | \text{Rx}_1, \dots, \text{Rx}_{n_{\text{Rx}}}, r_{0_2}, r_2) \\
p_{\text{Rx}_3}^{\text{SIMO}}(t | \text{Rx}_1, \dots, \text{Rx}_{n_{\text{Rx}}}, r_{0_3}, r_3) \\
\vdots \\
p_{\text{Rx}_{n_{\text{Rx}}}}^{\text{SIMO}}(t | \text{Rx}_1, \dots, \text{Rx}_{n_{\text{Rx}}}, r_{0_{n_{\text{Rx}}}}, r_{n_{\text{Rx}}})
\end{bmatrix}
= \mathcal{L}^{-1} \left\{ \begin{bmatrix}
P_{\text{Rx}_1}^{\text{SIMO}}(s) \\
P_{\text{Rx}_2}^{\text{SIMO}}(s) \\
P_{\text{Rx}_3}^{\text{SIMO}}(s) \\
\vdots \\
P_{\text{Rx}_{n_{\text{Rx}}}}^{\text{SIMO}}(s)
\end{bmatrix} \right\}, \quad (4.57)$$

and the framework to derive the closed-form solutions of the molecular SIMO absorption rates of MMs by all Rxs is compatible with the results for the molecular SIMO expressions for 2 Rx scenario.

We see that the solution is nontrivial, and hard to derive. Therefore we can simplify the derivation by utilizing the simplified model. By changing the molecular SIMO term in (4.47) with its molecular SISO counterpart –whose justification is presented above– we obtain the modified version of the simplified model adapted to model the

molecular SIMO systems with more than 2 Rxs, as

$$\hat{p}_{\text{Rx}_i}^{\text{SIMO}}(t | \text{Rx}_1, \dots, \text{Rx}_{n_{\text{Rx}}}, r_{0_i}, r_i) = p_{\text{Rx}_i}^{\text{SISO}}(t | r_{0_i}, r_i) - \sum_{\substack{j=1 \\ j \neq i}}^{n_{\text{Rx}}} \int_0^t p_{\text{Rx}_j}^{\text{SISO}}(\tau | r_{0_j}, r_j) p_{\text{Rx}_i}^{\text{SISO}}(t - \tau | r_{0_{i|j}}, r_i) d\tau, \quad (4.58)$$

which now gives the approximation of the absorption rate of MMs by  $\text{Rx}_i$  in presence of  $n_{\text{Rx}} - 1$  other Rxs. We may approach to the closed-form solution of the simplified channel modeling, presented in (4.58) by transforming the terms into Laplace domain as

$$\hat{P}_{\text{Rx}_i}^{\text{SIMO}}(s) = P_{\text{Rx}_i}^{\text{SISO}}(s) - \sum_{\substack{j=1 \\ j \neq i}}^{n_{\text{Rx}}} P_{\text{Rx}_j}^{\text{SISO}}(s) P_{\text{Rx}_i|j}^{\text{SISO}}(s). \quad (4.59)$$

Similar to the approach above, we shape the relations into matrix notation, as

$$\begin{bmatrix} \hat{P}_{\text{Rx}_1}^{\text{SIMO}}(s) \\ \hat{P}_{\text{Rx}_2}^{\text{SIMO}}(s) \\ \hat{P}_{\text{Rx}_3}^{\text{SIMO}}(s) \\ \vdots \\ \hat{P}_{\text{Rx}_{n_{\text{Rx}}}}^{\text{SIMO}}(s) \end{bmatrix} = \begin{bmatrix} 1 & -P_{\text{Rx}_1|2}^{\text{SISO}}(s) & \dots & -P_{\text{Rx}_1|n_{\text{Rx}}}^{\text{SISO}}(s) \\ -P_{\text{Rx}_2|1}^{\text{SISO}}(s) & 1 & \dots & -P_{\text{Rx}_2|n_{\text{Rx}}}^{\text{SISO}}(s) \\ -P_{\text{Rx}_3|1}^{\text{SISO}}(s) & -P_{\text{Rx}_3|2}^{\text{SISO}}(s) & \dots & -P_{\text{Rx}_3|n_{\text{Rx}}}^{\text{SISO}}(s) \\ \vdots & \vdots & \ddots & \vdots \\ -P_{\text{Rx}_{n_{\text{Rx}}}|1}^{\text{SISO}}(s) & -P_{\text{Rx}_{n_{\text{Rx}}}|2}^{\text{SISO}}(s) & \dots & 1 \end{bmatrix} \begin{bmatrix} P_{\text{Rx}_1}^{\text{SISO}}(s) \\ P_{\text{Rx}_2}^{\text{SISO}}(s) \\ P_{\text{Rx}_3}^{\text{SISO}}(s) \\ \vdots \\ P_{\text{Rx}_{n_{\text{Rx}}}}^{\text{SISO}}(s) \end{bmatrix}. \quad (4.60)$$

In this case, all we need to do is matrix multiplication of a known matrix and a known vector, provided that the spatial parameters are known. Since there are no inversion operations, the solution is trivial, and one can derive the time domain solutions by just inverse Laplace transforming the resultant vector, as

$$\begin{bmatrix} \hat{p}_{\text{Rx}_1}^{\text{SIMO}}(t | \text{Rx}_1, \dots, \text{Rx}_{n_{\text{Rx}}}, r_{0_1}, r_1) \\ \hat{p}_{\text{Rx}_2}^{\text{SIMO}}(t | \text{Rx}_1, \dots, \text{Rx}_{n_{\text{Rx}}}, r_{0_2}, r_2) \\ \hat{p}_{\text{Rx}_3}^{\text{SIMO}}(t | \text{Rx}_1, \dots, \text{Rx}_{n_{\text{Rx}}}, r_{0_3}, r_3) \\ \vdots \\ \hat{p}_{\text{Rx}_{n_{\text{Rx}}}}^{\text{SIMO}}(t | \text{Rx}_1, \dots, \text{Rx}_{n_{\text{Rx}}}, r_{0_{n_{\text{Rx}}}}, r_{n_{\text{Rx}}}) \end{bmatrix} = \mathcal{L}^{-1} \left\{ \begin{bmatrix} \hat{P}_{\text{Rx}_1}^{\text{SIMO}}(s) \\ \hat{P}_{\text{Rx}_2}^{\text{SIMO}}(s) \\ \hat{P}_{\text{Rx}_3}^{\text{SIMO}}(s) \\ \vdots \\ \hat{P}_{\text{Rx}_{n_{\text{Rx}}}}^{\text{SIMO}}(s) \end{bmatrix} \right\}, \quad (4.61)$$

and the framework proposed is compatible with the results of the simplified version of the channel model for the molecular SIMO system with 2 Rxs.

#### 4.4. Performance Evaluations

##### 4.4.1. Angular Analysis

We present a basic molecular SIMO system in Figure 4.1. As one can see, there are spatial parameters  $r_{0_i}$  and  $r_{0_j}$ , topological parameters  $r_i$  and  $r_j$ , and the separation angle  $\phi$  to define a molecular SIMO system with 2 Rx antennas. The variability of these parameters actively impacts the channel response of the channel, therefore the performance of the proposed models needs to be evaluated within the topologies of different parameters.

The analysis of this study is performed on three different molecular SIMO systems with 2 Rxs whose parameters are defined based on the relative sizes of Rxs. The absorption probability functions of the topologies, which are to be used as benchmarks are obtained by computer-based simulations. The performance evaluations and comparisons are operated between the computer-based results and the absorption probability functions acquired via the recursive model.

For small separation angles  $\phi$ , the Rx placed closer to Tx blocks the line of sight of Tx towards the Rx placed farther to Tx. Without any blocking, the coverage between the Tx and an Rx is as wide as it is proposed in Chapter 2.1.1. However, when an Rx blocks the line of sight of another Rx fully or partially, the coverage area is constricted. This blockage is called the shadowing phenomenon [22]. The shadowing affects the absorption of MMs by the shadowed Rx, since the MMs cannot arrive at the Rx towards the line of sight. There are two significant angles to be examined regarding this phenomenon, which are the half-eclipse angle and the no-eclipse angle. The half-eclipse angle is the angle at which the center of the farther Rx lies on the tangent of the closer Rx, causing roughly one-half of the farther Rx to be shadowed.

The no-eclipse angle is the angle at which the tangents of both Rxs coincide and there is no shadowing. These angles can be calculated as

$$\phi_{\text{Half-eclipse}} = \arcsin \frac{r_1}{r_{0_1}}, \quad (4.62)$$

$$\phi_{\text{No-eclipse}} = \arcsin \frac{r_1}{r_{0_1}} + \arcsin \frac{r_2}{r_{0_2}}. \quad (4.63)$$

Table 4.1. Spatial parameters for Scenario 1.

Parameters	$r_1$	$r_2$	$r_{0_1}$	$r_{0_2}$
Values	$2 \mu\text{m}$	$5 \mu\text{m}$	$6 \mu\text{m}$	$16 \mu\text{m}$

4.4.1.1. Scenario 1–Smaller Rx to be Closer to Tx. This configuration of Rxs offers a molecular SIMO topology where the smaller Rx between Rxs of different radii is placed closer to the Tx. The maximum shadowing occurs when the separation angle  $\phi$  is close to 0 rad. The selection of the radii of the Rxs helps that the closer Rx cannot completely shadow the farther Rx. The shortest distance between the Rxs is  $3 \mu\text{m}$  in the case of  $\phi = 0 \text{ rad}$ , at which the Rxs and the Tx are perfectly aligned.

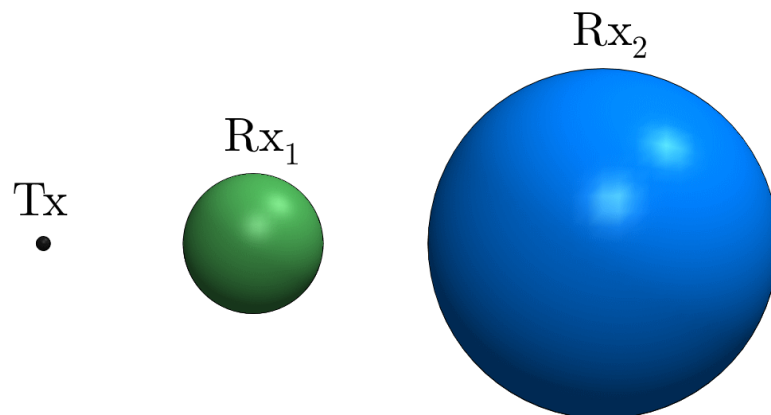


Figure 4.3. An illustration of the molecular SIMO topology examined in Scenario 1.

As the separation angle  $\phi$  increases, the shadowing on the farther Rx decreases, and disappears after the no-eclipse angle. The virtual release point towards Rx<sub>2</sub> from Rx<sub>1</sub> becomes more distant and direct which represents the competition among the Rxs. The root mean squared (RMS) error then decreases as the separation angle  $\phi$  decreases, as shown in Figure 4.4.

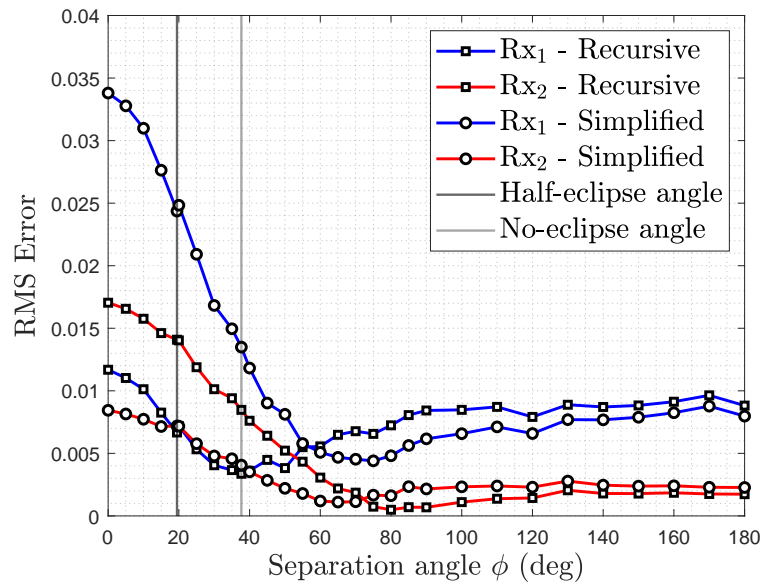


Figure 4.4. The graph of RMS error between the computer-based absorption probability of MMs and the absorption probability of MMs acquired by the recursive model versus the separation angle  $\phi$  for Scenario 1.

As one can see, the absorption rates of MMs and the absorption probabilities of MMs for two distinct separation angles differ slightly, since  $r_{0_{12}}$  and  $r_{0_{21}}$  changes. Since the half-eclipse angle causes Rx<sub>2</sub> to be shadowed, the decrease in the absorption probability of Rx<sub>2</sub> deviates from the absorption probability estimated by the recursive model. As the shadowing disappears, the visual accuracy of the estimation compared to the computer-based absorption probability enhances.

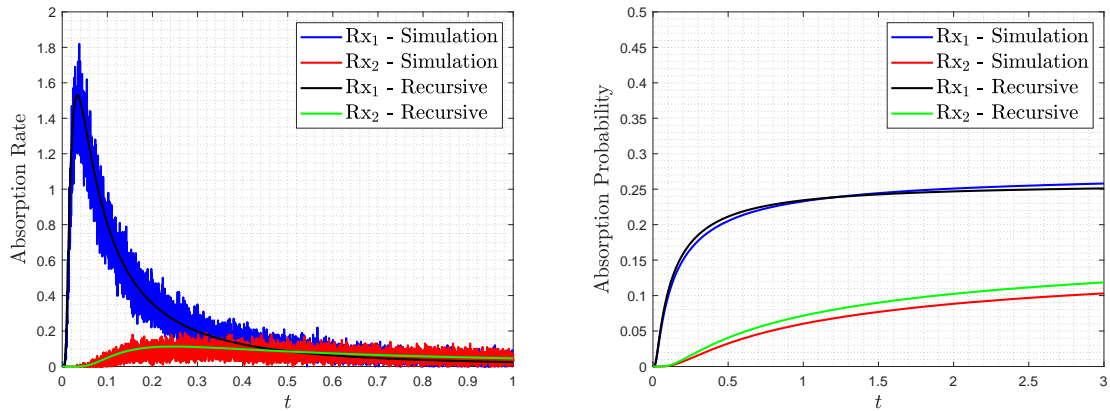


Figure 4.5. The graphs of absorption rate of MMs and absorption probability of MMs over time for Scenario 1, when the separation angle  $\phi$  is half-eclipse angle  $\arcsin \frac{r_1}{r_{01}}$ .

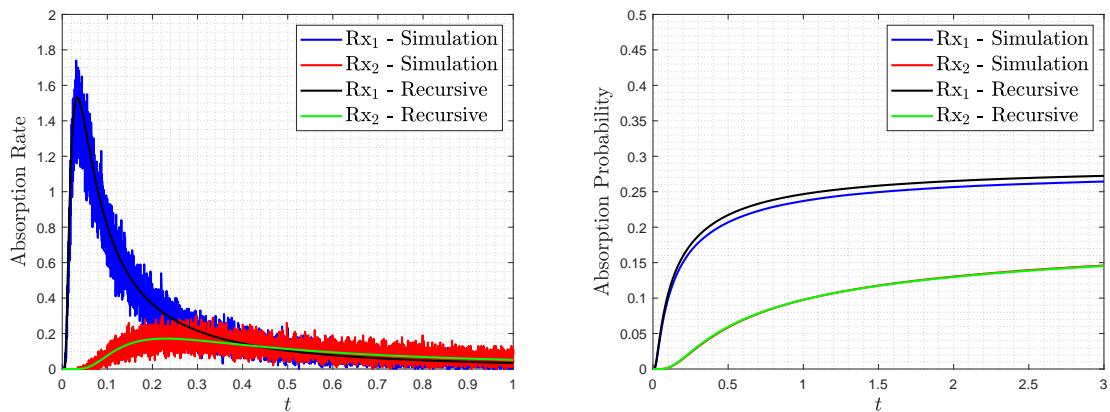


Figure 4.6. The graphs of absorption rate of MMs and absorption probability of MMs over time for Scenario 1, when the separation angle  $\phi$  is  $\frac{\pi}{2}$ .

4.4.1.2. Scenario 2–Larger Rx to be Closer to Tx. This configuration of Rxs offers a molecular SIMO topology where the larger Rx between Rxs of different radii is placed closer to the Tx. The maximum shadowing occurs when the separation angle  $\phi$  is close to 0 rad. The selection of the radii of the Rxs causes that the closer Rx can completely shadow the farther Rx easily. The shortest distance between the Rxs is  $3 \mu\text{m}$  in the case of  $\phi = 0$  rad, at which the Rxs and the Tx are perfectly aligned.

Table 4.2. Spatial parameters for Scenario 2.

Parameters	$r_1$	$r_2$	$r_{0_1}$	$r_{0_2}$
Values	$5 \mu\text{m}$	$2 \mu\text{m}$	$9 \mu\text{m}$	$19 \mu\text{m}$

As the separation angle  $\phi$  increases, the shadowing on the farther Rx decreases, and disappears after the no-eclipse angle. The half-eclipse angle and the no-eclipse angle are close since  $Rx_1$  is large, and the  $Rx_2$  is distant.

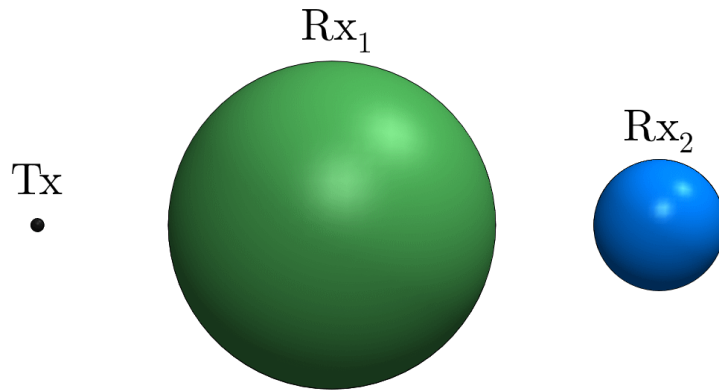


Figure 4.7. An illustration of the molecular SIMO topology examined in Scenario 2.

The virtual release point towards  $Rx_1$  from  $Rx_2$  is close for a small separation angle, which causes the estimation of the absorption probability of MMs by  $Rx_1$  to be slightly lower than the computer-based absorption probability of MMs by  $Rx_1$ . The RMS error is lower in general, and the estimation of the recursive model has a slightly higher RMS error since it takes unnecessarily more terms into account compared to the simplified model. The general trend shows RMS error decrease when the separation angle increases, as shown in Figure 4.8. After the separation angle exceeds the no-eclipse angle, the separation between receivers becomes sufficiently distant, therefore co-dependent impact between receivers drops significantly, hence the steady-trending RMS error.

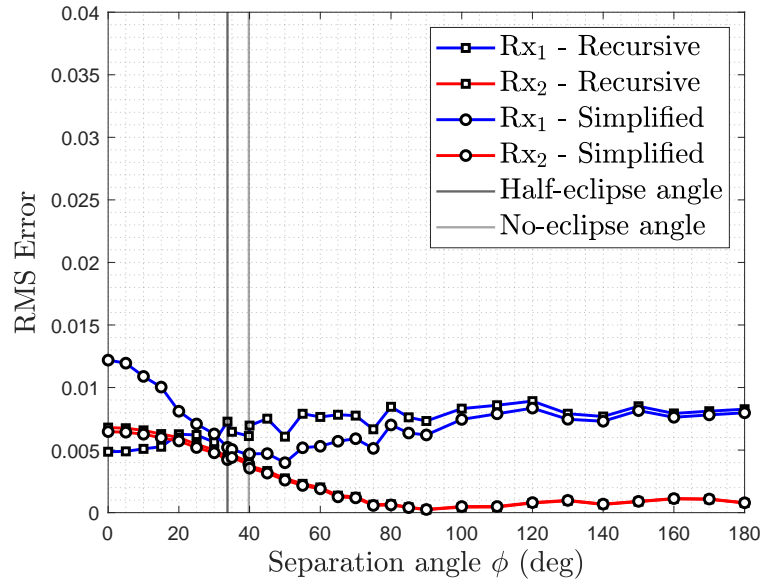


Figure 4.8. The graph of RMS error between the computer-based absorption probability of MMs and the absorption probability of MMs acquired by the recursive model versus the separation angle  $\phi$  for Scenario 2.

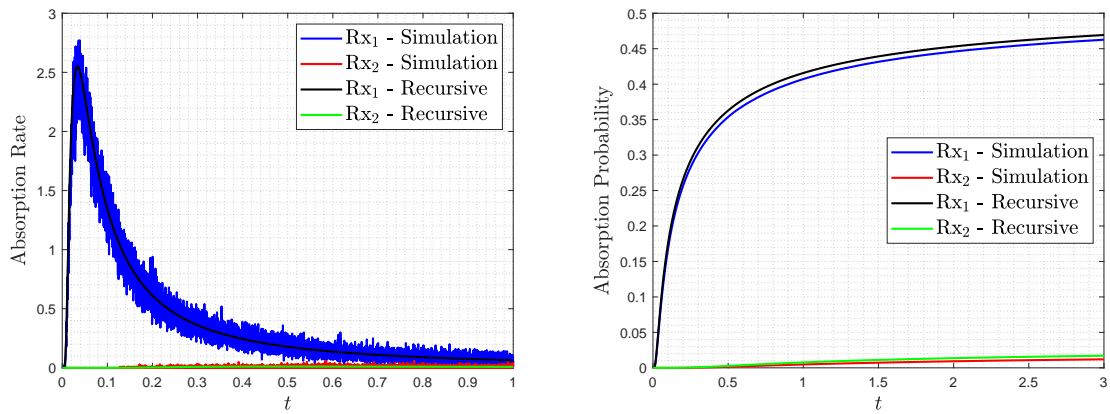


Figure 4.9. The graphs of absorption rate of MMs and absorption probability of MMs over time for Scenario 2, when the separation angle  $\phi$  is half-eclipse angle  $\arcsin \frac{r_1}{r_{01}}$ .

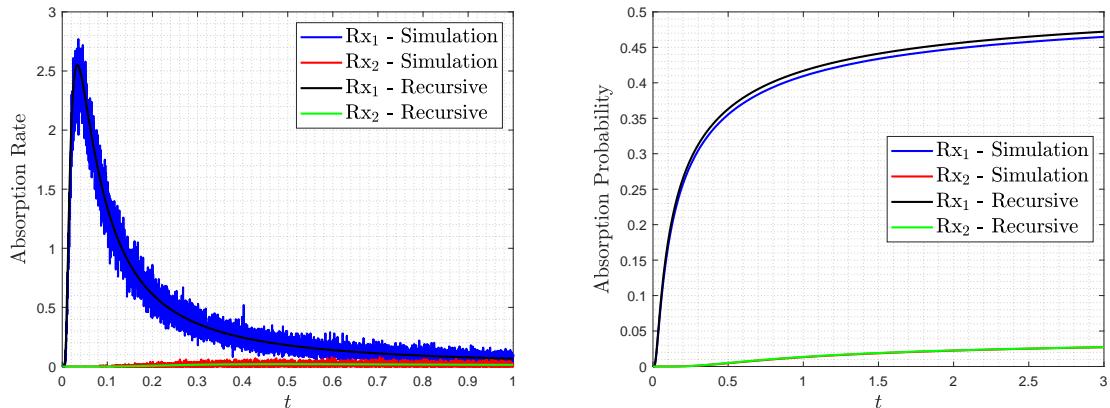


Figure 4.10. The graphs of absorption rate of MMs and absorption probability of MMs over time for Scenario 2, when the separation angle  $\phi$  is  $\frac{\pi}{2}$ .

The absorption rate and the absorption probability of MMs by Rx<sub>2</sub> are quite low, since it is small and placed at a relatively distant point. Therefore, the reciprocal interaction between the Rxs is at lower levels. The recursive model then estimates the amount of MMs captured by Rx<sub>2</sub> for the absorption probability of MMs by Rx<sub>1</sub> marginally lower, therefore the estimation deviates from the computer-based absorption probability of MMs by Rx<sub>1</sub>, as shown in Figure 4.10.

Table 4.3. Spatial parameters for Scenario 3.

Parameters	$r_1$	$r_2$	$r_{01}$	$r_{02}$
Values	5 $\mu\text{m}$	5 $\mu\text{m}$	9 $\mu\text{m}$	22 $\mu\text{m}$

**4.4.1.3. Scenario 3–Same Radii Rxs.** This configuration offers a molecular SIMO system where the Rxs have the same radii, and one of them is placed closer to the Tx. The selection of the radii of the Rxs causes the closer Rx can completely shadow the farther Rx easily, since the tangent lines of the closer Rx span a larger angle centered by Tx, the closer Rx still shadows the farther Rx when the separation angle  $\phi$  is close to 0 rad. The shortest distance between the Rxs is 3  $\mu\text{m}$  in the case of  $\phi = 0$  rad, at

which the Rx's and the Tx are perfectly aligned.

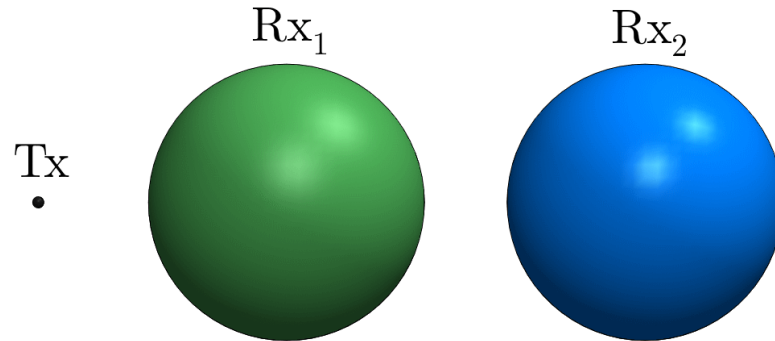


Figure 4.11. An illustration of the molecular SIMO topology examined in Scenario 3.

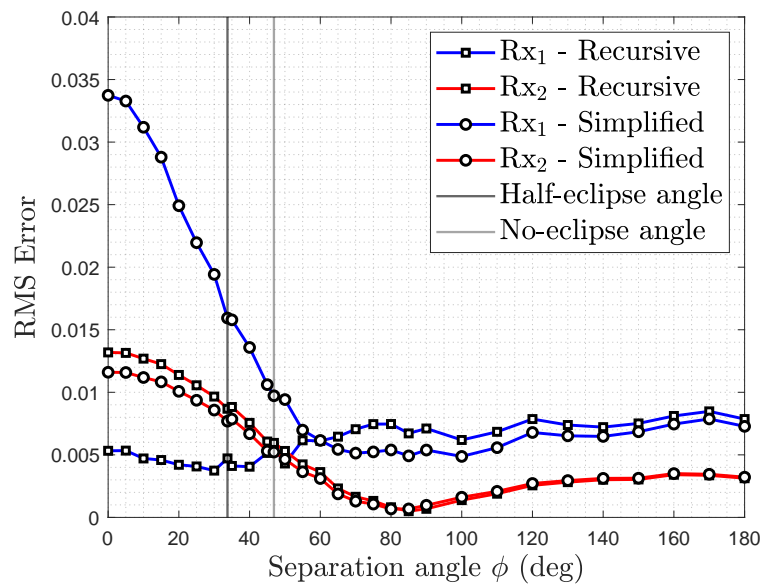


Figure 4.12. The graph of RMS error between the computer-based absorption probability of MMs and the absorption probability of MMs acquired by the recursive model versus the separation angle  $\phi$  for Scenario 3.

As the separation angle  $\phi$  increases, the shadowing on the farther Rx decreases, and disappears after the no-eclipse angle. The RMS error is lower in general, and the

estimation of the recursive model has a slightly higher RMS error since it takes unnecessarily more terms into account compared to the simplified model. Co-dependence between receivers drops eventually after the no-eclipse angle, hence the steady-trending RMS error on both receivers, as shown in Figure 4.12. The virtual release point placement is the main reason for the steady RMS error.

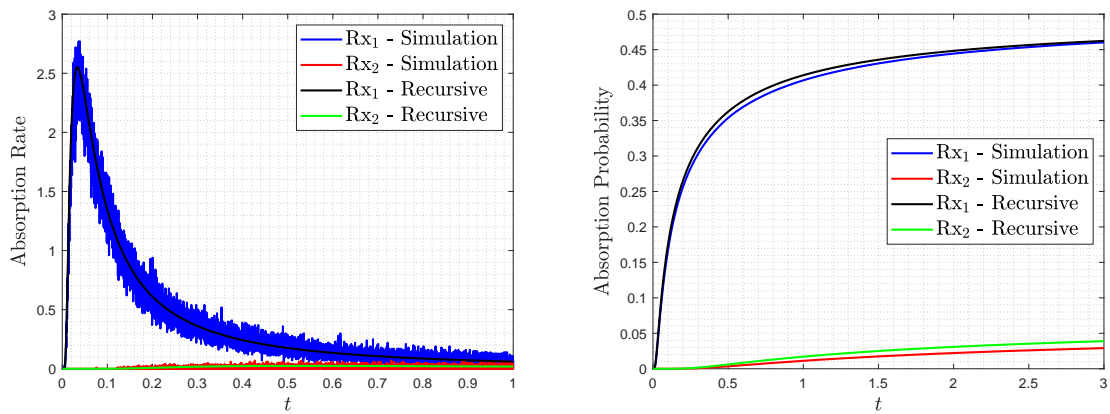


Figure 4.13. The graphs of absorption rate of MMs and absorption probability of MMs over time for Scenario 3, when the separation angle  $\phi$  is half-eclipse angle

$$\arcsin \frac{r_1}{r_{01}}.$$

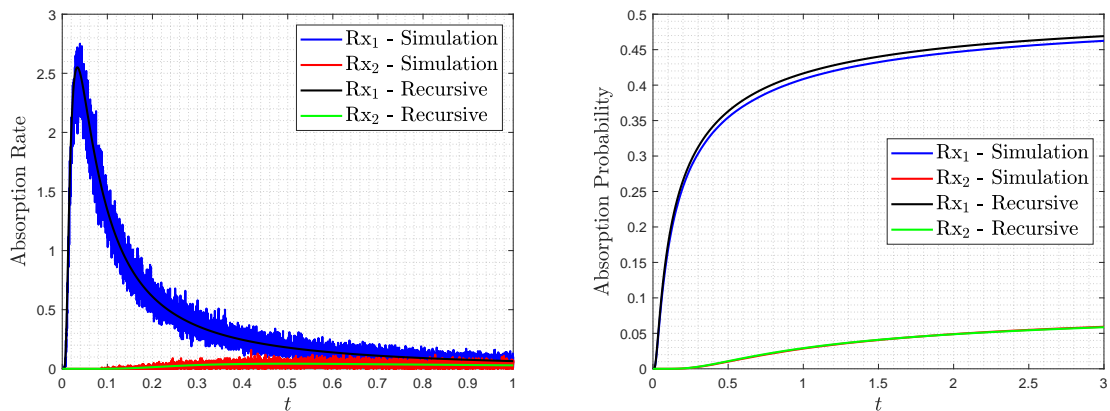


Figure 4.14. The graphs of absorption rate of MMs and absorption probability of MMs over time for Scenario 3, when the separation angle  $\phi$  is  $\frac{\pi}{2}$ .

The absorption rate and the absorption probability of MMs by  $Rx_2$  are quite low, since it is small and placed at a relatively distant point. Therefore, the reciprocal interaction between the Rxs is at lower levels. The recursive model then estimates the amount of MMs captured by  $Rx_2$  for the absorption probability of MMs by  $Rx_1$  marginally lower, therefore the estimation deviates from the computer-based absorption probability of MMs by  $Rx_1$ , as shown in Figure 4.14.

As expected, the shadowing phenomenon impacts the performance of the channel modeling significantly. The recursive model provides a well-fit channel estimation with marginally small error. RMS error decreases monotonically as the shadowing diminishes. One of the reasons for the error increase is the virtual release point assumption. For close Rx pairs, as the separation angle between Rxs goes to 0 rad, the virtual release point towards Rxs with relatively small radii is drastically influenced. On the other hand, the virtual release point towards Rxs with relatively large radii is not impacted in a comparable significance. This causes Rxs with relatively large radii to be robust against a considerable margin of error in the virtual release point assumption.

Considering the RMS error order of magnitudes, the errors that are encountered are significantly small. Provided that the distance between the virtual release points and the centers of regarded Rxs is sufficiently large, the recursive model-based absorption probability of MMs fits the computer-based absorption probability of MMs with sufficiently low RMS error.

#### 4.4.2. Compatibility Between Models

Although the recursive model provides a higher-accuracy model for molecular SIMO channel response, it is analytically derived as an infinite sum. Coefficients of further terms tend to go to 0, however, it still requires a significant amount of calculations. The comparison between the recursive model and the simplified model exhibits a significant correlation between the models, as shown in Figure . In given topologies, the smaller separation angles correspond to closely-placed Rx pairs, which require higher

degree terms which are explained in Chapter 4.1 to be taken into account. In cases where the separation angle is smaller than the no-eclipse angle, the simplified model slightly deviates from the recursive model, as shown in Figure 4.15 and Figure 4.16.

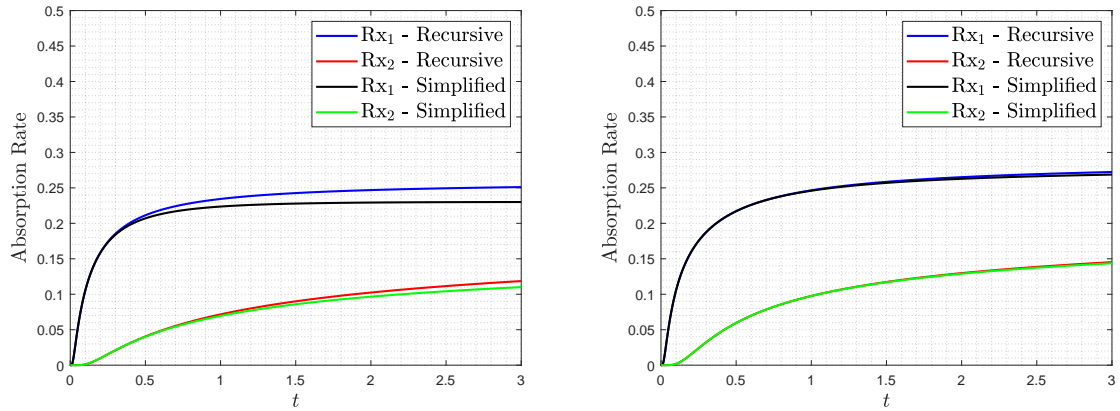


Figure 4.15. The graphs of absorption probability of MMs over time for Scenario 1 by the recursive model and the simplified model, when the separation angle  $\phi$  is half-eclipse angle  $\arcsin \frac{r_1}{r_{01}}$  on the left,  $\frac{\pi}{2}$  on the right.

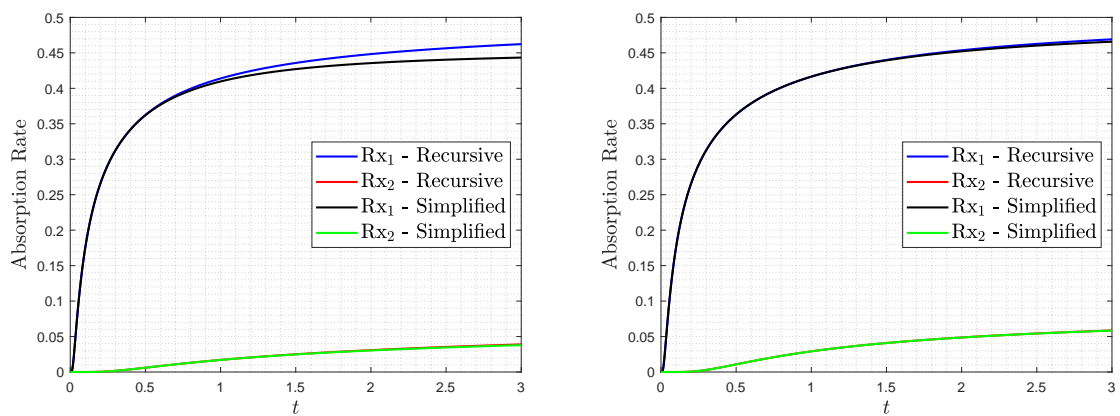


Figure 4.16. The graphs of absorption probability of MMs over time for Scenario 3 by the recursive model and the simplified model, when the separation angle  $\phi$  is half-eclipse angle  $\arcsin \frac{r_1}{r_{01}}$  on the left,  $\frac{\pi}{2}$  on the right.

In cases where the angular separation is quite large, the reciprocal effect among Rxs is sufficiently weakened, and the models correlate quite eloquently. Considering the fitness between the absorption probabilities of MMs estimated by the recursive model and the simplified model, it can be said that the models are compatible with each other, provided that the placements of Rxs are sufficiently distant.

#### 4.5. Applications of Channel Modeling in Molecular SIMO Systems

Channel model analytics of MC systems are essential to examine the channel characteristics and develop sophisticated system designs. Almost in all communication systems, practical problems such as synchronization, positioning, and localization are realistic constraints to solve. Proper characterization of molecular channels helps to offer robust and feasible solutions to such problems. In this section, we utilize the proposed models to offer systematic frameworks for dealing with positioning, localization, and synchronization as an example of the applications of channel modeling in molecular SIMO systems.

##### 4.5.1. Positioning & Localization of Tx

The absorption rate of MMs by an Rx in a molecular SIMO system can be found by the closed-form solution of the recursive model in (4.31). The expression depends on several spatial parameters which define the topology. The mathematical relation between these spatial parameters and time can be found by analyzing the expression. The peak time in the absorption rate of MMs by an Rx is a characteristic feature of the channel response of the Rx [14]. Therefore, we can relate the peak time with spatial parameters to infer from one another. As an example, in molecular SISO systems, the absorption rate of MMs by one single Rx is given in (1.4). The only spatial parameters in the equation are  $r_r$  and  $r_0$ . Differentiating (1.4) with respect to  $t$  to find the peak

time of the absorption rate of MMs [14] gives

$$\frac{\partial}{\partial t} p_{\text{Rx}}^{\text{SISO}}(t | r_0, r_r) = \frac{\partial}{\partial t} \left( \frac{r_r}{r_0} \frac{1}{\sqrt{4\pi Dt}} \frac{r_0 - r_r}{t} \exp \left[ -\frac{(r_0 - r_r)^2}{4Dt} \right] \right), \quad (4.64)$$

$$= \frac{r_r}{r_0} \frac{r_0 - r_r}{\sqrt{4\pi D}} \exp \left[ -\frac{(r_0 - r_r)^2}{4Dt} \right] \left( \frac{(r_0 - r_r)^2 - 6Dt}{4Dt^3 \sqrt{t}} \right). \quad (4.65)$$

Setting the expression equal to 0 to find the expected value of the peak time gives

$$E[t_{\text{peak}}] = \frac{(r_0 - r_r)^2}{6D}. \quad (4.66)$$

The distance between Tx and Rx can be inferred from the peak time  $t_{\text{peak}}$ , provided that the Tx and Rx are synchronized. However, inferring spatial parameter  $r_0$  only gives Rx a sphere with the center being the center of Rx and the radius of  $r_0$ , and the whereabouts of Tx is unclear, which is on the surface of the sphere but the exact position is not known.

4.5.1.1. Topology-Peak Time Relationship via The Recursive Model. In a similar approach, we differentiate (4.31) with respect to  $t$ . Our first instinct is that, since the presence of  $\text{Rx}_j$  reduces the MMs absorbed by  $\text{Rx}_i$  over time, we expect the peak time to get closer to  $t = 0$ . Starting with differentiation, we arrive at

$$\begin{aligned} \frac{\partial}{\partial t} p_{\text{Rx}_i}^{\text{SIMO}}(t | \text{Rx}_j, r_{0_i}, r_i) = \\ \sum_{k=0}^{\infty} \frac{A_{ik} B_{ik}}{\sqrt{4\pi}} \frac{\partial}{\partial t} \left[ \frac{1}{t\sqrt{t}} \exp \left( -\frac{B_{ik}^2}{4t} \right) \right] - \sum_{k=0}^{\infty} \frac{A_{jk} B_{jk}}{\sqrt{4\pi}} \frac{\partial}{\partial t} \left[ \frac{1}{t\sqrt{t}} \exp \left( -\frac{B_{jk}^2}{4t} \right) \right]. \end{aligned} \quad (4.67)$$

Placing the derivatives, we obtain

$$\begin{aligned} \frac{\partial}{\partial t} p_{\text{Rx}_i}^{\text{SIMO}}(t | \text{Rx}_j, r_{0_i}, r_i) = \\ \sum_{k=0}^{\infty} \frac{A_{ik} B_{ik}}{\sqrt{4\pi}} \exp \left( -\frac{B_{ik}^2}{4t} \right) \left[ \frac{B_{ik}^2 - 6t}{4t^3 \sqrt{t}} \right] - \sum_{k=0}^{\infty} \frac{A_{jk} B_{jk}}{\sqrt{4\pi}} \exp \left( -\frac{B_{jk}^2}{4t} \right) \left[ \frac{B_{jk}^2 - 6t}{4t^3 \sqrt{t}} \right]. \end{aligned} \quad (4.68)$$

Setting the expression equal to 0 to find the expected value of the peak time gives the equality of

$$\sum_{k=0}^{\infty} \frac{A_{ik}B_{ik}}{\sqrt{4\pi}} \exp\left(-\frac{B_{ik}^2}{4t_{\text{peak}_i}}\right) \left[\frac{B_{ik}^2 - 6t_{\text{peak}_i}}{4t_{\text{peak}_i}^3 \sqrt{t_{\text{peak}_i}}}\right] = \sum_{k=0}^{\infty} \frac{A_{jk}B_{jk}}{\sqrt{4\pi}} \exp\left(-\frac{B_{jk}^2}{4t_{\text{peak}_i}}\right) \left[\frac{B_{jk}^2 - 6t_{\text{peak}_i}}{4t_{\text{peak}_i}^3 \sqrt{t_{\text{peak}_i}}}\right]. \quad (4.69)$$

As one may see, the equation is transcendental and offers no analytical solution. Therefore, we conclude that the exact analytical approach does not pay off. The infinite number of terms is also an obstacle in derivation. However, we previously made an observation, that is,  $B_{jk}$  terms are relatively too large compared to  $B_{ik}$  terms, therefore the right-hand side of (4.69) is negligibly small. Therefore the change in  $t_{\text{peak}_i}$  is infinitesimally small.

4.5.1.2. Topology-Peak Time Relationship via The Simplified Model. For additional simplification, the relationship between the spatial parameters and the peak time of the absorption rate of MMs is reconstructed on the simplified model expression. When we look at (4.43), we see that the coefficients are again in form of (4.27), as

$$\begin{aligned} \frac{r_i}{r_{0_i}} &= A_{i0}, & \frac{r_j r_i}{r_{0_j} r_{0_{i|j}}} &= A_{j0}, \\ \frac{r_{0_i} - r_i}{\sqrt{D}} &= B_{i0}, & \frac{(r_{0_j} + r_{0_{i|j}}) - (r_j + r_i)}{\sqrt{D}} &= B_{j0}, \end{aligned}$$

where these are the coefficients for  $k = 0$ . Therefore, we can represent (4.43) with these coefficient in a clearer way as

$$\hat{p}_{\text{Rx}_i}^{\text{SIMO}}(t | \text{Rx}_j, r_{0_i}, r_i) = \frac{A_{i0}B_{i0}}{\sqrt{4\pi}} \frac{1}{t\sqrt{t}} \exp\left(-\frac{B_{i0}^2}{4t}\right) - \frac{A_{j0}B_{j0}}{\sqrt{4\pi}} \frac{1}{t\sqrt{t}} \exp\left(-\frac{B_{j0}^2}{4t}\right). \quad (4.70)$$

The derivative of (4.70) with respect to  $t$  becomes

$$\frac{\partial}{\partial t} p_{\text{Rx}_i}^{\text{SIMO}}(t | \text{Rx}_j, r_{0_i}, r_i) = \frac{A_{i0} B_{i0}}{\sqrt{4\pi}} \exp\left(-\frac{B_{i0}^2}{4t}\right) \left[\frac{B_{i0}^2 - 6t}{4t^3 \sqrt{t}}\right] - \frac{A_{j0} B_{j0}}{\sqrt{4\pi}} \exp\left(-\frac{B_{j0}^2}{4t}\right) \left[\frac{B_{j0}^2 - 6t}{4t^3 \sqrt{t}}\right]. \quad (4.71)$$

Setting the expression equal to 0 to find the expected value of the peak time gives the equality of

$$\frac{A_{i0} B_{i0}}{\sqrt{4\pi}} \exp\left(-\frac{B_{i0}^2}{4t_{\text{peak}_i}}\right) \left[\frac{B_{i0}^2 - 6t_{\text{peak}_i}}{4t_{\text{peak}_i}^3 \sqrt{t_{\text{peak}_i}}}\right] = \frac{A_{j0} B_{j0}}{\sqrt{4\pi}} \exp\left(-\frac{B_{j0}^2}{4t_{\text{peak}_i}}\right) \left[\frac{B_{j0}^2 - 6t_{\text{peak}_i}}{4t_{\text{peak}_i}^3 \sqrt{t_{\text{peak}_i}}}\right]. \quad (4.72)$$

Since  $B_{j0}$  is relatively large compared to  $B_{i0}$ , the right-hand side of (4.72) is assumed to converge to 0, at a cost of precision. The equation (4.72) then becomes

$$\frac{A_{i0} B_{i0}}{\sqrt{4\pi}} \exp\left(-\frac{B_{i0}^2}{4t_{\text{peak}_i}}\right) \left[\frac{B_{i0}^2 - 6t_{\text{peak}_i}}{4t_{\text{peak}_i}^3 \sqrt{t_{\text{peak}_i}}}\right] \approx 0. \quad (4.73)$$

The solution of this equation for  $t_{\text{peak}_i}$  is

$$B_{i0}^2 \approx 6t_{\text{peak}_i}, \quad (4.74)$$

$$E[t_{\text{peak}_i}] \approx \frac{(r_{0_i} - r_i)^2}{6D}, \quad (4.75)$$

$$r_{0_i} \approx \sqrt{6Dt_{\text{peak}_i}} + r_i. \quad (4.76)$$

The most significant inference from this result is that, the presence of another Rx,  $\text{Rx}_j$  in this scenario, does not considerably affect the peak time of an Rx in consideration, hence the same result as the one from the molecular SISO channel analytics [14]. Following that, we estimate the center-to-center distance between Tx and  $\text{Rx}_i$  based on the peak time of the absorption rate of MMs by  $\text{Rx}_i$ . Therefore, the position of Tx is inferred to be on the surface of a sphere with a radius of  $r_{0_i}$  centered by the center of  $\text{Rx}_i$ .

For each Rx, one distinct sphere with distinct radius is defined. As known from Euclidean geometry, the intersection of two distinct spheres defines a circle, provided that the spheres are not identical, not tangent to each other, and they intersect. For a molecular SIMO system with 2 Rxs,  $Rx_i$  and  $Rx_j$ , whose centers are placed at  $C_i = \begin{bmatrix} x_i & y_i & z_i \end{bmatrix}$  and  $C_j = \begin{bmatrix} x_j & y_j & z_j \end{bmatrix}$  in 3D space, the spheres with radii of  $r_{0_i}$  and  $r_{0_j}$  centered by Rxs are defined as

$$(x - x_i)^2 + (y - y_i)^2 + (z - z_i)^2 = r_{0_i}^2 = \left( \sqrt{6Dt_{\text{peak}_i}} + r_i \right)^2, \quad (4.77)$$

$$(x - x_j)^2 + (y - y_j)^2 + (z - z_j)^2 = r_{0_j}^2 = \left( \sqrt{6Dt_{\text{peak}_j}} + r_j \right)^2. \quad (4.78)$$

Similarly, the intersection of three distinct spheres defines two points, provided that the spheres intersect, and their pairwise intersections are not tangent to each other. Subsequently, the intersection of four distinct spheres defines a single point, provided that the intersection point exists. Therefore, utilizing four Rxs in a molecular SIMO system analytically guarantees Tx localization, provided that all Rxs are in coordination.

#### 4.5.2. Synchronization in Molecular SIMO Systems

The synchronization in communication systems is an essential feature for the sake of communication performance. Like all communication systems, MC systems are vulnerable to synchronization errors. The time calibration between Tx and Rxs is crucial for not only communication performance, but also for other channel characteristics. Synchronization is again employed by utilizing the relationship between the spatial parameters and the peak time. The only difference is that, for this case, the spatial parameters are assumed to be known, and the peak time is the parameter to be inferred.

Starting with the synchronization approaches in molecular SISO systems, the same expressions proposed in [14] are used, such as the expected value of the peak

time of the absorption rate of MMs by Rx as

$$E[t_{\text{peak}}] = \frac{(r_0 - r_r)^2}{6D}. \quad (4.79)$$

Provided that the spatial parameter  $r_0$  and the diffusion coefficient  $D$  are known by the Rx, the peak time –which is the time difference between the time at the peak absorption and the starting time– is estimated effortlessly. Then, a synchronization error  $\tau$  can comfortably be determined as

$$\tau = \hat{t}_{\text{peak}} - E[t_{\text{peak}}], \quad (4.80)$$

$$= \hat{t}_{\text{peak}} - \frac{(r_0 - r_r)^2}{6D}, \quad (4.81)$$

where  $\hat{t}_{\text{peak}}$  is the observed peak time. Following the detection of an error in synchronization, Rx can be calibrated accordingly.

The relationship between the spatial parameters and the peak time for molecular SIMO systems is a more rigorous process. The analytical solution of peak time as a function of spatial parameters cannot be found, due to the transcendental nature of the equality in 4.69. An estimation can be made by using the approximations of the exponential terms, such as finite Maclaurin expansion and Padé approximation [46]. However, since the exponents can be quite large depending on the spatial parameters, the approximations may deviate from the real values significantly, which decreases the success of the estimation of the peak time.

At a cost of precision, the estimation of peak time proposed in 4.75 can be utilized for synchronization in molecular SIMO systems. The only difference is that the synchronization error is individual for each Rx. Therefore, the calibration is done

for each Rx separately. The synchronization error of Rx<sub>*i*</sub> can be represented as

$$\tau_i = \hat{t}_{\text{peak}_i} - E [t_{\text{peak}_i}], \quad (4.82)$$

$$= \hat{t}_{\text{peak}_i} - \frac{(r_{0_i} - r_i)^2}{6D}. \quad (4.83)$$

where  $\hat{t}_{\text{peak}_i}$  is the observed peak time of the absorption rate of MMs by Rx<sub>*i*</sub>. Therefore, each Rx can be calibrated accordingly.

### 4.5.3. Applicability to Molecular MIMO Systems

In Chapter 4, a thorough channel modeling approach for molecular SIMO systems is proposed. The channel characterization of molecular SISO systems was proposed in [14] earlier, however, there is no proper channel analytics for molecular multiple-receiver systems, other than several works in the literature [23–26, 47, 48]. The method we propose overcomes the practical problems of these works, such as the receivers having to be the same radii [23, 49], and intractable expressions that are too complex and lack providing channel characteristics and parameters [24, 25].

One of the first assumptions made is that the Tx<sub>s</sub> are modeled as point objects that have no volume to interact with MMs. Thus, the existence of any Tx has no interruption on the movement of MMs. Based on this observation, a molecular MIMO system can be considered multiple individual molecular SIMO systems with overlapping Rx antennas. From the perspective of every Tx, the Rx array forms a molecular SIMO system with distinct spatial parameters. Each Rx then belongs to the molecular SIMO systems perceived by each Tx. Supported by this, the absorption rate of MMs by an Rx in a molecular MIMO system can be represented as the superposition of individual absorption rates of MMs by the regarded Rx in molecular SIMO systems perceived by each Tx. Therefore, the employed channel modeling for molecular SIMO systems can be adapted to molecular MIMO systems to channel characterization.

## 5. CONCLUSION

Molecular communication is a promising cutting-edge technology that utilizes molecular diffusion to convey information through diffusive media. There is a wide array of molecular methods in the literature, and the MCvD systems are the systems to focus on in the scope of this thesis. Molecular SISO systems are one of the most basic systems ever proposed, and have strong foundations in the literature [7, 14, 18, 45]. Although the molecular SISO systems are analytically well-examined [14], they do not meet the requirements of today's technological world. The higher data transmission rate demand and the need for the coexistence of the multiple entities in a nanonetwork require higher-complexity molecular system designs and sophisticated modulation schemes built on those systems to match the demand. Motivated by the rising potential of the molecular multiple-entity networks, a thorough analysis of the molecular multiple-receiver networks is performed. The thesis focuses on two specific molecular multiple-receiver networks. The first system is the molecular MIMO system whose number of Tx and the number of Rx are equal, and the antennas are placed on a UCA [11]. The second one is the molecular SIMO systems with a single Tx and multiple Rx [22].

The thesis can be investigated in three parts. In the first part, we have thoroughly investigated the molecular MIMO systems. There are several parameters to define a molecular MIMO system, such as the number of Tx and Rx antennas,  $n_{\text{TRx}}$ , the shortest distance between the Tx plane and the Rx plane  $d_x$ , and the radius of the Rx UCA  $d_{yz} + r_r$ , where the variable part is  $d_{yz}$ . These parameters are uniquely selected according to the purpose of the application. At the beginning of the part, we have proposed a numerical method to estimate the spatial parameters depending on the number of antennas. The distance between the Tx and Rx planes directly affects the coverage angle between each Tx-Rx pair, which governs the number of MMs absorbed by the Rxs. The radius of the Rx UCA, on the other hand, governs the displacement among the Rxs, which influences the ILI among Rxs. Subsequently, we have examined

the communication performances and the CSI behaviors of molecular MIMO systems with a varying number of antennas. Finally, we have investigated the effect of the spatial parameters of  $d_x$  and  $d_{yz}$  on both the communication performance and the CSI behaviors.

In the second part, we proposed several modulation schemes for the molecular MIMO systems. Primarily, we regarded the molecular MIMO system with 8 antennas. In this regard, we have reviewed the molecular index modulation examples in the literature [11]. Based on the foundations of the molecular index modulation applications, MSSK in particular, we have proposed the MGSSK, which is another index modulation application that utilizes more than 1 antenna, 2 for the scope of this thesis, to convey information via the indices of the antennas [31]. In this regard, the increased number of antennas eventually causes the ILI to increase. On the other hand, the potential number of symbols increases from 8 to 16, which enhances the length of bit packages by 1 bit. Therefore symbol duration  $t_s$  lengthens accordingly, which decreases the ISI. Selection of the bit duration causes a trade-off between ISI and ILI, in which the longer bit durations cause the ISI to reduce, but the ILI to increase. Therefore, increased symbol durations  $t_b$  combine with the increased number of antennas used per symbol duration, hence the increased ILI despite the reduction in ISI. Additionally, we have reviewed an ISI-mitigating modulation scheme proposed for molecular SISO systems [35]. The method to mitigate ISI in the time domain of molecular SISO systems is adapted to mitigate ILI in the spatial domain of molecular MIMO systems. The CWC-based ISD to mitigate ILI iteratively to estimate the symbols enables the communication performance, especially for MGSSK. Another application to mitigate ISI in the time domain of molecular SISO systems is pre-equalization [34]. Utilizing another MM type to represent minus signals, the modulation scheme aims to remove the ISI at the Rx side, by releasing the other MM type with a delay as a poison signal. Aiming to mitigate the ILI in the spatial domain of molecular MIMO systems, we have proposed the pre-equalization by releasing the other MM type from neighboring Tx's of the Tx to transmit the information. The calculation of the amount of MMs as poison is optimized by two metrics, which are SIR and SID. The increase in communication

performance is marginal since the pre-equalization aims to mitigate the interference while reducing the signal power. The gain is higher for shorter bit durations or faster data transmission rates, due to increased ISI.

In the final part, we have presented a unique and newly-proposed channel model for molecular SIMO systems. This is the heart of the thesis, as it offers a new method to the literature. The channel modeling of molecular multiple-receiver networks is still an open case, due to the statistical dependence among the fully-absorbing Rxs. We propose a probabilistic approach to derive an analytical expression to calculate the amount of MMs stolen by the bystander Rx. This way, the channel characteristics, such as the absorption rate of MMs and absorption probability of MMs, can be analytically derived. To simplify the derivation, one significant assumption is made, that is, the MMs absorbed by the bystander Rx are assumed to have been absorbed in a single point, namely the virtual release point. To calculate the amount of MMs to have been stolen by the bystander Rx, the MMs absorbed by the bystander Rx are assumed to have been released from the virtual release point towards the intended Rx. In this way, we calculate the absorption probability of MMs to be subtracted from the absorption probability of MMs by the intended Rx. We then proposed a simplification of this model. The computer-based simulations showed that the proposed model offers a well-fit channel characterization with relatively low RMS error. Finally, the simplified model is observed to correlate with the recursive model for most topologies, provided that the Rxs are placed sufficiently distant.

To conclude this thesis, we have proposed a thorough analysis of molecular MIMO systems. The analysis shows the channel characterizations of the molecular MIMO systems in detail, examining all aspects. Additionally, we have adapted several interference-mitigating applications proposed for molecular SISO systems into molecular MIMO systems aiming to mitigate ILI. Finally, we have proposed a comprehensive and well-structured channel modeling for molecular SIMO systems, which is thought to be the pioneer of incoming studies in the field.

## REFERENCES

1. Nakano, T., A. W. Eckford and T. Haraguchi, *Molecular Communication*, Cambridge University Press, 2013.
2. Fick, A., “On Liquid Diffusion”, *The London, Edinburgh, and Dublin Philosophical Magazine and Journal of Science*, Vol. 10, No. 63, pp. 30–39, 1855.
3. Einstein, A., “Über die von Der Molekularkinetischen Theorie Der Wärme Geforderte Bewegung von in Ruhenden Flüssigkeiten Suspensierten Teilchen”, *Annalen der Physik*, Vol. 322, No. 8, pp. 549–560, 1905.
4. Einstein, A., *Investigations on The Theory of The Brownian Movement*, Dover Books on Physics, Dover Publications, Mineola, NY, 1956.
5. von Smoluchowski, M., “Zur Kinetischen Theorie Der Brownschen Molekularbewegung und Der Suspensionen”, *Annalen der Physik*, Vol. 326, No. 14, pp. 756–780, 1906.
6. Yilmaz, H. B., N. R. Kim and C. B. Chae, *Modulation Techniques for Molecular Communication via Diffusion*, pp. 99–118, Springer International Publishing, 2017.
7. Kuran, M. S., H. B. Yilmaz, T. Tugcu and I. F. Akyildiz, “Modulation Techniques for Communication via Diffusion in Nanonetworks”, *IEEE International Conference on Communications (ICC)*, 2011.
8. Kabir, M. H., S. M. Riazul Islam and K. S. Kwak, “D-MoSK Modulation in Molecular Communications”, *IEEE Transactions on NanoBioscience*, Vol. 14, No. 6, pp. 680–683, 2015.
9. Garralda, N., I. Llatser, A. Cabellos-Aparicio, E. Alarcón and M. Pierobon, “Diffusion-Based Physical Channel Identification in Molecular Nanonetworks”,

*Nano Communication Networks*, Vol. 2, pp. 196–204, 2011.

10. Akdeniz, B. C., A. E. Pusane and T. Tugcu, “Position-Based Modulation in Molecular Communications”, *Nano Communication Networks*, Vol. 16, pp. 60–68, 2018.
11. Gursoy, M. C., E. Basar, A. E. Pusane and T. Tugcu, “Index Modulation for Molecular Communication via Diffusion Systems”, *IEEE Transactions on Communications*, Vol. 67, No. 5, pp. 3337–3350, 2019.
12. Honary, V. and T. A. Wysocki, “Molecular Communication System with Non-Absorbing Receiver”, *Nano Communication Networks*, Vol. 28, No. 100335, p. 100335, 2021.
13. Trinh, D. P., Y. Jeong and S.-H. Kim, “Molecular Communication with Passive Receivers in Anomalous Diffusion Channels”, *IEEE Wireless Communication Letters*, Vol. 10, No. 10, pp. 2215–2219, 2021.
14. Yilmaz, H. B., A. C. Heren, T. Tugcu and C. B. Chae, “Three-Dimensional Channel Characteristics for Molecular Communications with An Absorbing Receiver”, *IEEE Communications Letters*, Vol. 18, No. 6, pp. 929–932, 2014.
15. Akkaya, A., H. B. Yilmaz, C.-B. Chae and T. Tugcu, “Effect of Receptor Density and Size on Signal Reception in Molecular Communication via Diffusion With an Absorbing Receiver”, *IEEE Communications Letters*, Vol. 19, No. 2, pp. 155–158, 2015.
16. Srinivas, K. V., A. W. Eckford and R. S. Adve, “Molecular Communication in Fluid Media: The Additive Inverse Gaussian Noise Channel”, *IEEE Transactions on Information Theory*, Vol. 58, No. 7, pp. 4678–4692, 2012.
17. Tyrrell, H. J. V. and K. R. Harris, *Diffusion in Liquids: A Theoretical and Experimental Study*, Monographs in Chemistry, Butterworth-Heinemann, Oxford, England, 1984.

18. Nakano, T., Y. Okaie and J.-Q. Liu, “Channel Model and Capacity Analysis of Molecular Communication with Brownian Motion”, *IEEE Communications Letters*, Vol. 16, No. 6, pp. 797–800, 2012.
19. Kara, O., G. Yaylali, A. E. Pusane and T. Tugcu, “Molecular Index Modulation using Convolutional Neural Networks”, *arXiv Computing Research Repository (CoRR)*, 2021.
20. Yilmaz, H. B., C.-B. Chae, B. Tepekule and A. E. Pusane, “Arrival Modeling and Error Analysis for Molecular Communication via Diffusion with Drift”, *Proceedings of the Second Annual International Conference on Nanoscale Computing and Communication*, 2015.
21. Box, G. E. P., , W. G. Hunter and J. S. Hunter, *Statistics for Experimenters, Probability & Mathematical Statistics S.*, John Wiley & Sons, Nashville, TN, 1978.
22. Yaylali, G., B. C. Akdeniz, T. Tugcu and A. E. Pusane, “Channel Modeling for Multi-Receiver Molecular Communication Systems”, *arXiv Computing Research Repository (CoRR)*, 2021.
23. Bao, X., J. Lin and W. Zhang, “Channel Modeling of Molecular Communication via Diffusion with Multiple Absorbing Receivers”, *IEEE Wireless Communications Letters*, Vol. 8, No. 3, pp. 809–812, 2019.
24. Sabu, N., N. Varshney and A. Gupta, “3-D Diffusive Molecular Communication With Two Fully-Absorbing Receivers: Hitting Probability and Performance Analysis”, *IEEE Transactions on Molecular, Biological and Multi-Scale Communications*, Vol. 6, pp. 244–249, 2020.
25. Kwak, J. W., H. B. Yilmaz, N. Farsad, C.-B. Chae and A. J. Goldsmith, “Two-Way Molecular Communications”, *IEEE Transactions on Communications*, Vol. 68, No. 6, pp. 3550–3563, 2020.

26. Zoofaghari, M., H. Arjmandi, A. Etemadi and I. Balasingham, “A Semi-Analytical Method for Channel Modeling in Diffusion-Based Molecular Communication Networks”, *IEEE Transactions on Communications*, Vol. 69, No. 6, pp. 3957–3970, 2021.
27. Basar, E., M. Wen, R. Mesleh, M. Di Renzo, Y. Xiao and H. Haas, “Index Modulation Techniques for Next-Generation Wireless Networks”, *IEEE Access*, Vol. 5, pp. 16693–16746, 2017.
28. Basar, E., “Index Modulation Techniques for 5G Wireless Networks”, *IEEE Communications Magazine*, Vol. 54, No. 7, pp. 168–175, 2016.
29. Basar, E., U. Aygolu, E. Panayirci and H. V. Poor, “Orthogonal Frequency Division Multiplexing With Index Modulation”, *IEEE Transactions on Signal Processing*, Vol. 61, No. 22, pp. 5536–5549, 2013.
30. Jeganathan, J., A. Ghayeb, L. Szczecinski and A. Ceron, “Space Shift Keying Modulation for MIMO Channels”, *IEEE Transactions on Wireless Communications*, Vol. 8, No. 7, pp. 3692–3703, 2009.
31. Jeganathan, J., A. Ghayeb and L. Szczecinski, “Generalized Space Shift Keying Modulation for MIMO Channels”, *IEEE 19th International Symposium on Personal, Indoor and Mobile Radio Communications*, pp. 1–5, 2008.
32. Mesleh, R., H. Haas, C. W. Ahn and S. Yun, “Spatial Modulation - A New Low Complexity Spectral Efficiency Enhancing Technique”, *First International Conference on Communications and Networking in China*, pp. 1–5, 2006.
33. Mesleh, R. Y., H. Haas, S. Sinanovic, C. W. Ahn and S. Yun, “Spatial Modulation”, *IEEE Transactions on Vehicular Technology*, Vol. 57, No. 4, pp. 2228–2241, 2008.
34. Tepekule, B., A. E. Pusane, M. S. Kuran and T. Tugcu, “A Novel Pre-Equalization Method for Molecular Communication via Diffusion in Nanonetworks”, *IEEE Com-*

*munications Letters*, Vol. 19, No. 8, pp. 1311–1314, 2015.

35. Ulkar, M. G., A. E. Pusane and T. Tugcu, “Novel Decoding Methods of Constant Weight Coding for Molecular Communications”, *Nano Communication Networks*, Vol. 19, pp. 157–167, 2019.
36. Ahuja, M. and M. R. Bhatnagar, “A Spatio-Temporal Coded Modulation Scheme for Molecular MIMO Systems”, *International Conference on COMMunication Systems NETWORKS (COMSNETS)*, pp. 140–144, 2021.
37. GURSOY, M. C., A. CELIK, E. BASAR, A. E. PUSANE and T. TUGCU, “Molecular Index Modulation With Space-Time Equalization”, *IEEE Wireless Communications Letters*, Vol. 9, No. 5, pp. 702–705, 2020.
38. Skachek, V. and K. A. S. Immink, “Constant Weight Codes: An Approach Based on Knuth’s Balancing Method”, *IEEE Journal on Selected Areas in Communications*, Vol. 32, No. 5, pp. 909–918, 2014.
39. Etzion, T. and A. Vardy, “A New Construction for Constant Weight Codes”, *International Symposium on Information Theory and its Applications*, pp. 338–342, 2014.
40. Brouwer, A., J. Shearer, N. Sloane and W. Smith, “A New Table of Constant Weight Codes”, *IEEE Transactions on Information Theory*, Vol. 36, No. 6, pp. 1334–1380, 1990.
41. Lin, M.-C., “Constant Weight Codes for Correcting Symmetric Errors and Detecting Unidirectional Errors”, *IEEE Transactions on Computers*, Vol. 42, No. 11, pp. 1294–1302, 1993.
42. Van Veen, B. and K. Buckley, “Beamforming: A Versatile Approach to Spatial Filtering”, *IEEE ASSP Magazine*, Vol. 5, No. 2, pp. 4–24, 1988.

43. Wang, S., W. Guo and M. D. McDonnell, “Transmit Pulse Shaping for Molecular Communications”, *IEEE Conference on Computer Communications Workshops (INFOCOM WKSHPS)*, pp. 209–210, 2014.
44. Akdeniz, B. C., A. E. Pusane and T. Tugcu, “Optimal Reception Delay in Diffusion-Based Molecular Communication”, *IEEE Communications Letters*, Vol. 22, No. 1, pp. 57–60, 2017.
45. Akdeniz, B. C., N. A. Turgut, H. B. Yilmaz, C.-B. Chae, T. Tugcu and A. E. Pusane, “Molecular Signal Modeling of a Partially Counting Absorbing Spherical Receiver”, *IEEE Transactions on Communications*, Vol. 66, No. 12, pp. 6237–6246, 2018.
46. Baker, G. A. and P. Graves-Morris, *Padé Approximants*, Encyclopedia of Mathematics and Its Applications, Cambridge University Press, Cambridge, England, 2 edn., 1996.
47. Zoofaghari, M., A. Etemadi, H. Arjmandi and I. Balasingham, “Modeling Molecular Communication Channel in the Biological Sphere With Arbitrary Homogeneous Boundary Conditions”, *IEEE Wireless Communications Letters*, Vol. 10, No. 12, pp. 2786–2790, 2021.
48. Huang, X., Y. Fang, A. Noel and N. Yang, “Channel Characterization for 1-D Molecular Communication With Two Absorbing Receivers”, *IEEE Communications Letters*, Vol. 24, No. 6, pp. 1150–1154, 2020.
49. Berezhkovskii, A. and Y. Makhnovskii, “Mutual Influence of Traps on The Death of A Brownian Particle”, *Chemical Physics Letters*, Vol. 175, No. 5, pp. 499–504, 1990.

## APPENDIX A: REGION OF CONVERGENCE OF THE LAPLACE TRANSFORMATIONS OF THE ABSORPTION RATE FUNCTIONS IN THE RECURSIVE MODEL

Here, we derive the ROC of the absorption rate functions presented in the recursive model. The Laplace transformation of an absorption rate function in form of (1.4) becomes in form of

$$\mathcal{L} \left\{ \frac{a}{\sqrt{4\pi t}} \frac{b}{t} \exp \left( -\frac{b^2}{4t} \right) \right\} = a \exp(-b\sqrt{s}). \quad (\text{A.1})$$

To be used in further analysis, we need to expand

$$\frac{1}{1 - a \exp(-b\sqrt{s})}, \quad (\text{A.2})$$

for which we need to state

$$|a \exp(-b\sqrt{s})| < 1. \quad (\text{A.3})$$

Let  $-b\sqrt{s}$  be a complex number in form of  $x + yi$ , where  $i = \sqrt{-1}$  is the imaginary unit,  $\Re(-b\sqrt{s}) = x$ , and  $\Im(-b\sqrt{s}) = y$ . Then, (A.3) becomes

$$|a \exp(-b\sqrt{s})| = |a \exp(x) \exp(yi)|. \quad (\text{A.4})$$

The expression  $a \exp(x + yi)$  can be separated as magnitude term  $a \exp(x)$  and phase angle term  $\exp(yi)$ . The phase angle term does not contribute to the magnitude, then can be neglected within the inequality (A.3), which becomes

$$|a \exp(x)| < 1 \longrightarrow a < \exp(-x). \quad (\text{A.5})$$

Recalling the equality  $-b\sqrt{s} = x + yi$ , it becomes

$$-b\sqrt{s} = x + yi \longrightarrow \sqrt{s} = \frac{x}{-b} + \frac{yi}{-b}. \quad (\text{A.6})$$

Let  $s = \sigma + i\omega$ , then we obtain

$$\sqrt{\sigma + i\omega} = \frac{x}{-b} + \frac{yi}{-b}. \quad (\text{A.7})$$

Implementing basic algebra gives

$$\frac{x}{-b} = \sqrt{\frac{\sqrt{\sigma^2 + \omega^2} + \sigma}{2}}, \quad (\text{A.8})$$

$$\frac{y}{-b} = \sqrt{\frac{\sqrt{\sigma^2 + \omega^2} - \sigma}{2}}. \quad (\text{A.9})$$

Placing the expression in (A.5) gives

$$a < \exp \left( b \sqrt{\frac{\sqrt{\sigma^2 + \omega^2} + \sigma}{2}} \right), \quad (\text{A.10})$$

and this concludes the derivation of the ROC of the denominator of the Laplace transformation of the absorption rate function modeled by the recursive model.